MATHEMATICAL MODELING OF THE PRESSURE-DRIVEN PERFORMANCE OF MCMASTER PORE-FILLED MEMBRANES

by

JESUS GARCIA-ALEMAN, B. S., M. ENG.

A Thesis

Submitted to the School of Graduate Studies

In Partial Fullfilment of the Requirements

For the Degree

Doctor of Philosophy

McMaster University, Hamilton, Ontario, Canada

MODELING OF THE PERFORMANCE OF MCMASTER PORE-FILLED MEMBRANES

Doctor of Philosophy (2002)	**McMaster University**
(Chemical Engineering)	**Hamilton, Ontario**

TITLE:	**Mathematical Modeling of the Pressure-Driven Performance of McMaster Pore-filled Membranes**
AUTHOR:	**Jesus Garcia-Aleman** **Master of Engineering (McMaster University), Bachelor of Science (Instituto Tecnologico y de Estudios Superiores de Monterrey, Campus Monterrey)**
SUPERVISOR:	**Dr. James M. Dickson**
NUMBER OF PAGES:	**xxv, 227**

Abstract

The McMaster Pore-filled (MacPF) membranes are a new class of nanofiltration membranes prepared by co-polymerizing a polyelectrolyte (PEL) gel into a microporous substrate. The PEL gives unique characteristics to the MacPF membranes that make them suitable for water softening and fractionation.

The main objective of this investigation is to develop a procedure that can be used to design MacPF membranes for specific applications from theory *a priori*. This procedure involves the combination of two mechanistic models. The first model (gel model) predicts the physicochemical structure (i.e., membrane parameters) of the pore-filling gel (Mika and Childs, 2001). The second model (transport model) can be used in combination with the parameters predicted by the gel model to predict the pressure-driven transport of the MacPF membranes. The transport model is developed in this dissertation.

The design procedure and mathematical models outlined in here would be the first time a membrane design is attempted using only theoretical arguments.

The membrane transport model is a pseudo 2-dimensional transport model that consists of the extended Nernst-Planck equation (viscous flow and frictional model), a modified Poisson Boltzmann equation, and hydrodynamic calculations to relate the frictional and steric forces to the membrane structure. The model has three fitting parameters that describe four structural properties of the membrane:

pore radius, pure water permeability, surface charge density and the ratio of effective membrane thickness to water content.

The model successfully predicts and explains the performance of the MacPF membranes as well as one commercial thin-film composite membrane tested simultaneously. The model parameters estimated here are statistically significant and are comparable to previous results (Garcia-Aleman, 1998).

A comparison of the performance of the commercial and MacPF membrane was performed using experimental data and the transport model. This analysis shows that the rejection and transport mechanisms are the same in the commercial and MacPF membranes. Convection, diffusion and electromigration are the main mechanisms of solute transport. However, their contribution is different for each type of membrane. Solute rejection in NF membranes is determined primarily by steric and electrostatic effects. For the MacPF membranes separation and selectivity are primarily determined by the latter. The contribution of steric effects to rejection is significantly smaller compared to commercial membranes.

Additionally, the membrane parameters were estimated using both the gel and transport models. At this point, the results obtained separately from the two models show similar parameter estimates and separation. However, additional work has to be done to improve the agreement between the models before the procedure outline here can be used to truly tailor-make the MacPF membranes.

Acknowledgements

First, I would like to thank **God** for giving me such opportunity in life. I want to extend my love to **my family** for their moral and emotional support.

Special thanks to **Dr. James M. Dickson** for his knowledge and guidance, especially for his encouragement. You cannot reach the summit without a good belay! My supervisory committee: Dr. Heather Sheardown and Dr. Nicholas Kevlahan. Alijcia Mika for her insight on the MacPF membranes. I wish to thank Kathy Showkenik, Lynn Falkiner, Julie Birch, Justyna Derkach, Gordon Slater, and Paul Gatt for their invaluable help.

I wish to extend my gratitude to the Science and Technology National Council (**CONACYT**) of Mexico and **McMaster University** for their financial support.

I wish to thank **JED** (Jesus, Ken, Ed) for countless hours of ruthless insults. **Ella**, thank-you for listening, spilling, and threatening. The old and new graduate crowd: Meghan, Tracy, Manish, Jose, Jason, Carl, Adam, JF, Brandi and Sal. My crazy friends: Barb, Becs, Iris, Kevin, Trevor, Tree, Mo, and Kim. Thanks to the Pulse crew: Kelly and Sandy. A million thanks to Sabrina, Andrea D., Lee and Diane for those special moments!

I wish to thank the **undergraduate students** that performed most of the experiments during the course of this project: Jane Challen, Dave Latulippe, Laura Allsop, Andrea Podrebarac, and Allanna Chisholm. I am infinitely grateful... I cannot overstate this!

Table of Contents

List of Figures

List of Tables

Chapter I

Introduction

1.1 Membranes - Background

A membrane is a semi-permeable barrier, which separates mixtures by controlling the rate of transport of the particular components of the mixture. Membrane processes have been an emerging technology for the past 25-30 years. These processes present practical advantages over other separation processes (Mulder, 1996), such as,

- Energy savings since no phase changes required.
- No chemical reactions required and therefore no chemical alteration.
- The ability to separate temperature sensitive solutions since the separation can be carried out at ambient temperature.
- Membrane physical and physicochemical properties are variable and can be adjusted.

Membrane processes can be classified according to the main driving force: pressure (reverse osmosis, nanofiltration, ultrafiltration, microfiltration), concentration (dialysis), temperature (membrane distillation) and electrical potential (electrodialysis). This dissertation focuses on the performance of pressure-driven membrane processes, specifically nanofiltration.

1.2 Membrane Structures

Synthetic membranes can be categorized by their morphology into symmetric and asymmetric membranes (Fig. 1.1). Symmetric membranes are typically made of a single polymer or a polymer blend. Asymmetric membranes are composed of several layers of different polymers or of layers of a single polymer, but with different characteristics. These membranes can be fabricated with a homogeneous (dense) or a heterogeneous (porous) structure.

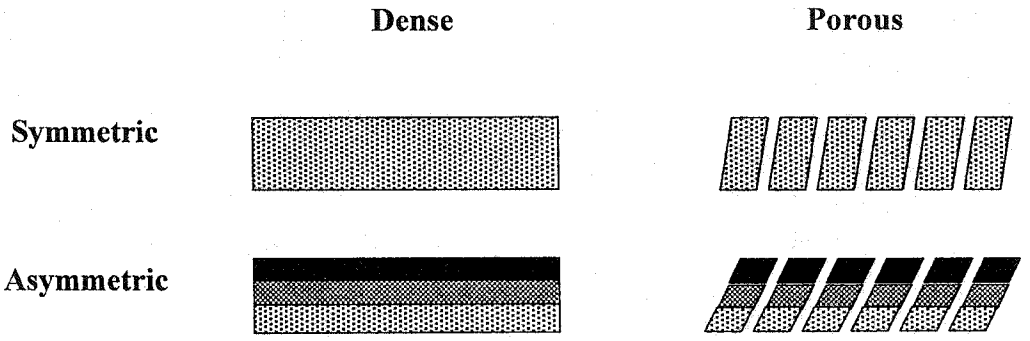

Figure 1.1 Schematic representation of the structure of a membrane.

1.3 Operating Modes

Membrane processes are commonly operated in two modes: dead-end filtration and cross-flow filtration (see section 2.2 for measures of performance). In dead-end filtration, all the feed is forced to flow perpendicular to the membrane (Fig 1.2a). Therefore, the rejected solute accumulates at the surface of the membrane creating a cake layer. The thickness of this layer increases with time, and thus rejection and flux decrease. Cross-flow membrane filtration is the major

membrane configuration used in industry (Ho and Sirkar, 1992). The feed flows across the membrane and only a portion of it permeates through the membrane (Fig 1.2b). Therefore, fouling is less severe compared to dead-end filtration. Concentration is a function of position in the module. However, flux and rejection decline can be minimized by proper selection of the module configuration and cross-flow velocities.

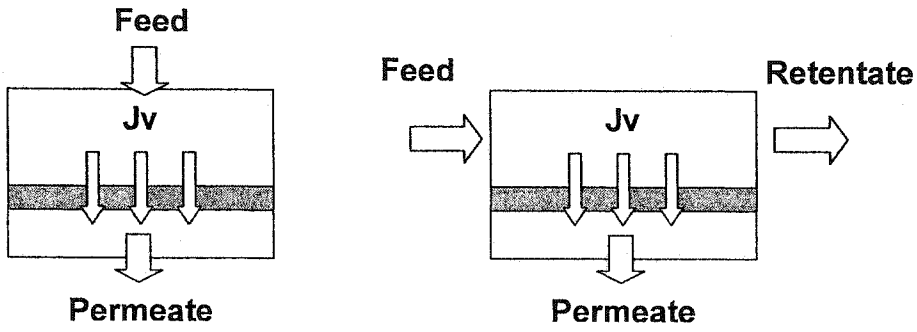

Figure 1.2 Schematic representation of two operating modes (a) dead-end and (b) cross-flow filtration.

1.4 Membrane Modules

Industrial membranes can be arranged into various configurations: tubular, hollow-fiber, flat-sheet or spiral-wound. Due to their relative efficiency and economy, spiral-wound membrane elements are by far the most popular for cross-flow operation. Flat-sheet configurations are not commonly used for pressure-driven separation, except for experimental setups. Hollow fiber modules are predominantly used for hemodialysis and gas separations. Tubular modules are preferred in the food industry (high feed concentrations).

1.4.1 Spiral-Wound Module

These modules can be thought of as a plate-and-frame device that has been rolled up into a cylinder (Fig. 1.3). The spiral design allows for a large membrane surface area and adequate fluid dynamics to produce a high permeate flow. Advantages: inexpensive, wide pressure range, several modules can be operated in series. Disadvantages: pre-treatment required, difficult to clean.

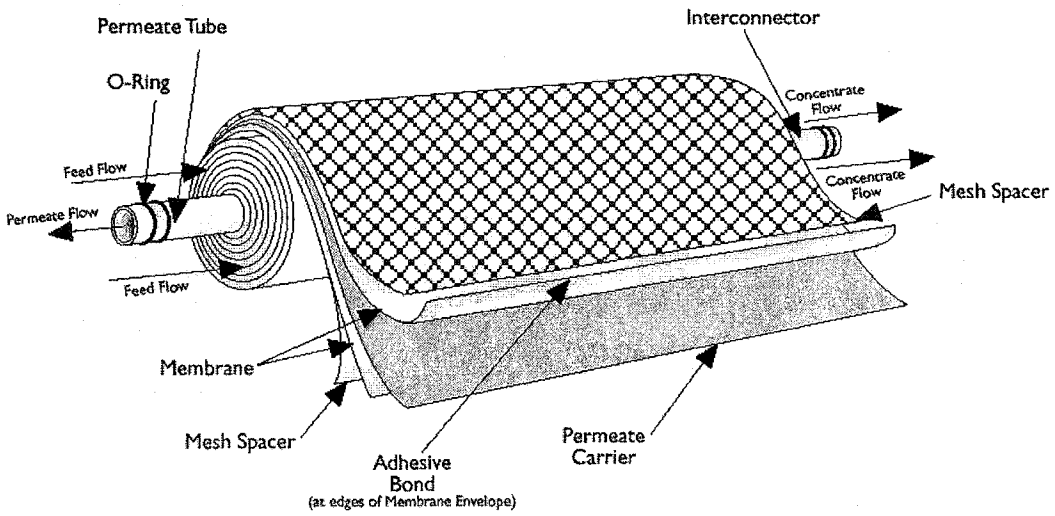

Figure 1.3 Spiral-wound module (Pure Water Handbook, Osmonics)

1.4.2 Hollow Fiber Module

Hollow fiber elements (Fig. 1.4) consist of hollow fibers each roughly the size of a human hair. Thousands of fibers are closely bundled in each housing. The pressurized feed flows slowly over the outside of the fibers and pure water permeates to the center. Then the permeate stream is collected out of perforated tube sheet. Advantages: high membrane area to volume ratio, high flow rates.

Disadvantages: the amount of pre-filtration required to keep the tightly-packed membrane surface free of severe fouling due to the laminar flow in the element.

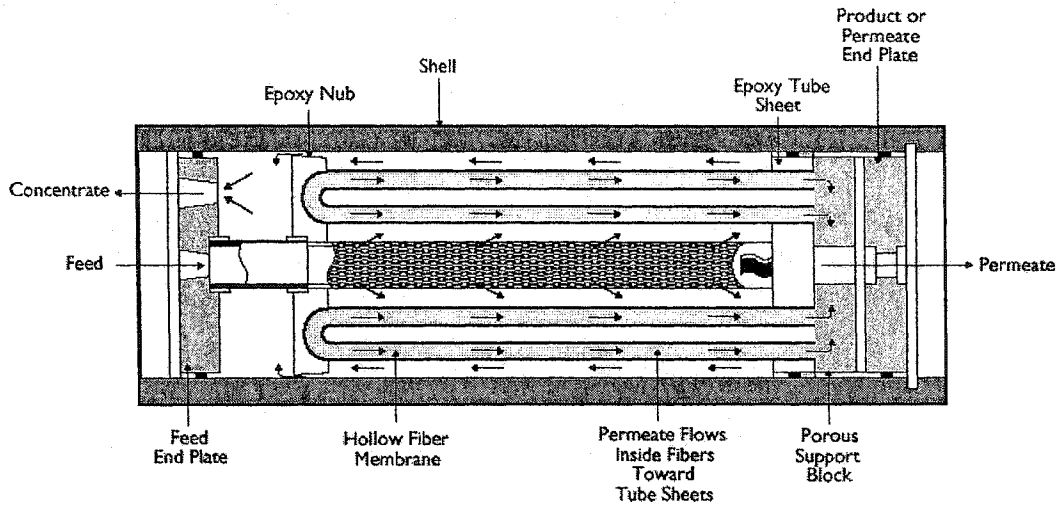

Figure 1.4 Hollow fiber module (Pure Water Handbook, Osmonics)

1.4.3 Tubular Module

The membrane is positioned on the inner circumference of the tubular casing (Fig. 1.5). Advantages: handles high concentrations, resistance to fouling, the module is cleaned easily, minimal pre-treatment required. Disadvantages: High capital and energy costs. Low membrane area to volume ratio.

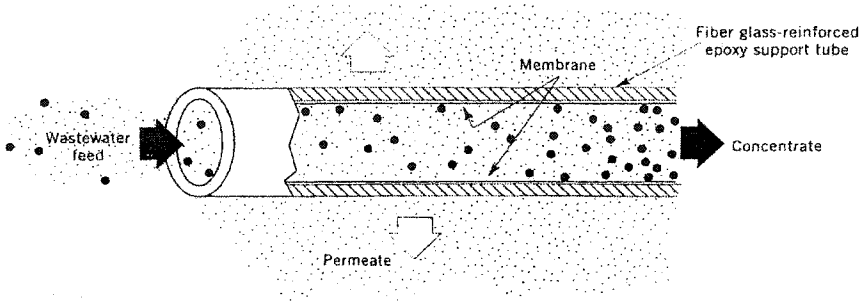

Figure 1.5 Tubular membrane module (Appelgate, 1984)

1.5 Pressure-driven Membrane Processes

Three of the most important pressure-driven membrane processes are reverse osmosis (RO), nanofiltration (NF) and ultrafiltration (UF). Microfiltration (MF) is not discussed in this dissertation.

Reverse osmosis was the first pressure-driven membrane separation process to be widely commercialized. Reverse osmosis removes most organic compounds and up to 99% of all ions, viruses and bacteria. Operating pressures are typically in the range of 1.4 to 10 MPa (see Table 1.1).

Ultrafiltration membranes reject solutes of large molecular weight, such as, larger organics, colloids, bacteria and pyrogens, while allowing most ions and small organics (sucrose, lactose) to permeate through the membrane. Operating pressures are typically in the range of 20 to 100 kPa.

Nanofiltration membranes remove substances in the 250 to 1000 molecular weight range at lower pressures (0.1-1.4 MPa). However, multi-ionic solutions can be fractionated according to the valence and concentration of the ions in solution.

Table 1.1 Typical pressure and selectivity ranges for reverse osmosis, nanofiltration, and ultrafiltration (Ho and Sirkar, 1992; Rautenbach et al., 1996).

Type of Membrane	Pressure (kPa)	MW cut-off (g/mol)
Reverse Osmosis (RO)	1,400 – 10,500	< 200 - 500
Nanofiltration (NF)	100 – 1,400	200 – 1,000
Ultrafiltration (UF)	20 – 100	1,000 – 100,000

Reverse osmosis is primarily used for applications in which demineralization is required. Generally the solvent permeates through the membrane and most of the solutes are concentrated in the retentate. Ultrafiltration is used primarily for fractionation. Large molecules, such as, proteins and colloids are rejected by the membrane. The solvent and smaller solutes permeate through the membrane.

1.6 Nanofiltration

Most NF membranes are typically charged and have intermediate pore sizes between RO and UF. These characteristics make NF optimal for the fractionation of solutes of similar sizes and/or the simultaneous desalting and fractionation of solutions. For example, NF membranes can remove hardness (Mg^{++}, Ca^{++}) from well water, without removing monovalent salts.

Therefore, nanofiltration is of special interest in applications where fractionation of charged molecules or selective desalination is required. See section 1.6.3 for industrial applications.

1.6.1 Commercially-available Nanofiltration Membranes

Loeb and Sourirajan (1962) designed the first RO membrane (asymmetric cellulose acetate membrane) capable of producing significant permeate flux and separation. Later in the 1960's, the introduction of thin-film composite (TFC)

membranes allowed for higher permeate fluxes at lower operating pressures compared to earlier membranes, see for example, Ho and Sirkar (1992).

Subsequently, TFC membranes were developed with characteristics more similar to ultrafiltration and the first NF membranes were produced. In the 1970's, Israel Desalination Engineering introduced the first description, Hybrid Filtration, for a process between RO and UF with an intermediate rejection of sodium chloride and high rejection of organics (Eriksson, 1988). Later, the term nanofiltration was adopted for such processes.

Nanofiltration membranes are generally made from synthetic polymers, which can be fabricated as thin-film composites or as a single-polymer asymmetric membrane. The single-polymer membranes consist of a thin surface skin layer, which gradually changes to a porous layer. Thin-film composite membranes are characterized by a barrier coating, which determines flux and separation, and a support layer, which provides mechanical stability.

Mulder (1996) and Petersen (1993) review membrane preparation methods and materials for commercial membranes. A comparison of the performance and general characteristics of several commercial membranes is shown in Table 1.2.

The polymers used presently in commercially-available NF membranes include: polyamide, sulfonated polysulfone, sulfonated polyethersulfone, cellulose acetate, polyvinyl alcohol, alumina, polyphenylene oxide, carboxylated polysulfone, poly(piperazineamide) and polyethylenimine, among others (Ho and Sirkar, 1992; Petersen, 1993; Mulder, 1996).

Table 1.2 Properties and performance characteristics of some commercially-available nanofiltration membranes (adapted from Raman et al., 1994; additional data from Comstock, 1989; Wang et al., 1995b; Bowen and Mukhtar, 1996).

Company	Membrane	Active layer	Charge	$L_P \times 10^6$ $m^3/m^2/hr/kPa$	NaCl Conc., %	R, %	$MgSO_4$ Conc., %	R, %
DDS	HC50	PA	Neg.	20.8	0.25	60	N/A	N/A
Desalination Systems	Desal-5	SPS	Neg.	47.1	0.1	50	0.1	96
FilmTec	NF-40	PA	Neg.	25.0	0.2	45.0	0.2	97.0
	NF-70	PA	Neg.	72.0	0.2	70.0	0.2	98.0
	XP-20	N/A	N/A	50.0	0.2	25.0	0.2	75.0
	XP-45	N/A	N/A	30.7	0.2	75.0	0.2	98.0
Nitto-Denko	NTR-7250	PVA	Neg.	62.5	0.2	50.0	0.2	98.0
	NTR-7410	SPS	Neg.	500	0.5	10.0	0.5	9.0
	NTR-7450	SPES	Neg.	92.0	0.5	50.0	0.5	32.0
PCI	AFC-30	PA	Neg.	25	0.2	35	0.2	97
Toray	SC-L100	CA	Neutral	31.3	0.2	75.0	0.2	97.0
	UTC-20HF	PA	Neg.	94.7	0.2	66.0	0.2	99.0
	UTC-60	PA	Amphoteric	47.3	0.1	85.0	0.2	99.0

CA = cellulose acetate; PA = polyamide; PVA polyvinyl alcohol; SPS = sulfonated polysulfone; SPES = sulfonated polyethersulfone.

1.6.2 Characteristics and Performance of Commercial NF Membranes

A membrane suitable for nanofiltration must meet specific requirements in relation to process economics, e.g. selectivity for solvent over solute, high permeation rate per unit pressure gradient and good membrane durability. Most nanofiltration membranes are thin-film composite membranes of synthetic polymers with charged groups.

The charge on the membrane may result from the dissociation of a functional group in the membrane matrix and/or the adsorption of ions on the membrane. This charge is sufficiently large as to affect the electrical potential developed across the membrane, which significantly affects membrane performance. As a result, the selectivity of NF for ions of different valences is

significantly different. Typically, for negatively charged NF membranes, the rejection for chlorides is about 50%, but for sulfates is higher than 95%, as is shown in Table 1.3.

Table 1.3 Typical chloride and sulfate rejections of commercial reverse osmosis and nanofiltration membranes (adapted from Rautenbach et al., 1996).

Reverse Osmosis		**Nanofiltration**	
Membrane	**Rejection**	**Membrane**	**Rejection**
Chloride			
FilmTec FT30SW	99.1	FilmTec NF45	55
Desal 3S	99.2	Desal 5	50
Toray UTC80	99.4	Toray UTC60	60
Nitto NTR 759H	99.5	Nitto NTR7450	50
Sulfate			
FilmTec FT30SW	>99.8	FilmTec NF45	98.5
		Desal 5	96.4-98

When mixed solutes are present the competition between various permeating ions becomes large and is greatly influenced by Donnan exclusion (see section 2.6.2.1). Several authors have reported negative rejections of monovalent ions in the presence of divalent electrolytes (Jonsson, 1980; Tsuru et al., 1991b; Nielsen and Jonsson, 1994; Bowen and Mukhtar, 1996; Garcia-Aleman, 1998).

The rejection of charged membranes is determined in part by the partitioning of the solute into the membrane. Solute partitioning depends on

membrane (pore size, pore geometry, charge density, etc.) and solute (valence, solute radius, etc.) characteristics. The rate at which the solute is transported through the membrane depends primarily on three mechanisms: convection (pressure difference), diffusion (concentration gradient), and electromigration (potential difference). See sections 2.5 and 2.6 for more details.

1.6.3 Industrial Applications

Nanofiltration has advantages for fractionation of monovalent salts from organics. These separations cannot be carried out with reverse osmosis or ultrafiltration membranes, and, competing processes such as electrodialysis or ion exchange require additional treatment (van der Horst et al., 1995). NF has the unique advantage of simultaneously desalting and concentrating the organics in the same separation step (Eriksson, 1988).

Nanofiltration is mainly used in the following industrial applications: water purification and softening (Rautenbach et al., 1996), pulp and paper processing (Petersen, 1993), whey demineralization (dairy industry) (van der Horst et al., 1995), treatment of metal-containing waste waters from metal finishing industries, decolorization of textile dye house wastes (Linde and Jönsson, 1995), and concentration of organics dyes (Perry and Linder, 1989).

The following are specific examples of applications where nanofiltration have been used successfully:

1.6.3.1 Dairy Industry

Some of the most successful membrane applications are in the dairy industry. Whey is the watery part of milk that separates from the curds in the process of making cheese. Whey effluents are of great environmental concern and economical impact. Approximately 9-10 kg of milk are used to produce a kg of cheese, resulting in 6-9 kg of whey. Cheese whey contains approximately 6% solids and has a biological oxygen demand (BOD) of 30-40 g/L (Gillies, 1974).

Although whey consists of high-quality protein and lactose, the high ratio of lactose to protein and the low solids content make it unusable as is. A combination of membrane processes (UF, NF, RO) can be used to convert whey into protein powder, concentrated lactose, and reusable process water. Typically, whey is first treated with UF to concentrate the protein fraction, from which protein powder is then produced. The UF permeate, containing the lactose and salts, is then filtered by NF to concentrate the lactose. Finally, the NF permeate (salty water) can be demineralized by RO and recycled into the process.

1.6.3.2 Sugar Industry

NF and UF membranes are routinely used to concentrate sugar and clarify sugar streams in the sugar industry. NF typically is used where traditional heat concentration processes are undesirable or inefficient. NF membranes separate sugars of a specific molecular weight and remove 40-50 percent of the water, concentrating raw sugar juice (Pure Water Handbook, Osmonics).

1.7 McMaster Pore-filled Membranes

The McMaster pore-filled (MacPF) membranes are a new class of polyelectrolyte-filled NF membranes. These membranes are prepared by co-polymerizing a polyelectrolyte gel into a microporous substrate (details are found in Section 5.2.1). In commercial TFC membranes the active layer is relatively thin (<1 μm) and is incorporated on top of a UF substrate membrane (Fig. 1.6). On the other hand, the active layer of the MacPF membranes is larger than 100 μm since the polyelectrolyte gel fills completely the MF substrate pores.

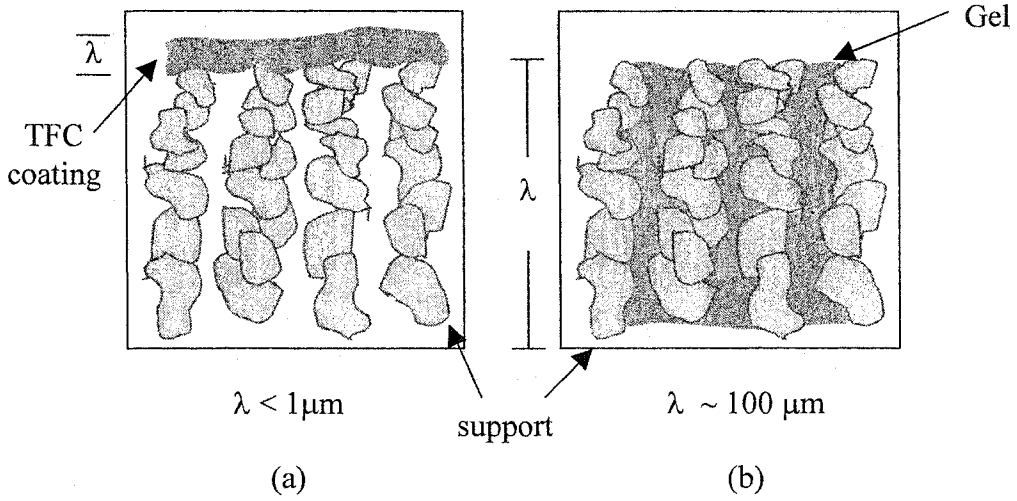

Figure 1.6 Schematic representation of a (a) typical commercial thin-film composite nanofiltration membrane, and a (b) MacPF membrane.

The pore-filling polyelectrolyte gives unique characteristics to the MacPF membrane, that increase the dependency of ion rejection on pressure and concentration compared to commercial membranes. Also these characteristics make these membranes a viable option for water softening and fractionation of mixed-solute solutions.

1.8 Objectives

The objective of this investigation is to develop a mechanistic model that describes the pressure-driven performance of the MacPF membranes, especially for mixed-electrolyte solutions. The intended research focuses in the following areas:

- Understanding and analysis of the pressure-driven performance of the MacPF membranes, from a practical (experiments) and theoretical (mathematical model) point of view.
- The collection of experimental data to analyze the behavior of the MacPF membranes, and to find potential research and industrial applications for these membranes. The experimental data consist of single-salt, mixed-electrolyte, and mixed-solutes experiments.
- Develop a mathematical model that describes the performance of the MacPF membranes when used with mixed-solute and mixed-electrolyte solutions.
- Develop a procedure that can be used to design MacPF membranes for specific applications from theory. This procedure involves two mechanistic models. The first model describes the conformation of the pore-filling gel in the MacPF membranes (Mika and Childs, 2001). The second model describes the pressure-driven transport of charged and uncharged solutes (this dissertation).

1.9 Theoretical Design of the McMaster Pore-filled Membranes

As mentioned above, the main objective of this dissertation is to develop a model that describes the pressure-driven performance of the MacPF membranes. However, this dissertation is part of a larger objective. This larger objective is the design of the MacPF membranes from theory using two mathematical models.

One important factor in membrane design is the relationship between the membrane fabrication procedure and membrane performance (flux and separation). The membrane fabrication procedure determines the morphology and physicochemical properties of the membrane, which in turn determine membrane parameters and performance.

However, there is not a reliable technique (model or measurement) that allows the *a priori* determination of membrane parameters, and thus performance, from the fabrication procedure (Fig. 1.7). Another challenge in membrane fabrication is the reproducibility of membrane parameters between samples of a same batch. A membrane fabrication procedure that addresses these two challenges, *a priori* determination of membrane parameters (section 4.3) and sample reproducibility (section 5.2.1), is presented in this dissertation. An overview of this procedure is outlined in section 1.9.2.

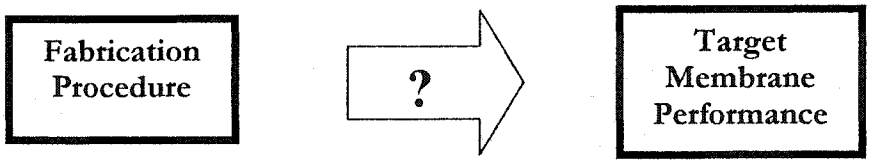

Figure 1.7 Schematic diagram of membrane design.

1.9.1 Traditional Approach to Membrane Design

Traditionally, a trial and error procedure is used to design a membrane for a specific application. Each iteration consists of two steps: membrane fabrication and membrane testing (Fig. 1.8). In the first step, a membrane sample is prepared. In the second step membrane performance is examined and interpreted using experimental data and a mathematical model. Once the model parameters are obtained, the actual and target membrane performances are compared each other. Usually these performances differ significantly from each other. Therefore, a new membrane sample with different characteristics has to be prepared and tested. These two steps are repeated until the desired membrane parameters and the target membrane performance are achieved.

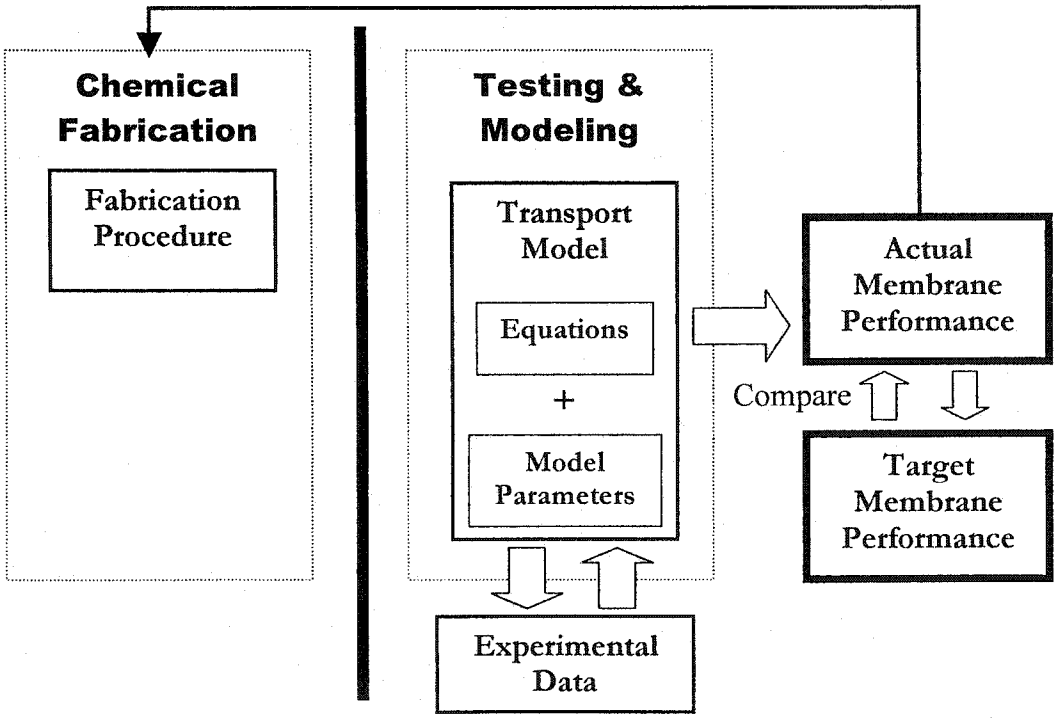

Figure 1.8 Schematic diagram of the traditional method of membrane design.

This procedure is time consuming. Membrane design takes months using the traditional method. Extensive sets of experimental data are required.

1.9.2 Proposed Approach to Membrane Design

One of the goals of this dissertation is to reduce the number of iterations involved in membrane design. In theory, mechanistic models can be used to predict the membrane parameters and performance; hence, reducing the number of iterations to one (Fig. 1.9).

In the proposed approach to membrane design, a mechanistic model is used to predict the morphology and physicochemical properties of the membrane (membrane parameters). The key structural element in this project is the polyelectrolyte gel. The fabrication procedure of the MacPF membrane has been refined such that, in theory, the membrane parameters (charge density, effective thickness, pore radius, permeability) can be estimated *a priori* using polyelectrolyte theory (Mika et al., 1999; Mika and Childs, 2001).

A transport model and the predicted membrane parameters can then be used to predict membrane performance (flux and separation). Hence, an iterative procedure is not required in the design of the MacPF membranes.

The advantages of this approach over the traditional approach are the following: ideally, only one iteration is required; no experimental data are required; and, the design of an optimum membrane for a specific application can be achieved in considerably less time.

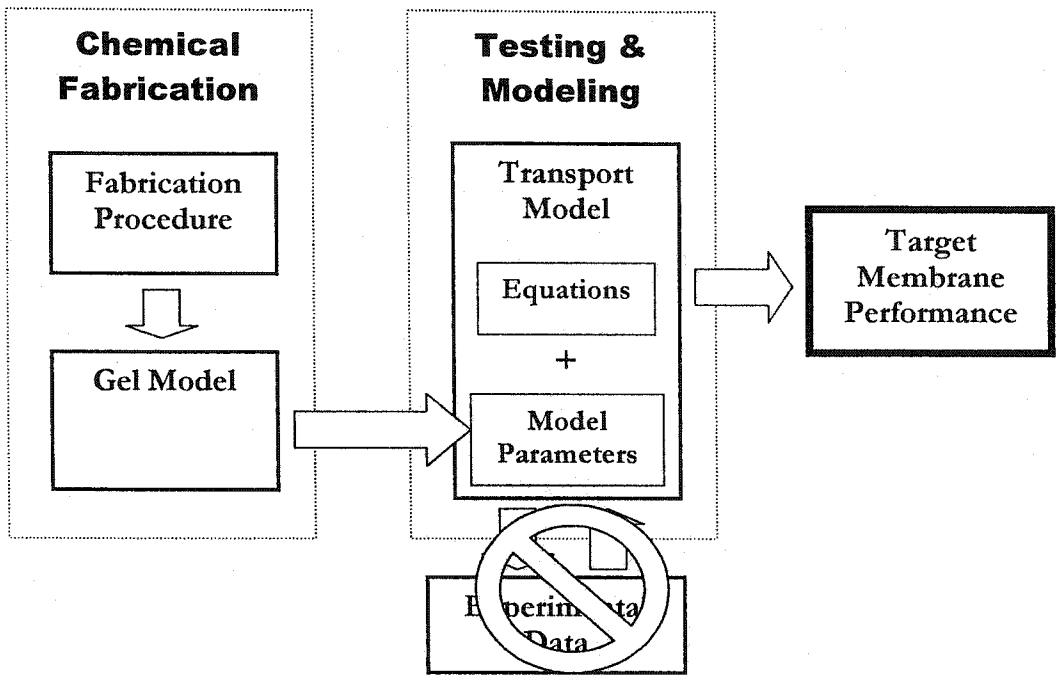

Figure 1.9 Schematic diagram of the proposed method of membrane design.

The ultimate application of this concept (model-based tailor-making) is the design of a membrane using the two mathematical models and experimental data from an intended application. The concept is depicted in Fig. 1.10 and explained here. The desired performance from a process (pressure, flux and rejection) is entered into the transport model. The transport model then estimates the membrane parameters required to achieve the desired performance. So far we have information about the structure of the membranes. However, there is no indication on how to manufacture the membrane to obtain such structure. The gel model is used to relate the structure of the membrane to the fabrication procedure. Once the membrane parameters (transport model) are known, the gel model

estimates the type (Flory-Higgins interaction parameter) and formulation (i.e., volume fraction, degree of cross-linking, degree of quaternization, etc.) of the polyelectrolyte required to obtain that membrane structure.

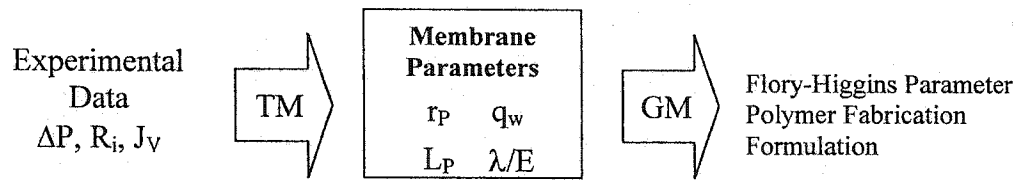

Figure 1.10 Schematic diagram of the model-based membrane design.

1.9.3 Contribution to the Field of Membrane Science

The main contributions of the intended research to the field of membrane science are the following:

- The membrane-design procedure and mathematical models outlined in here are the first attempt to design a membrane completely from theory. Such a goal has not been achieved before due to inadequate models to characterize the separation layer of the membrane, the lack of control on membrane formation parameters, and the reproducibility of membrane fabrication procedures. The membrane design procedure is successfully outlined in this dissertation. However, at this point, the design procedure is not fully implemented, as described in section 7.4.
- The transport model presented here is the first successful model to describe transport through the MacPF membranes.
- The model for gel structure is the first attempt to combine and modify

existing polyelectrolyte theory to model a pore-filled membrane.

1.10 Thesis Outline

This thesis contains seven chapters. Chapter II provides the basic background on membrane theory. This review includes information on mass transfer resistance in membrane applications, transport mechanisms, and selectivity mechanisms in NF membranes.

Chapter III reviews relevant transport models found in the literature. Models based on black-box approaches and mechanistic models are reviewed. Chapter IV is concerned with model development, including theory, derivations, underlying assumption and limitations. This chapter includes the derivation of the mechanistic model for solute transport and the model for gel conformation.

Chapter V details the experimental procedure, including the NF apparatus, a detailed experimental design and conditions, sample analysis, and general safety considerations. A detailed description of the McMaster pore-filled membranes is included. In Chapter VI the results are presented and discussed in terms of the analysis of the experimental data, the transport model solution, and the numerical techniques used to calculate membrane performance and estimate the parameters.

Finally, in Chapter VII the pertinent conclusions from the analysis performed in the preceding chapters are presented. Recommendations are made for future work in the field.

Chapter II

Membrane Theory

This chapter presents the general theory behind nanofiltration (NF) in the context of the membranes and solutions used in this investigation. A description of the transport and selectivity mechanisms in the membrane are provided. This discussion focuses only on the factors and mechanisms that are important to the membrane-solution systems used in this dissertation. More detailed information, on other aspects of NF membranes not covered in this chapter, can be found in Mulder, 1996. Transport models are reviewed on Chapter III.

2.1 Osmotic Pressure (Osmosis and Reverse Osmosis)

When a salt solution and solvent (water) are separated by a semi-permeable membrane (impermeable to salt), water migrates across the membrane from the pure water compartment to the salt solution compartment. Water flow is driven by a gradient in the chemical potential across the membrane. Thus, the chemical potential of the pure solvent is higher than that of the solution. This process is called osmosis.

If the solutions are allowed to come to equilibrium, then the resulting pressure difference is the osmotic pressure (Figure 2.1). If pressure is applied to the salt solution, then water flows in the opposite direction, which is called reverse osmosis. In order to have solvent flow across the membrane, the applied

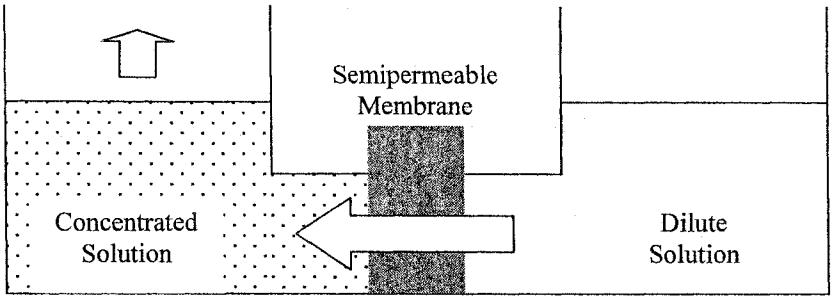

(a)

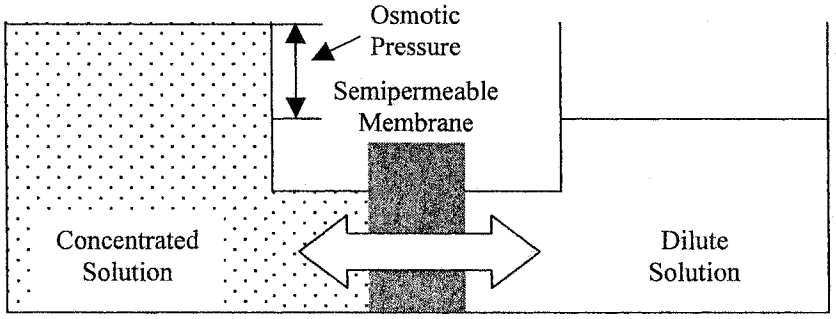

(b)

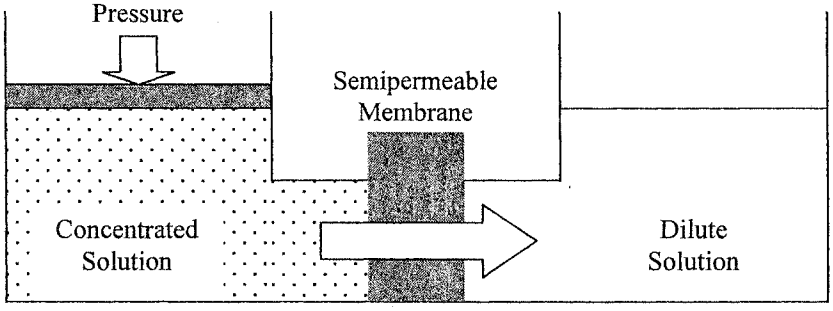

(c)

Figure 2.1 Osmotic phenomena (a) osmotic equilibrium, (b) osmotic flow, and (c) reverse osmosis (adapted from Applegate, 1984)

pressure must be higher than the osmotic pressure of the salt solution. NF membranes allow salt passage through the membrane, and so the osmotic pressure on both sides of the membrane must be considered.

2.2 Measures of Performance (Continuous Operation)

Typical measures of NF performance are separation (also known as rejection or retention) and solution flux (also known as volume flux or permeate flux).

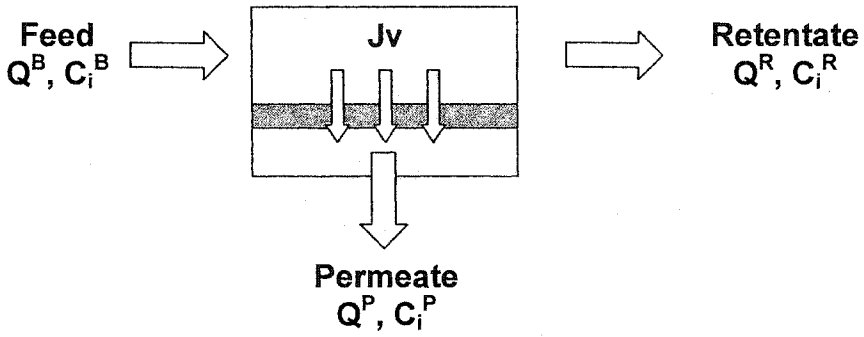

Figure 2.2 Schematic representation of a pressure-driven membrane separation process.

The observed rejection, for the i^{th} species, is defined as (Sourirajan, 1970):

$$R_i = \frac{m_i^B - m_i^P}{m_i^B} \tag{2.1}$$

where m_i^B is the feed molality, and m_i^P is the permeate molality. For dilute solutions molalities can be replaced by molar concentrations:

$$R_i = \frac{C_i^B - C_i^P}{C_i^B} \tag{2.2}$$

Considering the effects of concentration polarization (see section 2.3), the concentration just outside the membrane ($C_{i,m}^{B}$) is greater than the concentration in the bulk solution. The theoretical rejection is defined as:

$$R_i' = \frac{C_{i,m}^B - C_i^P}{C_{i,m}^B} \tag{2.3}$$

The solution flux, based on membrane area, is related to the applied pressure (ΔP) and osmotic pressure ($\Delta\pi$) (hence solute concentration) by the following relationship (Kedem and Katchalsky, 1958):

$$J_V = L_P(\Delta P - \sigma_i \Delta\pi) \tag{2.4}$$

were σ_i is the reflection coefficient (Staverman, 1951).

The recovery of the module, Q, is defined as the fraction of feed solution that permeates through the membrane.

$$Q = \frac{Q^P}{Q^B} = \frac{J_V Area}{Q^B} \tag{2.5}$$

The degree of fractionation of a membrane can be interpreted as the ratio of concentrations between a desired solute or ion and another one.

$$DF_i = \frac{C_i^P / C_i^B}{C_j^P / C_j^B} \tag{2.6}$$

2.3 Mass Transfer Resistances

There are several mass transfer resistances that may be accounted for in addition to those within the active membrane layer: concentration polarization at

the feed side, resistances associated with pore entrances and exits, and mass transfer resistance of the porous support. In this dissertation, it is assumed that the gel layer formation and fouling are negligible, and that the structure of the porous support does not interfere with solute or solvent transport. Also mass transfer resistances associated with pore entrances and exits are neglected since the pore length is much larger than the pore radius (Deen, 1987).

When a solution is transported through a membrane, the salt that is held back concentrates in a layer next to the membrane surface. This phenomenon of salt build-up at the boundary layer is called concentration polarization (Figure 2.3). Concentration polarization has a number of undesirable effects, often reducing both flux and rejection (Nakao, 1986; Mulder, 1996).

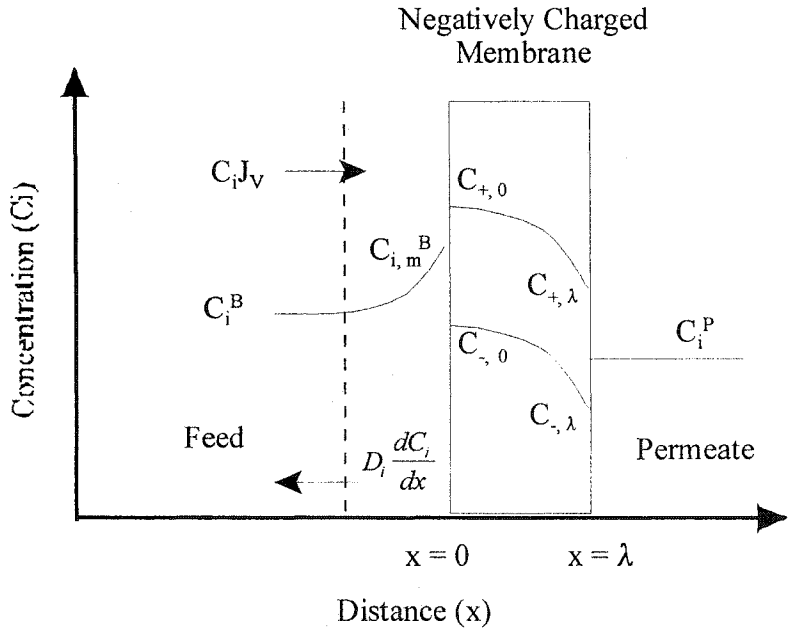

Figure 2.3 Ion permeation through a negatively charged membrane. Concentration polarization effects and counter- and co-ion partitioning into the membrane (adapted from Xu et al., 1997).

Since NF membranes transmit some of the salt present in the feed, the concentration of salt in the product increases with the concentration at the feed-membrane interface. Salt build-up at the interface increases the osmotic pressure of the solution at the interface, which in turn decreases effective pressure (driving force). Further, excessive concentration polarization may cause precipitation of dissolved components, which can foul or destroy sensitive membrane surfaces.

The extent of concentration polarization depends primarily on the competition between convection of salt towards the membrane and diffusion away from the membrane. Concentration polarization also depends of the fraction of salt rejected by the membrane and by mixing which includes: the presence or absence of cross-flow over the surface of the membrane, the kind of cross-flow (laminar or turbulent), the geometry of the permeation cell, and the number and identity of the dissolved components (Dresner and Johnson, 1980).

The concentration on the surface of the membrane (just outside the membrane) of the i^{th} species is related to the volumetric flux by the film theory model (Bird et al., 1960):

$$\left(\frac{C_{i,m}^{B} - C_{i}^{P}}{C_{i}^{B} - C_{i}^{P}}\right) = \exp\left(\frac{J_V}{k}\right) \tag{2.7}$$

where k is the mass transfer coefficient in the layer and can be described by a generalized mass transfer correlation, such as (Sourirajan, 1970):

$$Sh = \frac{kd}{D_i} = a\,\mathrm{Re}^{b}\,Sc^{c} \tag{2.8}$$

where Sh, Re, and Sc are the Sherwood, Reynolds and Schmidt numbers, respectively. The parameters a, b, and c have to be determined experimentally, as described by Nakao (1986) and Murthy and Gupta (1997).

2.4 Fundamental Mechanisms in Nanofiltration Membranes (Active Layer)

The transport and selectivity mechanisms of nanofiltration membranes are a result of gradients between the properties of the two phases separated by the membrane. This section details the relevant transport and selectivity mechanisms that are encountered inside the active layer of the nanofiltration membranes used in this dissertation. The membrane selectivity mechanisms are explained for neutral solutes, single electrolytes, and mixed salts.

2.5 Transport Mechanisms in Nanofiltration Membranes

The main driving forces for transport in membranes are pressure, concentration and electrical potential, which primarily influence the flux of solvent, solute, and electrical current, respectively (Dickson, 1985). However, the overall driving force is the chemical potential gradient, which normally consists of additive terms of these three main driving forces (Strathmann, 1985). Thus, a pressure differential may not result in a mass flux when it is counterbalanced by a concentration gradient (see osmotic equilibrium). Temperature, gravitational and magnetic forces are considered negligible in this investigation.

In addition to the primary effects, described above, the driving forces have a cross-influence on other fluxes (Table 2.1). For example, a concentration gradient across a membrane produces a mass flow, but can also produce a build-up of pressure (osmosis). A pressure gradient primarily affects the solvent flux, but can also produce a streaming current.

Table 2.1 Thermodynamic driving forces and fluxes in NF membranes. Adapted from Cussler (1984) and Mason and Lonsdale (1990).

Driving force / **Flux**	**Pressure gradient**	**Concentration gradient**	**Electrical potential**
Solvent	Darcy permeability	Osmosis	Electro-osmosis
Solute	Ultrafiltration	Diffusion	Electrophoresis
Current	Streaming current	Membrane potential	Electrical current

A pressure gradient inside the membrane leads to a viscous flow. The effective pressure gradient is composed of two parts: the hydrostatic pressure difference between the feed and permeate solutions; and, the osmotic pressure (cross-influence) caused by the concentration difference between the feed and permeate solutions.

A concentration gradient in the membrane results in a diffusive flux. The rate of transport is controlled by the diffusivity and concentration of each species inside the membrane.

The electrical potential gradient influences the permeability of charged solutes inside the membrane. The rate of transport is controlled by the mobility of each species, which in turn, depends on the valence, size, and diffusivity of each ion and the charge density of the membrane.

Although the overall flux through the membrane is directly related to driving forces, the transport of any chemical species also depends on the physical and physicochemical nature of the permeating species and the membrane. Some of these characteristics include, but are not limited to (Chevalier, 1999):

- Membrane (pore size, porosity, pore size distribution, tortuosity, morphology of polymer matrix, charge density, sign of charge, affinity for solutes, etc.)
- Solute (size, volume, molecular weight, flexibility of macromolecular chains, valence, charge, affinity for membrane, solubility, etc.)
- Operating conditions (pressure, temperature, concentration, tangential velocity)

2.6 Rejection Mechanisms in Nanofiltration Membranes

The selectivity of a membrane results from the interaction of different forces of physical, chemical, and electrostatic origin. Chevalier (1999) discusses such forces in greater detail. This dissertation focuses only on the following mechanisms of rejection: physical (steric exclusion and frictional forces), chemical (adsorption), and electrostatic (coulombic forces). Other selectivity

mechanisms are considered negligible for the solution-membrane systems used here, or cannot be quantified accurately, as discussed later.

The selectivity (hence rejection) of charged membranes is determined, in part, by the solute partitioning into the membrane. Solute partitioning depends, among others, on steric effects and electrostatic repulsion. These factors are interrelated to the membrane and solute characteristics. For an ideal solution, the partition coefficient (K_i) can be defined as:

$$K_i = C_{i,p} / C_i \tag{2.9}$$

In this thesis, activity coefficients are assumed to be unity, see section 4.1.2, so that concentrations can be used in eq. 2.9. Therefore, the activities of these phases have no influence on the exclusion mechanism.

Ion partitioning may be influenced by a change of the dielectric constant of the solvent going from the solution to the membrane phase. It has often been discussed in the literature that the dielectric constant in narrow pores may be lower than in the bulk, but a quantitative description is not available (Bontha and Pintauro, 1994; Hagmeyer and Gimbel, 1998).

Basu and Sharma (1997) attempted to quantify the radial distribution of the dielectric constant of water in nanopores at neutral pH in the presence of aqueous salts. The variations of the dielectric constant were smaller than 10% at salt concentrations up to 50 mol/m^3, which are the concentrations used in the present dissertation. Given these findings, dielectric exclusion is not taken into account in this dissertation.

2.6.1 Neutral Solutes

Neutral solutes are rejected primarily by a sieving mechanism (steric exclusion) and frictional forces. The rejection of any given neutral organic molecule is a function of membrane pore size, size of the molecule, and the geometry of the molecule (i.e., length to diameter ratio). However, some organic molecules, such as alcohols and amines, can have strong polar interactions (hydrogen bond) with the membrane material, thus affecting solute rejection. Van der Bruggen et al. (1999) determined experimentally that molecular charge and polarity have no effect on the retention of polysaccharides (e.g., sucrose).

2.6.2 Charged Solutes

The rejection of ionic species by charged nanofiltration membranes is controlled primarily by steric/friction and electrostatic effects. Short-range interactions (van der Waal forces) are assumed to be negligible (see section 2.6) and ion-solvation or dielectric effects are not taken into account, as discussed earlier. Normally ions have low permeability inside the membrane. However, in charged membranes this permeability can be enhanced or diminished depending on the charge of the ions and the membrane.

The charge in nanofiltration membranes can be generated by the inherited charge of the polymer material in the membrane and/or by co-ion adsorption (Tsuru et al., 1991b; Garcia-Aleman, 1998). Bowen et al. (1997) determined that this adsorption is of a chemical nature and reversible. The main contribution of

co-ion adsorption to selectivity is an increase of the effective charge density of the membrane. However, it is unclear whether co-ion adsorption also affects selectivity by reducing the number of permeating ionic pairs through the membrane; and, by reducing the effective pore radius of the membrane.

2.6.2.1 Donnan Exclusion

The potential that arises at the interface of a charged membrane contributes to ion rejection by the membrane. This phenomenon was first described by Donnan (1924) and is discussed in more detail in subsequent sections. Mathematically, Donnan equilibrium is typically described by two models: the Donnan exclusion model (eq. 2.10) or the Poisson Boltzmann equation (PBE) (section 4.1.7.1).

Donnan exclusion model is important when the Debye length is greater than the pore radius. The PBE is valid for any physically significant ratio of the Debye length to pore radius. In the absence of steric effects, the partition coefficient (eq. 2.9) can be related to the Donnan potential ($\Delta\Psi_D$) by,

$$K_i\left(\frac{\gamma_{i,p}}{\gamma_i}\right) = \exp\left(-\frac{z_i F}{RT}\Delta\Psi_D\right) \tag{2.10}$$

where γ_i, z_i, R, T, and F are the activity coefficient of the ion in solution, the valence of the ion, the universal gas constant, temperature, and Faraday's constant, respectively.

2.6.2.2 Membrane Selectivity for Single-electrolyte Solutions

Consider the case of a NaCl solution and a negatively charged membrane. An excess of Na^+ ions must be present in the membrane compared to the bulk solution concentration to compensate for the membrane charge. But as Cl^- ions exist in the bulk solution that means that a small amount of these ions must be present in the membrane. The condition of electroneutrality demands the same amount of Na^+ ions to enter the membrane. This small amount of Na^+ and Cl^- ions determine the membrane rejection because only these ions are able to leave membrane pores. Ion partitioning decreases with increasing membrane fixed charge and, hence, rejection increases (Garcia-Aleman, 1998).

The rejection of sodium chloride decreases with increasing feed concentration. More cations are available to shield the negative charges on the membrane as the feed concentration of salt increases, making it easier for the anions to pass through the membrane.

In NF membranes co-ion repulsion determines primarily the solute rejection of salt solutions. Rejection increases with increasing valence of the co-ion due to a higher repulsion by the membrane (e.g., the rejection of sulfate ions is considerably higher than the rejection of chloride ions in negatively charged membranes). The counter-ions are rejected to the same extent as the co-ions due to the requirement of electroneutrality.

However, the degree of rejection can decrease with increasing valence of the counter-ion, especially in the presence of a monovalent co-ion (Tsuru et al.,

1991b). This results in a lower rejection of $MgCl_2$ than of NaCl in negatively charged membranes. However, the valence of the co-ion has a larger effect on rejection than the valence of the counter-ion.

2.6.2.3 Membrane Selectivity for Mixed-electrolyte Solutions

The same factors that affect membrane selectivity for single-electrolyte solutions affect multi-ionic systems. Additionally, selectivity of one ion is affected by the presence of the other ions in the system, which makes the mechanism of rejection more complex. For example, in a solution with two salts having a common ion, the partition coefficient of the common ion is smaller than the partition coefficient of the more permeable ion (Jonsson, 1980). The partition coefficient of the corresponding counter-ion or co-ion is being increased by the presence of the less permeable salt (Garcia-Aleman, 1998).

This effect is relevant for nanofiltration of multi-component systems. The salt uptake and thus the salt permeability of a membrane may be increased by adding a highly rejected electrolyte with an ion in common with that salt of which the permeability should become enhanced (Levenstein et al., 1996).

In a mixed-salt solution of NaCl and Na_2SO_4, the concentration of sulfate influences the rejection of chloride (negatively charged membrane). When Na_2SO_4 is added to a solution of constant NaCl concentration, the rejection of Cl^- decreases as the concentration of Na_2SO_4 increases. The Na^+ ions, which readily pass through the membrane, must be accompanied by an anion in order to

maintain electroneutrality. The negatively charged ions are, however repelled by the negatively charged membrane. The Cl^- ions with the lower potential are forced to permeate preferentially compared with the $SO_4^=$ ions, and even a negative rejection of Cl^- has been observed (Linde and Jönsson, 1995).

Fractionation, the difference between chloride and sulfate rejection, increases with increasing sulfate feed concentration and increasing charge density. However, fractionation is more sensitive to an increase on sulfate feed concentration than on charge density (Garcia-Aleman, 1998).

2.7 Summary

The basic theory for pressure-driven separation with nanofiltration membrane has been reviewed. Useful measures of membrane performance have been presented. The three main transport mechanisms (convection, diffusion, electromigration) and their driving forces have been discussed. The mechanism for solute rejection has been explained for charged and uncharged species.

Chapter III

Literature Review

This chapter reviews the relevant mathematical models for nanofiltration (NF) membranes. Mechanistic and non-mechanistic models used to describe NF are discussed. Models for reverse osmosis (RO) membranes are briefly discussed.

Literature models for membranes are based either on irreversible thermodynamics (IT) or on some transport mechanism. The models based on IT treat the membrane as a black box ignoring the structure of the membrane or any transport mechanism. The mechanistic models assume a membrane structure and also relate fluxes to the driving forces. The model equations account for the effects of physical and chemical characteristics of both the membrane and the permeating solution.

3.1 Models for Pressure-Driven Separations

This section briefly reviews mathematical models that describe transport for pressure-driven separations, particularly for reverse osmosis. Such models are of historical importance; and, in some cases, have been adapted to nanofiltration membranes. However, these models have limited applicability to the membranes used in this investigation. A more detailed description of these models is provided elsewhere (Dickson, 1988; Mason and Lonsdale, 1990).

3.1.1 Models Based on Irreversible Thermodynamics

In irreversible thermodynamics (IT), it is assumed that the system can be divided into small subsystems in which local equilibrium occurs. For a sufficiently slow process, the relationships between the fluxes (J_i) and forces (X_j) are linear (phenomenological equations), as suggested by Onsager (1931).

$$J_i = \sum_j L_{i,j} X_j \tag{3.1}$$

Equation (3.1) states that in a system with 'n' simultaneous flows, any flow (J_i) depends in direct and linear manner not only on its conjugated force, but also on the non-conjugated forces in the proportion stated by (L_{ij}). This is a mathematical representation of the fluxes and forces presented in Table 2.1. Onsager (1931) also postulated that the transpose of each coefficient has the same value as that coefficient, therefore,

$$L_{i,j} = L_{j,i} \quad (i \neq j) \tag{3.2}$$

Kedem and Katchalsky (1958) derived the first model based on IT for a membrane. The authors developed linear equations for the solvent and solute fluxes. Consequently, the model was limited to systems where the pressure and concentration differences were small. Later, Spiegler and Kedem (1966) reformulated a similar set of equations in differential form to correct for the limitations found in the Kedem-Katchalsky (KK) model.

The Spiegler-Kedem (SK) model accounts for the variability of the concentration profile at large fluxes and high concentration gradients. This model

corrects the calculation of the average concentration inside the membrane. Thus, there is a milder dependency of the parameters (solvent permeability, solute permeability, reflection coefficient) on pressure and concentration in the Spiegler-Kedem model compared to the Kedem-Katchalsky model.

Perry and Linder (1989) extended the Spiegler-Kedem model to account for the Donnan exclusion mechanism in charged NF membranes. Schirg and Widmer (1992) used a power law to correlate the effect of feed concentration on salt permeability. The contribution of the solvent to solute flux was not included in these models.

These models are simple to solve and have only three fitting parameters (reflection coefficient, solute permeability, and solvent permeability). As always for IT, these models provide no insight on the transport mechanism or the structure of the membrane.

3.1.2 Nonporous Mechanistic Transport Models

This section summarizes the mathematical models that assume that the membrane is nonporous and that transport occurs through the dense membrane material. The first model to be developed in this area was the Solution Diffusion (SD) model (Lonsdale et al., 1965; Merten, 1966). The model assumes that the solvent and solute dissolve into the membrane, are transported through the membrane by diffusion, and then desorb into the permeate solution. The postulate is that the transport of solvent and of solute occur by non-interacting mechanisms,

and this is likely not correct. The osmotic pressure term on the solvent equation clearly accounts for the effect of the solute on solvent transport.

Sherwood et al. (1967) incorporated the concept of porosity or imperfections in the membrane. This model is the first compromise between nonporous and porous transport models and is known as the Solution Diffusion Imperfection (SDI) model. Transport occurs through a solution diffusion mechanism and leakage (bulk flow) through imperfections in the membrane material. As in the Solution Diffusion model, the Solution Diffusion Imperfection model postulates that solvent and solute transport occur independently in the nonporous regions.

3.1.3 Porous Mechanistic Transport Models

This section summarizes the mathematical models that assume that the membrane is composed of a bundle of straight capillaries (pores). Models for neutral and charged membranes are discussed.

3.1.3.1 Kimura-Sourirajan Analysis (KSA)

The Kimura-Sourirajan Analysis (KSA) is based on the preferential sorption-capillary flow mechanism (Sourirajan, 1963). This model assumes that water is preferentially sorbed by the membrane and forced to flow through the membrane pores by pressure. Solute flux and separation are determined by diffusion, convection and by physicochemical interactions. This model is

mathematically identical to the Solution Diffusion model. However, these models are based on different assumptions and, thus, the model parameters have a different physical interpretation.

3.1.3.2 Finely Porous (FP) Model

The Finely Porous (FP) model was developed by Merten (1966) and is based on the original frictional model proposed by Spiegler (1958) and later modified by Kedem and Katchalsky (1961). These models are based on a balance of applied and frictional forces. At steady state, the thermodynamic driving forces (chemical potential) for the solute and the solvent are counterbalanced by mechanical frictional forces. These mechanical forces are expressed as interactions among solute, solvent and the membrane. Details are found elsewhere (Jonsson and Boesen, 1975); Soltanieh and Gill, 1981). The model was further modified by Mehdizadeh and Dickson (1989b) to correct mistakes in the original formulation (Modified Finely Porous model).

3.1.3.3 Surface Force-Pore Flow (SF-PF) Model

Sourirajan and co-workers (Matsuura and Sourirajan, 1981; Matsuura et al., 1981) developed the Surface Force-Pore Flow (SF-PF) model using, in part, ideas from the Finely Porous model and the work of Anderson and Malone (1974). While the previously discussed models take a 1-dimensional approach (axial variations only), this model is 2-dimensional (variations in axial and radial

directions), which adds accuracy to the physical picture, but requires advanced numerical methods to solve the equations.

The model takes into account the effect of solute size, solute-membrane friction, and solute-membrane interaction (by a potential function). A balance of applied and frictional forces is made on the solute. The model was later modified (Modified Surface-Pore Flow model) by Mehdizadeh and Dickson (1989a; 1989b).

The models presented in this section cannot be directly applied to the nanofiltration membranes used in this investigation. However, models derived from these theories can be adapted to predict the pressure-driven performance of NF membranes. Such models are reviewed in the next section.

3.2 Mechanistic Models for Nanofiltration Membranes

Mechanistic models assume a membrane structure and the model equations account for the effects of physical and chemical characteristics of both the membrane and solution. Most mechanistic nanofiltration models use a form of the extended Nernst-Planck equation (ENPE). The models that describe the electrical properties of the membrane usually fall in two categories: models based on the Space-Charge (SC) model and models based on the Teorrell-Meyer-Sievers (TMS) model.

3.2.1 The Extended Nernst-Planck Equation

The origins of the Nernst-Planck equation can be traced back to the discussion of transport of dilute electrolytes across interfaces given by Nernst (1888) and by Planck (1890a; 1890b). Modern versions of this equation are reviewed elsewhere (Meares et al., 1972; Lightfoot, 1974; Buck, 1984).

The extended Nernst-Planck equation accounts for diffusion, convection and electromigration caused by gradients in concentration, pressure, and potential gradients. Most of the mathematical models discussed in the following sections use a version of the extended Nernst-Planck equation that was suggested by Schlögl (1966) and Dresner (1972) and later modified by Anderson and Quinn (1974).

$$J_i = \alpha_i C_{i,p} J_V - \frac{D_{i,\infty}}{b_i}\left(\frac{dC_{i,p}}{dx} - z_i C_{i,p}\frac{F}{RT}\frac{d\Psi}{dx}\right) \tag{3.3}$$

The parameters α_i and b_i account for steric hindrance and frictional forces that impede convective and diffusive transport, respectively. Other effects, such as adsorption or electrostatic effects, could affect solute transport; and, thus the interpretation of α_i and b_i (Dresner, 1972). However, most authors consider that α_i and b_i are based purely on mechanical forces (Nakao and Kimura, 1982; Deen, 1987) and other factors that restrict solute transport are accounted for elsewhere in their models.

3.2.2 Model Assumptions, Similarities and Differences

The relevant similarities and differences between the mathematical models presented in the following sections are summarized in this section. Minor assumptions and differences are not discussed. The models presented in section 3.2.5 are conceptually equivalent.

The models presented in the subsequent sections are based on the following common assumptions:

- The system is stationary and isothermal.
- The membrane is composed of straight cylindrical pores that are charged. The membrane tortuosity is taken into account. Pore entrance and exit effects are considered negligible.
- Transport occurs only through the pores of the membrane.
- The solutions at the interfaces are in equilibrium. Dilute solution theory applies. Activities can be replaced in terms of concentrations.
- Ionic flux can be described by the extended Nernst-Planck equation.
- The electroneutrality conditions inside the membrane and in the external solution are used. The condition of no-electric current is applied.
- Diffusion coefficients and friction parameters are independent of concentration at low concentrations.
- The membrane is described in terms of physically significant quantities, such as, pore radius, permeability, thickness, porosity, and charge density.

Some authors attempt to validate their mechanistic models by rearranging these models in terms of the parameters (reflection coefficient, solute permeability and transport number) proposed by irreversible thermodynamics.

The models presented in the subsequent sections differ in the following manner:

- The solution flux is described in different ways, varying from phenomenological approaches to the Navier-Stokes equation.
- One or more of the contributions to solute flux (diffusion, convection, and electromigration) are ignored in some approaches.
- The friction parameters, α_i and b_i, are handled in different ways, from being ignored to relationships based on the ratio of solute to pore radius.
- Different authors account for the dependency of the effective charge density of the membrane on feed concentration with different models (empirical, semi-empirical, and mechanistic models).
- The numerical challenge involved in solving the set of governing equations.

3.2.3 The Space Charge (SC) Model

Osterle and co-workers (Gross and Osterle, 1961; Oldham et al., 1963; Morrison and Osterle, 1965) developed the Space Charge model to explain electrokinetic phenomena in charged capillaries. The Space Charge model assumes that there is a radial distribution of the potential and concentration across

the pores (two dimensional approach). The ions are treated as point charges. Hence, steric effects are neglected.

The model is based on the Nernst-Planck equation for ion transport, the nonlinear Poisson-Boltzmann equation (PBE) for the radial distribution of electric potential and ion concentration, and the Navier-Stokes equation for volume flow. For a detailed derivation refer to Wang et al. (1995a).

Assuming that the axial contribution of the potential is small compared to the radial contribution (charge density), the PBE for a binary electrolyte can be written as,

$$\frac{1}{\bar{r}}\frac{d}{d\bar{r}}\left(\bar{r}\frac{dy(x,\bar{r})}{d\bar{r}}\right)=\frac{1}{2}\left(\frac{r_P}{\kappa}\right)^2(K_1-K_2) \tag{3.4}$$

The solution flux can be obtained from the Navier-Stokes equation in terms of the pressure difference, viscous forces and the electrical potential.

$$0=\frac{\partial P(x,r)}{\partial x}-\rho(x,r)\frac{\partial \Psi(x,r)}{\partial x}+\frac{\mu}{r}\frac{\partial}{\partial r}\left(r\frac{\partial u_x(r)}{\partial r}\right) \tag{3.5}$$

As proposed by Wang et al. (1995a), the membrane-solution system can be described with three parameters: the ratio of pore radius to Debye length (r_P/κ), the dimensionless membrane surface charge density (q_o), and the ratio of membrane thickness to porosity ($\Delta x/\varepsilon$). The first parameter (r_P/κ) takes into account the dependency of the transport parameters on feed concentration. The dimensionless surface charge density (q_w) is a function of the surface charge density and the pore radius (r_P).

It is common practice to define Space Charge-type models in terms of irreversible thermodynamics. The logic in this approach is that the membrane-solution system can be more effectively understood in terms of phenomenological coefficients. Therefore, for a charged membrane, three kinds of fluxes (J_i) and driving forces (X_i) can be related with phenomenological coefficients (L_{ij}) (Wang et al., 1995a), as in eq. 3.1, the terms become,

$$J_i = \begin{pmatrix} J_V \\ J_1 + J_2 \\ I \end{pmatrix} \qquad X_i = \begin{pmatrix} -dP/dx \\ -RTd\ln C/dx \\ -d\Psi/dx \end{pmatrix} \qquad L_{ij} = \begin{pmatrix} L_{11} & L_{12} & L_{13} \\ L_{21} & L_{22} & L_{23} \\ L_{31} & L_{32} & L_{33} \end{pmatrix} \quad (3.6)$$

These phenomenological coefficients ($L_{i,j}$) can be related to the parameters from irreversible thermodynamics (solute permeability, reflection coefficient, and transport number), as described, for instance, by Smit (1989).

The original formulation of the Space Charge model is mathematically complicated and computationally expensive (Neogi and Ruckenstein, 1981). Several attempts have been proposed to simplify the original formulation. Probstein and co-workers (Jacazio et al., 1972; Probstein et al., 1973) assumed that a parabolic velocity profile could be assumed inside the membrane pores. Thus, the Navier Stokes equation can be reduced to the Poiseuille equation. Smit and co-workers (Smit, 1989; Hijnen and Smit, 1995) proposed analytical solutions to the Poisson-Boltzmann equation under limiting conditions of the electrostatic potential of the membrane.

Wang et al. (1995a) adapted the Space Charge model to NF membranes for single electrolyte solutions and provided a more stable numerical solution.

Yaroshchuck and co-workers (Yaroshchuk and Vovkogon, 1994; Yaroshchuk et al., 1994) combined a phenomenological approach and the Space Charge model to specify the model parameters for ternary-electrolyte solutions (mixed electrolytes).

The main disadvantage of Space Charge-type models is that the numerical solution of these equations is computationally expensive, even with simplifying assumptions. This complexity increases as the number of permeating species increases. An additional disadvantage is the exclusion of steric and friction interactions in the derivation of these models. Such contributions are important in NF membranes, especially in commercial membranes. However, these interactions can be accounted for in a rigorous manner (Mehdizadeh, 1990; Basu and Sharma, 1997) or with averaged quantities (see section 3.2.4).

There is no clear understanding if the insight provided by the combination of Space Charge model and irreversible thermodynamics is superior or comparable to the insight provided by other mechanistic models (see later sections). However, this is a matter of debate that stems from the trade-off between providing an accurate physical picture and model simplicity.

3.2.4 Electrostatic and Steric-Hindrance (ES) Model

The Electrostatic and Steric-hindrance (ES) model was developed by Wang et al. (1997). The ES model is a simplification of the Space Charge model (Wang et al., 1995a) and an extension of the Steric-hindrance Pore (SHP) model

(Nakao and Kimura, 1982). The ES and Space Charge models use the nonlinear PBE to describe the radial distribution of the electrostatic potential and ionic species. Ionic fluxes are described by the extended Nernst-Planck equation. However, the ES model describes the solution flux using the Poiseuille equation (eq. 3.8). Steric-hindrance effects are accounted for by the SHP model. The ES model can be further simplified by using the Donnan Exclusion model (eq. 2.9) instead of the PBE.

The Steric-hindrance Pore model is a modification of the earlier adaptation by Haberman and Sayre (1958) to the pore model originally proposed by Ferry (1936). Convection is retarded according to eq. (3.7a) and diffusion is assumed to occur unhindered (eq. 3.7b). The rationale for this difference originates from the derivation of the model. The model was originally derived for ultrafiltration membranes, where diffusion is negligible compared to convection. This assumption is not valid for nanopores, even at high fluxes.

$$\alpha_i = 1 + (16/9)\eta_i^2 \tag{3.7a}$$

$$b_i = 1 \tag{3.7b}$$

The local solution flux (u_x), as a function of radial position and the average solution flux (J_V), is calculated from the Poiseuille equation:

$$u_x = 2J_V\left[1-\left(\frac{r}{r_P}\right)^2\right] \tag{3.8}$$

The Electrostatic and Steric-hindrance model characterizes the membrane-solution system with three parameters: the pore radius (r_P), the surface charge density (q_w), and the ratio of membrane thickness to porosity ($\Delta x/\varepsilon$)

The governing equations of the electrostatic and steric-hindrance (ES) model can be combined with the Spiegler-Kedem model to obtain the phenomenological parameters (solute permeability and reflection coefficient) in terms of the ES model parameters.

$$P_S = \frac{(\nu_1 + \nu_2) D_2 K_2 t_1}{\nu_2} \frac{\varepsilon}{\Delta x} \tag{3.9a}$$

$$\sigma_S = 1 - \alpha_2 K_2 - t_2 (\alpha_1 K_1 - \alpha_2 K_2) \tag{3.9b}$$

The model was experimentally verified using solutions containing a single organic salt (Wang et al., 1995c; Wang et al., 1997) under the assumption that the Donnan exclusion model was valid. The dependence of the effective charge density on electrolyte concentration was correlated using a Langmuir-type isotherm. The model was not tested with mixed-salt solutions.

3.2.5 Teorell-Meyers-Sievers (TMS) Model

The Teorell-Meyers-Sievers (TMS) model (Meyer and Sievers, 1936; Teorrell, 1953) is a less rigorous approach compared to the Space Charge model. A uniform radial distribution of fixed charges and mobile species is assumed. Bowen et al. (1997) corroborated that these assumptions are valid at low concentrations and in pores smaller than 2 nm. This assumption simplifies

mathematical analysis from 2- to 1- dimensional models. Mathematical models that described the membrane electrical properties using the TMS model are widely used to describe transport in nanofiltration membranes.

3.2.5.1 Frictional Model (FM)

Jonsson (1980) predicted negative rejection in reverse osmosis cellulose acetate membranes using the extended Nernst-Planck equation combined with a frictional and exclusion model. He assumed that the activity coefficients outside and inside the membranes were different and Donnan equilibrium applied through all the membrane thickness in heterogeneous structures (Helfferich, 1962). The model consists of 2n+1 parameters, where n is the number of mobile ions. These parameters are the ratio of activities ($K_{i,o}$) and the friction parameter (B_i) for an ion, i, and the ratio of effective membrane thickness to water content (λ/E). The parameter B_i accounts for friction and steric effects on both convective and diffusive transport for each ion.

In a further paper, Nielsen and Jonsson (1994) proposed an analytical solution to the same problem. Ion-pore friction interactions were neglected (unhindered diffusion), and the individual ion flux was defined as a fraction of the convective term. They developed a graphical method to calculate negative rejection of mixed-electrolyte solution in limiting cases. Thus, giving only a rough estimate of salt rejection.

The models proposed by Jonsson and co-workers (Jonsson, 1980; Nielsen and Jonsson, 1994) have an inherited value as qualitative tools. However, both models fail to describe accurately the following: ion-membrane interactions (friction/steric hindrance); and, the membrane in terms of structural parameters (pore radius, permeability, charge density).

3.2.5.2 Donnan-Steric-Pore (DSP) Model

The Donnan-Steric Pore (DSP) model was developed by Bowen and co-workers (Bowen et al., 1997). The model uses the extended Nernst-Planck equation to describe ion transport and the steric-Donnan equilibrium model to describe ion partitioning. Steric hindrance is taken into account explicitly in the equilibrium and transport equations. The solution flux is calculated from the Kedem-Katchalsky model and the Hagen-Poiseuille equation. The model has four structural parameters: the pure water permeability of the membrane (L_P), the pore radius (r_P), the ratio of effective membrane thickness over porosity ($\Delta x/\varepsilon$), and the effective charge density (C_X).

Kedem and Katchalsky (1958) proposed to calculate the solution flux as a function of the membrane permeability (L_P) and the effective pressure differential (ΔP-$\Delta\pi$) in the membrane. Assuming that the reflection coefficient is equal to unity, eq. (2.4) becomes (with σ_i assumed to be 1),

$$J_V = L_P(\Delta P - \Delta\pi) \tag{3.10}$$

For a cylindrical pore, where fully developed flow exists, the pure water permeability is described by the Hagen-Poiseuille equation.

$$L_P = \frac{r_P^2}{8\mu(\lambda / E)} \tag{3.11}$$

The authors proposed to describe ion partitioning by combining the classical Donnan equilibrium model (eq. 2.9) to account for electrostatic effects and the factor Φ_i to account for steric effects. Therefore, the Donnan-steric model is written as

$$K_i = \Phi_i \exp\left(-\frac{z_i F}{RT}\Delta\Psi_D\right) \tag{3.12}$$

where

$$\Phi_i = (1-\eta_i)^2 = (1-r_i/r_P)^2 \tag{3.13}$$

The factor Φ_i is the solution of the radially-averaged Boltzmann distribution for a spherical solute when the interactions between the solute and the pore wall are purely electrostatic (Deen, 1987).

The model assumes that convection (α_i) and diffusion (b_i) are hindered by the membrane. Bowen et al. (1997) developed two equations that relate the ratio of ion to pore radius (η) to the friction parameters. These equations are valid only when ($0 < \eta < 0.80$).

$$\alpha_i = \left[2-\Phi_i\right]\left(1+0.054\,\eta-0.988\,\eta^2+0.441\,\eta^3\right) \tag{3.14a}$$

$$b_i = \left(1-2.3\eta+1.154\,\eta^2+0.224\,\eta^3\right)^{-1} \tag{3.14b}$$

These two relationships were adapted from earlier work by Bowen and co-workers (Bowen and Sharif, 1994; Bowen and Mukhtar, 1996). The existence of cylindrical pores is directly assumed. Only steric and hydrodynamic interactions between the solute and pore wall were considered. Other forces, such as, electrostatic forces are not considered (Deen, 1987).

The model assumes that the effective charge density accounts for activities inside the membrane and non-idealities caused by solute-solute and solute-membrane interactions. The dependence of the effective charge density on the feed concentration was correlated with a Freundlich-type isotherm. The model parameters were obtained by fitting the model to data from permeation experiments of uncharged solutes and single salts.

3.2.5.3 Steric, Chemical and Electrical Retention (SCER) Model

This model was developed by Chevalier (1999) to describe the transport of neutral and charged species through commercial NF membranes. This model is equivalent to the Donnan-Steric Pore model. The extended Nernst-Planck equation describes ionic transport and the Donnan equilibrium model describes the membrane-solution interface. Ion partitioning is considered to be purely electrostatic (no steric effects). The solution flux is calculated from the Kedem-Katchalsky model and the Hagen-Poiseuille equation.

The hindrance factors (α_i, b_i) in the extended Nernst-Planck equation are derived from the work of Haberman and Sayre (1958). These equations are valid only when ($0 < \eta < 0.80$).

$$\alpha_i = \left[2\Phi_i - \Phi_i^2\right]\left(\frac{1 - 2/3\eta^2 - 0.20217\eta^5}{1 - 0.75857\eta^5}\right) \tag{3.15a}$$

$$b_i = \left[\Phi_i\right]\left(\frac{1 - 2..105\eta + 2.0865\,\eta^3 - 1.7068\eta^5 + 072603\,\eta^6}{1 - 0.75857\eta^5}\right) \tag{3.15b}$$

The dependence of the effective charge density on electrolyte concentration is accounted for by a Langmuir-type isotherm:

$$\theta_S = \frac{C_X}{C_{X,MAX}} = \frac{Ke_s C_s}{1 + \sum Ke_i C_i} \tag{3.16}$$

The model has three structural parameters: the pure water permeability of the membrane (L_P), the pore radius (r_P), the ratio of membrane thickness to porosity ($\Delta x/\varepsilon$), and the effective charge density (C_X).

The author determined these parameters from experimental measurements. The effective charge density was obtained by estimating the adsorption coefficients (Ke_S) from experimental measurements and a Langmuir-type isotherm.

3.2.5.4 Donnan-Steric-Gouy-Chapman (DSGC) Model

This model was developed by Garcia-Aleman (1998) and it is based on the frictional and viscous model developed by Jonsson (1980). The model is based

on the extended Nernst-Planck equation for solute transport, the Donnan-steric model for solute partitioning, and the Gouy-Chapman equation to correlate the dependency of the effective charge density on feed concentration. The solution flux is calculated from the Kedem-Katchalsky model and the Hagen-Poiseuille equation.

The steric parameters (α_i, b_i) in the extended Nernst-Planck equation are calculated from the Donnan-Steric Pore model. The effective surface charge density for multiple ions close to a flat surface can be approximated by:

$$q_W = \left(\frac{y}{|y|}\right)\sqrt{2\varepsilon_r\varepsilon_o RT}\left[\sum C_i^B\left(\nu_{i,+}e^{-Z_{i,+}y} + \nu_{i,-}e^{-Z_{i,-}y}\right) - \sum C_i^B\left(\nu_{i,+}+\nu_{i,-}\right)\right]^{\frac{1}{2}}$$

or for a binary solution enclosed by a cylindrical surface by: (3.17a)

$$q_W = -\frac{2FC^B z_+}{\kappa}\left[2\sinh\left(\frac{z_+ y}{2}\right) + 2\frac{\tanh\left(z_+ y/2\right)}{\kappa r_P}\right] \tag{3.17b}$$

where y is the dimensionless surface potential (eq. 3.18).

$$y = \frac{F\varphi}{RT} \tag{3.18}$$

The volumetric charge is therefore obtained from:

$$C_X = \frac{2q_w}{r_P F} \tag{3.19}$$

The model has three fitting parameters: the pure water permeability of the membrane (L_P), the pore radius (r_P), and the surface electrical potential (φ). The ratio of membrane thickness to water content (λ/E) is calculated from the Hagen-

Poiseuille equation. The parameters λ/E in the DSGC model is equivalent to the parameter $\Delta x/\varepsilon$ found in the previous models.

The advantage of this model over other literature models is that the dependency of charge density on feed concentration is described by mechanistic arguments as opposed to empirical or semi-empirical models.

3.3 Summary

The models presented in this chapter show an evolution in the approach to membrane modeling. The first models developed to calculate membrane performance were based on simple phenomenological relationships that did not provide any insight about the membrane structure. Such models were general enough that they could be applied to several membrane processes without compromise.

Over the last decade, the approach to membrane modeling has changed dramatically. With the development of high-speed computers and numerical methods, more complex models have been proposed to explain membrane processes. The recent trend is to develop models for specific membrane applications that will explain the main transport and physicochemical mechanisms involved in the process.

The mechanistic NF models presented in this chapter are based on a similar physical picture and similar assumptions. The governing equations and model parameters are essentially the same. The major difference between these

mathematical models is the quantification of physical and physicochemical interactions between the solute and the membrane (friction interactions, charge density). However, the model parameters and conclusions obtained by different models, especially those models based on the TMS model, are essentially the same (Garcia-Aleman, 1998)

The model developed in Chapter IV describes the transport and physicochemical mechanisms for NF membranes. The basis of the model is the Donnan-Steric-Gouy-Chapman model.

Chapter IV

Model Development

A mathematical model that describes the transport of mixed-solute solutions through nanofiltration membranes is developed in this chapter. The underlying assumptions and simplifications of the model are discussed. A description of the gel conformation model is presented later in this chapter. The basic theory equations that relate the physicochemical properties of the gel to its conformation in the McMaster Pore-filled membranes are presented (Mika and Childs, 2001). The algorithms for the solution of both mathematical models are presented.

A transport model described by Garcia-Aleman (1998) has been modified to account for additional phenomena not described in the original formulation. The model presented in this section can be used for solutions containing 'n' ions and neutral solutes. The model is based on a pseudo 2-dimensional approach. The model parameters are related to membrane structural parameters (effective thickness, pore radius, surface charge) using hydrodynamic calculations (Bowen, et al., 1997) and the Poisson-Boltzmann equation (PBE).

A procedure based on radially-averaged variables is proposed to reduced the computational expense associated with two-dimensional models for mixed-electrolyte solutions and the nonlinear PBE.

4.1. Transport Model

The following sub-sections describe the derivation of the transport model, including assumptions, simplifications and governing equations.

4.1.1 Assumptions in the Transport Model

The following section outlines the underlying and simplifying assumptions about the structure of the membrane, the treatment of the problem, and the development of the model. Other assumptions are given throughout this chapter.

The membrane is assumed to be macroscopically uniform in thickness and porous. The pores are modeled as capillaries that extend throughout the membrane. These pores are evenly distributed throughout the surface of the membrane (cross-section) and are not interconnected. Several researchers (Mika et al., 1995; Bowen and Mukhtar, 1996) have shown that these assumptions are unrealistic (cylindrical pores), but they use this approach anyway. A schematic representation of the theoretical membrane pore is presented in Fig. 4.1.

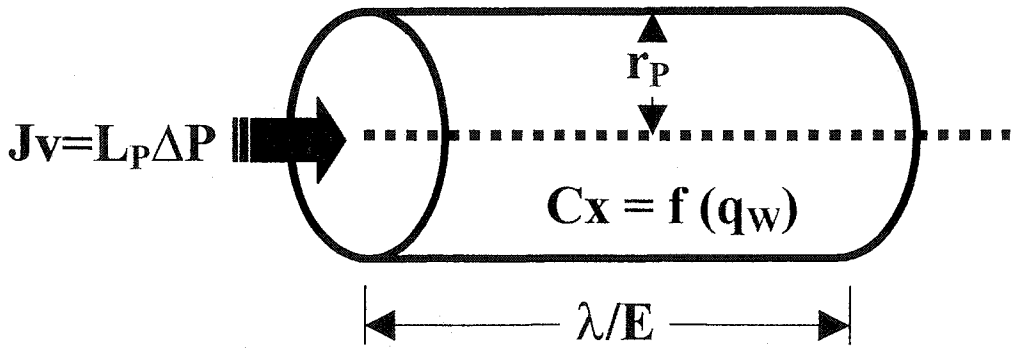

Figure 4.1 Schematic representation of a membrane pore. Each pore can be characterized by 4 parameters: the pure water permeability (L_P), the pore radius (r_P), the surface charge density (q_w) and the ratio of effective membrane thickness to water content (λ/E).

In reality, the membrane pores are tortuous paths in which the effective length of the pore is different from its linear thickness. These assumptions (uniform pore size and shape) are frequently used in transport models since the mathematical analysis is simplified and model calculations are usually in agreement with experimental results (Nakao and Kimura, 1982; Wang et al., 1995a).

Solvent and solute transport occurs only inside the pores. The membrane support does not contribute to the selectivity of the membrane (Hall et al., 1997; Chevalier, 1999). Entrance and exit effects are ignored since the membrane thickness is large compared to the pore radius ($\lambda/E >> r_P$). It is assumed that the membrane and adjacent solution (interfaces) are in equilibrium. This equilibrium phenomenon is described by the Donnan exclusion theory.

The membrane pores are charged capillaries. This charge is evenly distributed throughout the surface of the pore (axial direction). The distribution of charge density and mobile species within the pores are assumed to vary in the radial direction. Dilute-solution theory is applied to the analysis of the problem.

4.1.2 Governing Equations

The extended Nernst-Planck equation (ENPE) describes the three important mechanisms of solute transport in membranes: diffusion and electromigration, as a result of concentration and electrical potential gradients,

respectively, and convection caused by the pressure difference across the membrane. The ENPE in the axial direction is represented by (Jonsson, 1981),

$$J_{i,p}(x) = \underbrace{\frac{C_{i,p}(x)u(x)}{1+\chi_{i,p}/\chi_{i,w}}}_{Convection} - \underbrace{\frac{RT}{\chi_{i,p}+\chi_{i,w}}\frac{dC_{i,p}(x)}{dx}}_{Diffusion} - \underbrace{\frac{z_i C_{i,p}(x)RT}{\chi_{i,p}+\chi_{i,w}}\frac{F}{RT}\frac{d\Psi(x)}{dx}}_{Electromigration} \tag{4.1a}$$

and similarly in the radial direction is described by

$$J_{i,p}(r) = \frac{C_{i,p}(r)u(r)}{1+\chi_{i,p}/\chi_{i,w}} - \frac{RT}{\chi_{i,p}+\chi_{i,w}}\frac{dC_{i,p}(r)}{dr} - \frac{z_i C_{i,p}(r)RT}{\chi_{i,p}+\chi_{i,w}}\frac{F}{RT}\frac{d\Psi(r)}{dr} \tag{4.1b}$$

The solution velocity (u) and the ion flux ($J_{i,,p}$) are based on pore cross-sectional area. The ion concentrations ($C_{i,p}$) are concentrations inside the pore. In equation (4.1) the activities of the solution are replaced by concentration, which implies that the activity coefficients of the solutions are approximately equal to unity and that the pressure gradient has a negligible contribution to the activity of the solution.

4.1.3 Definition of the Hindered Diffusion and Hindered Convection Parameters

The friction coefficients ($\chi_{i,p}$, $\chi_{i,w}$) (Spiegler, 1958) account for membrane-ion and solvent-ion friction interactions, respectively. These two parameters can be related to the diffusivity of the solute in the membrane ($D_{i,,p}$) and the hindered diffusion ($b_{i,}$) and convection parameters ($\alpha_{i,}$) as shown below.

The individual ion velocities are different from the solution average velocity. For instance, inside the membrane, ions move slower than the solvent

due to ion-membrane friction interactions (hydrodynamic drag). Therefore, the individual velocity of an ion is a fraction of the average velocity of the solution, and this fraction is represented by the hindered convection parameter (α_i) (Deen, 1987). The hindered convection parameter, α_i, can replace the frictional coefficients using (Jonsson and Boesen, 1975),

$$1/\alpha_i \approx 1 + \chi_{i,p}/\chi_{i,w} \tag{4.2}$$

If the Nernst-Einstein relationship is assumed to be valid, the diffusivity inside the pore can be defined as:

$$D_{i,p} = RT/(\chi_{i,m} + \chi_{i,w}) \tag{4.3}$$

and the hindered diffusion parameter, b_i, is equal to the ratio of the solute diffusivity inside the pore and the diffusivity in free solution.

$$b_i = D_{i,\infty}/D_{i,p} \tag{4.4}$$

The diffusivity in free solution can be calculated from the equivalent ionic conductance, as described in Appendix C. The ionic flux is obtained by substituting eqs. (4.2) to (4.4) into eq. (4.1).

$$J_{i,p}(x) = \alpha_i C_{i,p}(x)u(x) - \frac{D_{i,\infty}}{b_i}\left(\frac{dC_{i,p}(x)}{dx} + z_i C_{i,p}(x)\frac{F}{RT}\frac{d\Psi(x)}{dx}\right) \tag{4.5a}$$

$$J_{i,p}(r) = \alpha_i C_{i,p}(r)u(r) - \frac{D_{i,\infty}}{b_i}\left(\frac{dC_{i,p}(r)}{dr} + z_i C_{i,p}(r)\frac{F}{RT}\frac{d\Psi(r)}{dr}\right) \tag{4.5b}$$

The ion flux and convective term in the radial direction are negligible compared to the diffusional and electromigration terms. This equation (4.5b) is

equivalent to the Boltzmann distribution, as described later in this chapter. By substituting eq. (4.5b) into eq. (4.5a), we obtain:

$$J_{i,p}(x) = \alpha_i K_i C_i(x) u(x) - \frac{D_{i,\infty}}{b_i} K_i \left(\frac{dC_i(x)}{dx} + z_i C_i(x) \frac{F}{RT} \frac{d\Psi(x)}{dx} \right) \tag{4.6}$$

where K_i is the partition coefficient and C_i is the virtual concentration inside the pore. The virtual concentration (C_i) represents a fictitious concentration, at a large distance from the pore wall where the electrostatic potential is zero, which is in equilibrium with the local concentration ($C_{i,p}$) inside the membrane.

4.1.4 Solution of the Concentration Gradient

The solution and solute fluxes through the membrane are obtained by multiplying the fluxes based on pore area by the membrane porosity, ϵ. The porosity is the ratio of the total area occupied by the pores to the surface area of the membrane.

$$J_i(x) = J_{i,p}(x)\varepsilon \tag{4.7}$$

$$J_V(x) = u(x)\varepsilon \tag{4.8}$$

The pores in the membrane can be modeled as cylinders. The tortuosity, t, of the membrane is accounted for by replacing the axial coordinate, x, by the effective distance, z.

$$x = zt \tag{4.9}$$

Hence, the water content of the membrane is obtained as a function of the porosity and the tortuosity of the membrane.

$$E = \varepsilon / t \tag{4.10}$$

Substituting eqs. (4.7) to (4.10) into eq. (4.6) the ion flux per membrane area is obtained as a function of ion concentration, solution flux and model parameters.

$$J_i(z) = \alpha_i K_i C_i(z) J_V(z) - \frac{D_{i,\infty}}{b_i} E K_i \left(\frac{dC_i(z)}{dz} + z_i C_i(z) \frac{F}{RT} \frac{d\Psi(z)}{dz} \right) \tag{4.11}$$

The differential concentration profile inside the membrane can be obtained by rearranging eq. (4.11).

$$\frac{dC_i(z)}{dz} = \frac{b_i}{D_{i,\infty} E} \left(\alpha_i C_i(z) J_V(z) - \frac{J_i(z)}{K_i} \right) - z_i C_i(z) \frac{F}{RT} \frac{d\Psi(z)}{dz} \tag{4.12}$$

4.1.5 Solution of the Electrical Potential Gradient

The electrical potential gradient can be derived in terms of measurable quantities by applying several known constraints to the solution. First, electroneutrality should prevail inside the membrane (eq. 4.13a) and in the external solutions (eq. 4.13b) so that no net charge is produced (electroneutrality condition).

$$\sum z_i C_{i,p}(z) + z_X C_X = 0 \tag{4.13a}$$

$$\sum z_i C_i = 0 \tag{4.13b}$$

Second, no net current should be produced inside the membrane as a consequence of ionic flux (condition of no-electric current).

$$I = F\sum z_i J_i(z) = 0 \tag{4.14}$$

Using the condition of electroneutrality (eq. 4.13b) and the condition of no electric current (eq. 4.14) the following equation is obtained:

$$\sum\left(z_i \frac{dC_i(z)}{dz}\right) = \frac{1}{E}\sum\left(z_i \frac{\alpha_i b_i}{D_{i,\infty}} C_i(z) J_V(z)\right)$$
$$-\frac{1}{E}\sum\left(z_i \frac{b_i}{D_{i,\infty}} \frac{J_i(z)}{K_i}\right) - \frac{F}{RT}\frac{d\Psi(z)}{dz}\sum\left(z_i^2 C_i(z)\right) \tag{4.15}$$

The term on the left-hand side is equal to zero (electroneutrality condition). The electrical potential gradient is obtained after algebraic manipulation of eq. (4.15), as,

$$\frac{d\Psi(z)}{dz} = \frac{RT}{F}\frac{1}{E}\frac{\sum b_i z_i / D_{i,\infty}\left(\alpha_i C_i(z) J_V(z) - \frac{J_i(z)}{K_i}\right)}{\sum\left(z_i^2 C_i(z)\right)} \tag{4.16}$$

Thus the extended Nernst-Planck equation, with the conditions of electroneturality and no-electric current, is reduced to a first order ordinary differential equation.

4.1.6 Equation of Continuity, Solution of the Material Balance for the Solute

When steady state is reached in the membrane, the ion concentration is independent of time and the flux is independent of distance. Thus the continuity equation (eq. 4.17) is equal to zero. Only the axial component of this equation is

used here. However, this equation simplifies to the steady state case, where no net change in flux occurs.

$$\frac{\partial C_{i,P}}{\partial t} + \nabla J_i = 0 \tag{4.17}$$

A solute material balance yields the following equation:

$$C_i^P = \frac{J_i}{J_V} \tag{4.18}$$

Equation (4.18) states that the permeate concentration is defined by the ratio of molar solute flux (J_i) to volumetric solution flux (J_V). The concentration and electrical potential profiles are obtained by substituting eq. (4.18) into eqs. (4.12) and (4.16).

$$\frac{dC_i(z)}{dz} = J_V \frac{b_i}{D_{i,\infty} E}\left(\alpha_i C_i(z) - \frac{C_i^P}{K_i}\right) - z_i C_i(z) \frac{F}{RT}\frac{d\Psi(z)}{dz} \tag{4.19}$$

$$\frac{d\Psi(z)}{dz} = \frac{RT}{F}\frac{J_V}{E}\frac{\sum\left(z_i b_i / D_{i,\infty}\right)\left(\alpha_i C_i(z) - \frac{C_i^P}{K_i}\right)}{\sum\left(z_i^2 C_i(z)\right)} \tag{4.20}$$

4.1.7 Derivation of the Partition Coefficients: Size Exclusion and the Poisson-Boltzmann Equation.

The partition coefficients for charged and uncharged solutes are derived in this section. The basic derivation of the Poisson-Boltzmann equation is provided. For uncharged solutes, in the absence of long- and short-range interactions between the solute and the pore wall, the average partition coefficient is only

dependent on the relative size of the solute and the membrane pore, see for example, Deen (1987).

$$\overline{K_i}(z) = \Phi_i = (1-\eta)^2 \tag{4.21}$$

where,

$$\eta_i = r_i / r_P \tag{4.22}$$

For solutions containing electrolytes, the average partition coefficients are calculated using the nonlinear Poisson-Boltzmann equation, as shown below.

4.1.7.1 Derivation of the Poisson-Boltzmann Equation

The electrical potential inside the membrane can be divided into two components: an axial component (ϕ) produced by the streaming potential and a component (φ) produced by the surface charge of the membrane (Gross and Osterle, 1968).

$$\Psi = \phi(z) + \varphi(z,r) \tag{4.23}$$

When the length of the capillary is considerably larger than the radius, the axial gradient ($\nabla\phi$) of the potential is negligible compared to the radial component ($\nabla\varphi$). Therefore, the total potential gradient can be reduced to the radial component of the potential.

The total electrical potential gradient is described by the Poisson equation.

$$\nabla\Psi = \frac{-\rho_C}{\varepsilon_r \varepsilon_0} \tag{4.24}$$

where ψ is the electric potential and ρ_c is the local charge density.

When local equilibrium exist, a Boltzmann distribution is established according to,

$$C_{i,p}(z,r) = K_i(z,r)C_i(z) \tag{4.25}$$

where the local partition coefficient is defined as,

$$K_i(z,r) = \exp\left(-\frac{z_i F\varphi(z,r)}{RT}\right) \tag{4.26}$$

Thus, the local charge density can be described as:

$$\rho_c = \sum z_i K_i(z,r)C_i(z) \tag{4.27}$$

The following dimensionless quantities can be defined: the dimensionless electrostatic potential,

$$y(z,r) = \frac{F\varphi(z,r)}{RT} \tag{4.28}$$

the dimensionless radial coordinate,

$$r^* = \frac{r}{r_P} \tag{4.29a}$$

and the dimensionless axial coordinate

$$z^* = \frac{z}{\lambda / E} \tag{4.29b}$$

Therefore, equations (4.25) and (4.27) are combined to obtain the radial component of the Poisson-Boltzmann equation for mixed-electrolyte solution in dimensionless coordinates:

$$\frac{1}{r^*}\frac{d}{dr^*}\left(r^*\frac{dy(z^*,r^*)}{dr^*}\right) = -\frac{F^2 r_P^2}{\varepsilon_r \varepsilon_0 RT}\sum z_i C_i(z^*)K_i(z^*,r^*) \tag{4.30}$$

This equation is equivalent to the form of the PBE proposed by Wang et al. (1995a). Equation (4.30) is valid for cases where the axial gradient of the potential is negligible in comparison to the radial gradient. Such is the case when the length of the capillary is considerably larger than its radius. The PBE is can be solved numerically subject to two boundary conditions. The condition of symmetry at the center of the pore is

$$\left.\frac{dy(z^*,r^*)}{dr^*}\right|_{r^*=0} = 0 \tag{4.31}$$

For the case of constant surface charge density the second boundary conditions is written in the form of Gauss Law as,

$$\left.\frac{dy(z^*,r^*)}{dr^*}\right|_{r^*=1} = \frac{F}{RT}\frac{r_P q_W}{\varepsilon_r \varepsilon_0} \tag{4.32a}$$

and for the case of constant potential this condition is written as,

$$y(z^*,r^*)\Big|_{r^*=1} = \zeta \tag{4.32b}$$

where ζ is the zeta potential (the electrostatic potential at the boundary of the Stern layer). A constant surface charge density is assumed in this investigation.

Thus, the average partition coefficient can be written as,

$$\overline{K_i}(z^*) = \Phi_i \xi_i = \Phi_i \left[2\int K_i(z^*,r^*) r^* dr^*\right] \tag{4.33}$$

Equation (4.33) contains a purely steric component (Φ_i) and a purely electrostatic component (ξ_i). The average volumetric charge density for a cylindrical pore can be obtained from,

$$\overline{C_X} = \frac{2\pi r_P}{\pi r_P^2}\frac{\overline{q_W}}{F} = \frac{2\overline{q_W}}{r_P F} \tag{4.34}$$

4.1.8 Average Solution Flux and Average Concentration Profile

The differential concentration and electrical potential gradients (eqs. 4.19 and 4.20) depend on radial position. These equations have to be integrated radially to obtain the average gradients. Kedem and Katchalsky (1958) derived a phenomenological equation (eq. 2.4) to describe the solution flux in terms of the membrane permeability (L_P) and the differential effective pressure gradient ($P_{eff} = \Delta P - \Delta\pi$). If we assume that the variations of the radial pressure gradient are negligible compared to the axial component and include the contribution of the streaming potential to the volume flux, then the average solution flux can be described as:

$$\overline{J_V}(z^*) = L_P\left(\frac{dP_{eff}}{dz^*} + F\overline{C_X}\frac{d\overline{\Psi}(z^*)}{dz^*}\right) \tag{4.35a}$$

This equation (eq. 4.35b) can be further simplified to,

$$\overline{J_V}(z^*) = L_P\left[\left(\Delta P - \sigma\Delta\pi\right) + F\overline{C_X}\Delta\overline{\Psi}/(\lambda/E)\right] \tag{4.35b}$$

Since the permeate concentration in the external solution is independent of radial position, equation (4.18) can be written as,

$$\overline{J_i} = \overline{J_V}C_i^P \tag{4.36}$$

The radially-averaged virtual concentrations can be obtained from the nonlinear Poisson-Boltzmann equation (section 4.1.7). Equations (4.37) and

(4.38) are obtained by substituting eqs. (4.33) and (4.36) into eqs. (4.19) and (4.20).

$$\frac{d\overline{C_i}(z^*)}{dz^*} = \overline{J_V}\frac{b_i}{D_{i,\infty}}\left(\alpha_i\overline{C_i}(z^*) - \frac{C_i^P}{\overline{K_i}}\right) - z_i\overline{C_i}(z^*)\frac{F}{RT}\frac{d\overline{\Psi}(z^*)}{dz^*} \tag{4.37}$$

$$\frac{d\overline{\Psi}(z^*)}{dz^*} = \overline{J_V}\frac{RT}{F}\frac{\sum\left(z_i b_i / D_{i,\infty}\right)\left(\alpha_i\overline{C_i}(z^*) - \frac{C_i^P}{\overline{K_i}}\right)}{\sum\left(z_i^2\overline{C_i}(z^*)\right)} \tag{4.38}$$

Equations (4.37) and (4.38) describe the radially-averaged differential concentration and electrical potential gradients inside the membrane as a function of concentration, solution flux, free-solution diffusivities, membrane thickness and steric factors (α_i, b_i). The concentration profile and the electrical potential gradient are solved using one of the following boundary conditions:

$$\overline{C_i}\left(z^* = 0\right) = C_i^B = \overline{C_{i,p}^B}\Big/\overline{K_i^B} \tag{4.39a}$$

$$\overline{C_i}\left(z^* = 1\right) = C_i^P = \overline{C_{i,p}^P}\Big/\overline{K_i^P} \tag{4.39b}$$

In theory, using either boundary condition yields the same result. However, in practice, using eq. (4.39a) and integrating the differential equation backwards yields the best results, as discussed in section 4.2.1.

The use of radially-averaged variables in the model reduces the computational time associated with two dimensional models and the nonlinear PBE equation. This feature is especially useful for solutions containing more than two permeating species. Numerical complexity increases with increasing number of ions in solution.

4.1.9 Hindered Diffusion and Hindered Convection Parameters in the Extended Nernst-Planck Equation as a Function of the Pore Radius

The hindered diffusion and convection parameters account for friction between the solute and the membrane pores. This friction is dependent on both ionic size and the structure of the pore, among other factors. Bowen et al. (1997) developed two equations that relate the ratio of ion to pore radius (η) to the friction parameters. These equations are valid only when ($0 < \eta < 0.80$).

$$\alpha_i = \left[2 - \Phi_i\right]\left(1 + 0.054\,\eta - 0.988\,\eta^2 + 0.441\,\eta^3\right) \tag{3.14a}$$

$$b_i = \left(1 - 2.3\eta + 1.154\,\eta^2 + 0.224\,\eta^3\right)^{-1} \tag{3.14b}$$

These two relationships were adapted from earlier work by Bowen and co-workers (Bowen and Sharif, 1994; Bowen and Mukhtar, 1996). The existence of cylindrical pores is directly assumed (see section 3.2.5.2. for details).

4.1.10 Pure Water Permeability

In the absence of compaction, the pure water permeability of the membrane (L_p) is obtained from the Hagen-Poiseuille equation.

$$L_p = \frac{r_p^2}{8\mu(\lambda / E)} \tag{3.11}$$

However, with compaction, L_p varies with applied pressure and can be described using a semi-empirical equation (eq. 4.40).

$$L_P = L_{PO} e^{-\alpha_O(\Delta P - \Delta\pi)} \tag{4.40}$$

The first parameter (L_{po}) is the pure water permeability of the membrane in the absence of applied pressure. The second parameter (α_o) is the degree of compaction of the membrane with effective pressure. A form of eq. (4.40) was originally proposed by Sourirajan (1970). The original equation omits the contribution of the hydrodynamic pressure caused by the solute (osmotic pressure). In this dissertation, the original equation is modified to take into account the effective pressure gradient in the membrane (eq. 4.40).

4.1.11 Effective Charge Density as a Function of Feed Concentration.

Several authors have found that the effective charge density of charged membranes increases with increasing electrolyte concentration due to adsorption (Tsuru et al. 1991b; Xu et al., 1997; Garcia-Aleman, 1998; Shaep et al., 1999).

This dependency can be described by mechanistic approaches (Garcia-Aleman, 1998) or semi-empirical approaches (Hall et al., 1997; Bowen et al., 1997; Shaep et al., 1999; Chevalier, 1999). The mechanistic approach proposed by Garcia-Aleman (1998) is valid only for NF membranes with small pore sizes (< 2 nm). Therefore, a semi-empirical approach is adopted to model the membranes used in this dissertation. If the relationship between the surface charge density (q_w) and ionic strength (I) is linear, the following relationship is used (Bowen et al., 1997; Shaep et al., 1999):

$$q_W = AI + B \tag{4.41a}$$

For non-linear relationships, a Langmuir-type isotherm can be used, as proposed by Chevalier (1999),

$$q_W = \frac{AI}{1+BI} \tag{4.41b}$$

where ionic strength (I) is defined as:

$$I = \sum z_i^2 C_i \tag{4.42}$$

The empirical coefficients A and B can be positive or negative depending on the sign of the charge density of the membrane.

4.1.12 Summary

The mechanistic model developed in this section consists of 'n-1' coupled ordinary differential equations for 'n' number of ions and solutes. The additional degree of freedom required to solve the equations comes from the electroneutrality condition (eq. 4.13) The membrane is described by four parameters (r_P, q_w, L_P, λ/E). The first three parameters (r_P, q_w, L_P) are fitting parameters. The ratio of membrane thickness to water content (λ/E) is calculated from the Hagen-Poiseuille equation, once the permeability (L_P) and pore radius (r_P) are known. A pseudo 2-dimensional approach with radially averaged concentration and potential gradients is used here to reduce the computational expense associated with full 2-dimensional approaches.

4.2 Model Solution

General theory and practical approaches for the solution of the model are described in this section. The discussion focuses on three major areas: practical solution of the model, nonlinear least squares, and optimization routines. All the routines used in this dissertation were coded in Matlab 6.1 (Mathworks, Inc.) using both built-in and our own routines.

4.2.1 Algorithm for the Solution of the Transport Model

The model can be solved on a personal computer using the algorithm described below:

1. The feed concentration, operating temperature, and operating pressure are the independent variables. Membrane parameters are known, as current estimates in a parameter estimation routine, for instance (r_P, q_w, L_{Po}, α_o). The parameter (λ/E) is calculated from eq. (3.11). The hindered diffusion and convection parameters are calculated from eqs. (3.14a) and (3.14b). The hydrodynamic radii are calculated from ionic diffusivities and the Stokes-Einstein equation.
2. The radially-averaged partition coefficients are obtained from eq. (4.21) when only uncharged solutes are present. For electrolytes the non-linear PBE (eqs. 4.30-4.32) must be solved numerically (see section 4.1.11.2) to obtain radial distribution of the electrical potential and ion concentrations inside the membrane. Then, the local electrical potential is integrated

numerically (Simpson's method, ⅓ rule) to obtain the radially-averaged electrical potential. The average partition coefficients inside the membrane are obtained from eq. 4.33. The average volumetric charge density can be calculated by solving equations (4.13) and (4.34), simultaneously.

3. The average solution flux and permeate concentration are obtained by solving eqs. (4.13b), (4.37), and (4.38) simultaneously with the appropriate boundary conditions (eq. 4.39a or 4.39b). This set of equations is integrated backwards (from the permeate side to the feed side). This procedure is iterative since an initial estimate of the permeate concentration is required. The reflection coefficients in eq. (4.35) are assumed to be unity for simplicity and since osmotic pressure effects are relatively small. Osmotic pressure is calculated from the van't Hoff equation.
4. The set of coupled ordinary differential equations, resulting from points 2 and 3, is solved numerically using a variable step predictor-corrector method (Shampine and Gordon, 1975). The membrane parameters are estimated using Levenberg-Marquardt non-linear parameter estimation method (Levenberg, 1944; Marquardt, 1963).

4.2.2 Analytical Solution of the Transport Model for Uncharged Solutes

The differential concentration profile inside the membrane can be solved analytically for solutions containing only uncharged solutes. For uncharged solutes, equation (4.37) can be transformed into,

$$\int_{K_i C_i^B}^{K_i C_i^P} \frac{dC_{i,p}}{\left(\alpha_i C_{i,p} - C_i^P\right)} = J_V \frac{b_i}{D_{i,\infty}} \int_0^1 d\left(z^*\right) \tag{4.43}$$

Integrating eq. (4.43) and after algebraic manipulation, we obtain the analytical solution to permeate concentration for an uncharged solute.

$$C_i^P = C_i^B \frac{\alpha_i K_i}{\left[1 + \left(\alpha_i K_i - 1\right) \exp\left(-J_V \frac{b_i \alpha_i}{D_{i,\infty}} \frac{\lambda}{E}\right)\right]} \tag{4.44}$$

4.2.3 Numerical Methods

The mathematical model consists of two sets of differential equations. The first set consists of n-1 ordinary differential equations (ODE), corresponding to the concentration profile of each solute permeating through the membrane. The second set consists of two coupled differential equations that correspond to the Poisson-Boltzmann equation.

These equations are solved numerically using a shooting method (iteratively). The shooting method is implemented with a nonlinear equation solver based on the least-squares algorithm (FSOLVE) and the differential equations are solved using a variable step predictor-corrector (ODE113) method based on the Adams-Bashforth-Moulton formulas.

The concentration and potential gradients (eqs. 4.37 and 4.38) are integrated backwards from the permeate side (eq. 4.39b) to the feed side (eq. 4.39a) of the membrane. An estimate of the permeate concentration is provided

as an initial guess. The nonlinear equation solver then compares the estimate of the feed concentration with the actual value, and updates the estimate of the permeate concentration accordingly. The procedure is repeated until the estimated and the actual values of the feed concentration are within a certain tolerance. At each point (z^*) the PBE equation is solved as described below and in point 2 of section 4.2.1.

The same procedure applies for the solution of the PBE (eq. 4.30). An initial estimate of the potential at the center of the pore is provided. The coupled differential equations are integrated from the center to the surface of the pore using the appropriate boundary conditions (eqs. 4.31 and 4.32a, respectively). The iterative procedure continues until the estimated and actual values of the zeta potential (eq. 4.32b) are within a certain tolerance.

4.2.4 Nonlinear Least Squares

The parameter estimation problem is approached using an algorithm based on nonlinear least squares (Fletcher, 1989). From nonlinear least squares the objective function is defined, in general, as:

$$f(h) = 1/2\, g(h)^T\, g(h) \tag{4.45}$$

where

$$g_i(h) = C^P_{i,\text{experimental}} - C^P_{i,calculated} \tag{4.46}$$

The applied pressure is the independent variable (h) and the permeate concentration is the dependent variable. Thom (1993) discussed the use of other

variables, for example rejection, although she emphasized that this practice is undesirable from the statistical point of view since rejection depends on both independent and dependent variables.

4.2.5 Optimization Routine

The nonlinear least squares objective function is minimized using an unconstrained optimization routine (LSQCURVEFIT) based on Levenberg (1944) and Marquardt (1963) method. Levenberg-Marquardt (LV) method is a modification of a Newton-type method that uses second order information (Hessian) to find the minimum of a function.

The authors suggested that the Hessian matrix be modified by a parameter at each stage of the search as needed to ensure that the modified Hessian is positive definite and well-conditioned (Dennis and Schnabel, 1983).

In essence the LV method initially behaves as a steepest descent method (first order) as the Hessian is forced to be positive definite (i.e., parameters are large). As the optimization advances and the value of the parameters decrease the search shifts to a Gauss Newton method (locally quadratic). The Jacobian and Hessian are determined numerically by finite differences as described in Gill et al. (1993).

4.3 Gel Conformation Model

In this section a brief description of the gel conformation model developed by Mika and Childs (2001) is presented. Model assumptions and advantages are discussed, and the governing equations are described.

The objective of this part of the investigation was to develop a mechanistic model that predicts quantitatively the conformation of the constrained gel inside the substrate pores. The model presented here predicts the Darcy permeability of the polyelectrolyte gel, the charge density of the gel, and the pore radius.

4.3.1 Basic Assumptions in Gel Conformation Model

This approach assumes that confined gels can be treated as semi-dilute polymer solutions of the same polymer concentration (volume fraction). Schaefer's model (Schaefer, 1984) of polymers in semi-dilute solutions coupled with the concept of electrostatic persistence length is used to estimate the correlation length of the solution (ξ_P). The hydrodynamic permeability of the gel is obtained by modeling the gel as an assemblage of spheres of diameter equal to the correlation length. Other assumptions are given throughout this section.

4.3.2 Governing Equations

In semi-dilute polyelectrolyte (PEL) solutions there are two different interactions, intra-chain and inter-chain. Many qualitative features can be obtained, however, using scaling arguments introduced by de Gennes (1979).

The so-called blob representation emerging from scaling arguments has been proved a very simple but powerful physical picture (Fig. 4.2). Inside a sphere of diameter ξ_P there are segments of a given chain that do not interact with segments of other chains. Hence, inside a blob, the chains behave like isolated chains under excluded volume effect. Therefore, semi-dilute solutions can be understood as a dense packed system of blobs with a characteristic length scale known as the correlation length (ξ_P).

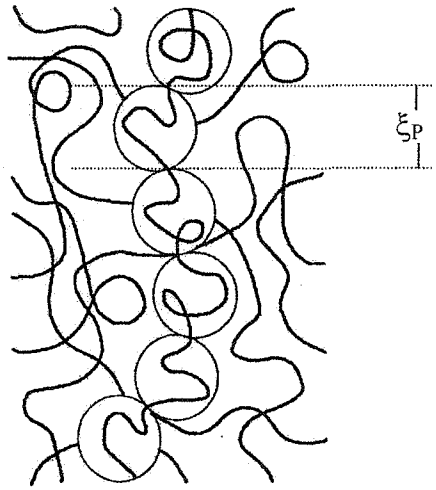

Figure 4.2 Blob representation of semi-dilute polymer solutions. The correlation length (ξ_P) is the average distance between inter-chain contacts.

The Schaefer equation (Schaefer, 1984) relates the correlation length (ξ_p) to the polymer volume fraction (δ), the three-body excluded volume parameter (w) and the Flory-Huggins interaction parameter (χ).

$$\xi_P = \frac{N^2 a}{\left[N(1-2\chi)\delta + wa^{-6}\delta^2\right]^{1/2}} \tag{4.47}$$

Based on the approach taken by Odijk (1979) for wormlike PEL chains, the electrostatic persistence length is defined as:

$$L_e = \frac{l_B}{4\kappa^2 A^2} \quad \text{for A} > l_B \tag{4.48a}$$

where l_B is the Bjerrum length and A is the contour distance between charged groups in the polymer unit. For A < l_B, Odijk adopted counter-ion condensation theory in the form proposed by Manning (1969) and Oasawa (1971) and modified the Odijk (1977), and Skolnick-Fixman (1977) (OSF) relation (eq. 4.48a) to:

$$L_e = \frac{1}{4\kappa^2 l_B} \quad \text{for A} \le l_B \tag{4.48b}$$

where κ is the Debye-Huckel parameter defined as

$$\kappa^2 = 4\pi Ac \tag{4.49}$$

The correlation length scales with concentration, c, as:

$$\xi_P \cong \left(L_{PE} + \frac{1}{16\pi l_B Ac} \right)^{-1/4} (4\pi Ac)^{1/8} (Ac)^{-3/4} \tag{4.50}$$

where L_{PE} is the bare persistence length (no charge). Equation (4.50) is only valid if the correlation length is much larger than the electrostatic persistence length (Odijk, 1979).

The next step of the model is to relate the fractional void volume of the PEL to the permeability. Happel (1958; 1973) modeled the gel network as an assemblage of hard spheres of radius R surrounded by a spherical fluid envelope of radius R_e. The fluid volume contained in the envelope is sufficient to make the

fractional void volume (ε_P) in the cell identical to that in the entire assemblage. This means that the following relationship is true.

$$\left(\frac{R}{R_e}\right)^3 = \delta = (1-\varepsilon_P) \tag{4.51}$$

Solving the Stokes equation the following relationship, the Happel equation, for permeability is obtained.

$$k_H = \frac{2R^2}{9\delta}\left[\frac{3-(9/2)\delta^{5/3}-3\delta^2}{3+2\delta^{5/3}}\right] \tag{4.52}$$

The permeability of the gel can then be related to the permeability of the pore-filled membrane by:

$$k_m = k_H \frac{\varepsilon_S}{t} \tag{4.53}$$

The charge density of the membrane can be obtained by calculating the number of charged groups (per volume) in the gel assemblage from the polymer volume fraction (δ) and the partial specific volume (v_2).

$$n_{qe} = \frac{\delta}{v_2} \tag{4.54}$$

If counter-ion condensation occurs A $\leq l_B$, then the effective charge density is obtained from:

$$q_W = \frac{n_{qe}}{l_B} \tag{4.55}$$

4.3.3 Algorithm for the Solution of the Gel Conformation Model

The gel structure model can be solved on a spreadsheet or any programming language without complex calculations. The parameters (χ, δ) used in the gel conformation model are readily available (experimentally or from the literature) for the polymers used in this investigation. A comparison between the parameters used in both models is presented in Table 4.1. The pore diameter is calculated from eq. (4.47) or eq. (4.50). The membrane permeability is obtained from eqs. (4.52) and (4.53). The surface charge density of the membrane is calculated from eq. (4.55).

Table 4.1 Parameter equivalences between transport model and gel conformation model.

Parameter	Gel Conformation Model	Transport Model
Pore radius	$\xi_P / 2$	r_P
Pure water permeability	$k_m / (\mu \lambda)$	L_P
Surface charge density	q_w	q_w

4.4 Summary

A mechanistic model for solute transport through nanofiltration membranes has been developed. The model is based on the extended Nernst-Planck equation that takes into account steric effects on the diffusive and convective fluxes and the PBE for the radial distribution of the membrane

potential and the ionic species. The model parameters consist of the pore radius, surface charge density, and ratio of membrane thickness to water content.

This model is used to calculate and predict the performance of commercial and pore-filled membranes using different feed solutions, as presented in Chapter VI. The membrane parameters in the transport model can be estimated using the gel model or fitted using experimental permeation data.

A model that predicts the conformation of the polyelectrolyte gel inside the MacPF membranes was also presented here. The model is used to calculate the membrane parameters from theory. These parameters are compared to those obtained from fitting data from permeation experiments.

Chapter V

Experimental

This chapter details the experimental apparatus, membranes, and procedures used in this investigation. A description of the experimental and analytical equipment is provided. The experimental conditions are summarized. Safety considerations are included.

5.1 Description of Experimental Apparatus

The nanofiltration apparatus, illustrated in Figure 5.1, consists of six radial-flow membrane cells connected in series. Each cell has an active cross sectional area of 15.08 cm^2. The feed solution flows from an 8 liter Pyrex bottle into a diaphragm (dual chambered) metering pump. The output from the pump is connected to a hydraulic nitrogen-gas accumulator to dampen the pressure fluctuation caused by the pump. A high/low automatic shutoff pressure protector is used to protect the pump in case of leaks or to protect the membranes and the test system from damage in case of pressure build-up. The feed solution is processed at room temperature. The permeate and concentrate streams may be either recycled to the feed bottle or dumped to the drain. Two sets of membranes where used in this investigation in two experimental apparatuses.

Pressure, feed flow rate, and feed concentration are controlled independently. The system temperature is controlled manually by adjusting the

cooling water flow rate to the heat exchanger and is monitored via an OMEGA 2176A digital thermometer.

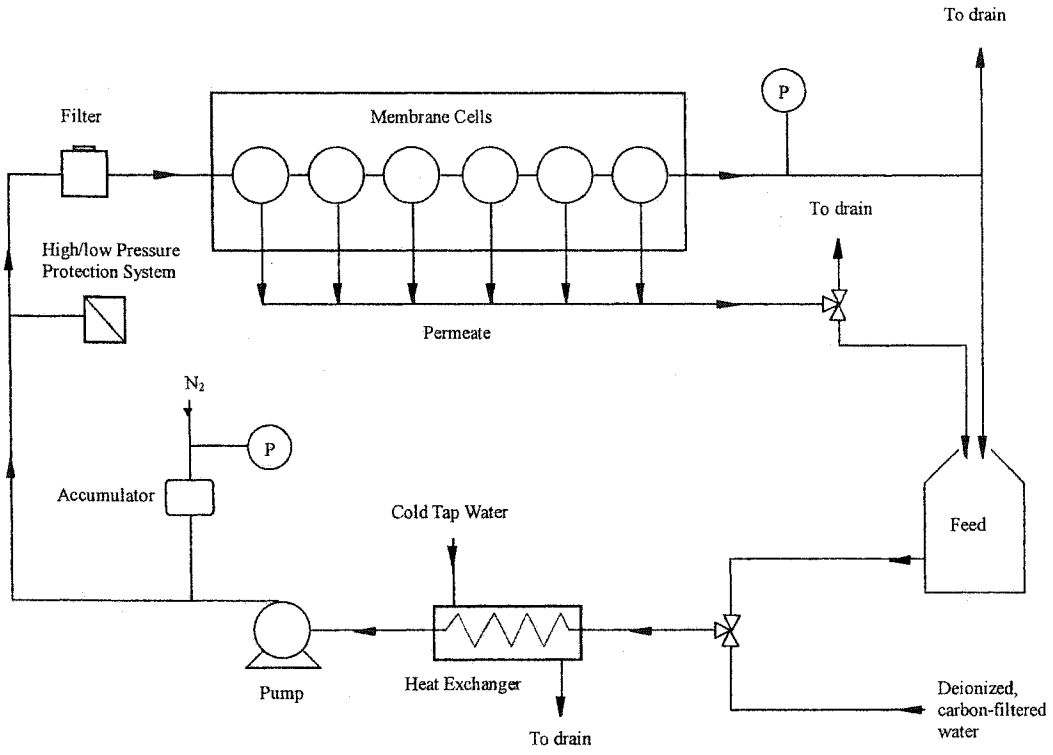

Figure 5.1 Schematic diagram of the nanofiltration testing apparatus. Each system contains six radial flow cells connected in series.

5.2 Nanofiltration Membranes

A total of seven different MacPF membranes and one commercial membrane were used in this investigation. All MacPF membranes are anion-exchangers (i.e., positively charged). The commercial membrane Hydranautics HN-4040-TFV-7450 (HN-7450) is negatively charged and it is similar to the Nitto Denko NTR-7450, which has a skin layer made of sulfonated polyethersulfone with a polysulfone support layer (Petersen, 1993).

The McMaster Pore-filled (MacPF) membranes are prepared by two methods: by photo-grafting of 4-vinylpyridine/divinylbenzene (4VP/DVB) onto polyethylene (PE) microfiltration substrates (Mika et al., 1995); or, by *in situ* cross-linking of 4VP with dibromo-*p*-xylene into polypropylene (PP) substrates (Mika et al., 2001). The MacPF membranes used in this study differ in substrate type, cross-linker type, degree of cross-linking, and degree of quaternization. A detail description of the preparation methods and materials of the MacPF membranes is presented in Appendix A.

An atomic force microscopy surface image of a PE substrate before and after pore-filling is presented in Fig. 5.2.

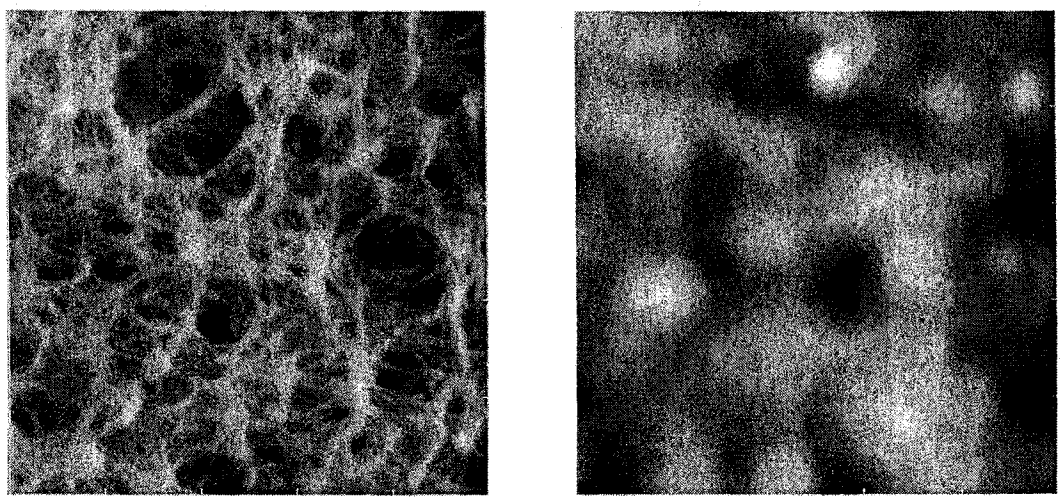

(a) (b)

Figure 5.2 Surface image (AFM) of the polyethylene substrate (a) before and (b) after pore-filling with 4VP and DVB.

The MacPF membranes were characterized according to the methods described elsewhere (Mika et al., 1995; Mika et al., 1997). A summary of these

characteristics is presented in Table 5.1. The mass gain represents the percentage mass increase of the dried substrate after grafting. The ion-exchange capacity of the membrane was determined by titration. The average charge densities in the membranes were determined from the equivalent number of the fixed charge and volume of a water-swollen membrane sample. The thickness of the pore-filled membrane was determined by picnometry (Mika et al., 1995).

Table 5.1 Physicochemical properties of the McMaster Pore-filled membranes used in this investigation.

Membrane	Substrate	Degree of Cross-linking Molar Ratio	Mass Gain %	Thickness μm	Charge Density eq/L	Water Content Vol-%
352	PE	0.5	188.4	158	0.59	N/A
324	PE	4	185	108	0.86	N/A
382	PE	4	57.7	78	0.36	N/A
515	PP5	0.1	N/A	129	0.425	92.4
508	PP5	0.2	N/A	124	0.52	90.6
509	PP5	0.25	N/A	119	0.52	90.3
AL7	PP3	0.104	N/A	122	0.18	92.5

5.3 Nanofiltration Experiments

This section is divided in five subsections covering the following: the definition of operating variables and the errors associated with its measurement, the experimental procedure, and the experimental conditions (solute, concentration, pressure) used in each run.

Two systems were used in these experiments. The membranes MacPF 352, 324, 382 and HN-7450 were contained in system one. The membranes 515, 508, 509 and AL7 were contained in system two. Cells 5 and 6 were not used.

Table 5.2 Physical arrangement of nanofiltration cells.

	System 1		System 2	
Cell	**Membrane**	**Substrate**	**Membrane**	**Substrate**
1	HN-7450	Polysulfone	MacPF 515	PP 5
2	MacPF 352	PE	MacPF 508	PP 5
3	MacPF 324	PE	MacPF 509	PP 5
4	MacPF 382	PE	MacPF AL7	PP 3

5.3.1 Materials

The solutes used were sodium chloride (BDH, analytical grade), sodium sulphate (BDH, analytical grade), magnesium chloride (BDH, analytical grade), β-D-lactose (Sigma-Aldrich) and polyethylene glycol (Sigma-Aldrich). The pure water was supplied from a RO unit and polished using high purity deionizer (Barnstead/Thermolyne) and activated carbon cartridges (Fisher).

5.3.2 Definition of Operating Variables and Experimental Error

The operating variables of the experimental apparatus were categorized into measurements, and independent and dependent variables. Solute type, solute concentration, pressure, and feed flow rate were the independent variables. Permeate concentration and flux were considered the dependent variables.

The variability in concentration between runs of the same concentration was ± 3.1%. The errors associated with measurements in the feed and permeate concentrations are discussed later. The values of the other operating variables and the error associated with these variables are presented in Table 5.3 for system 1 and 5.4 for system 2.

Table 5.3 Range and experimental error in operational variables and measurements for system 1.

Variable	Range	Error
Pressure	0.3-1.5 MPa	± 2%
Temperature	20°C	± 5°C
Feed flow rate	1 L/min	± 1.5%
Soln. Flux HN-7450	1.96-13.41 $x10^{-6}$ m/s	± 9.63%
Soln. Flux MacPF 352	0.55-2.35 $x10^{-6}$ m/s	± 8.45%
Soln. Flux MacPF 324	0.65-55.78 $x10^{-6}$ m/s	± 9.37%
Soln. Flux MacPF 382	3.41-16.56 $x10^{-6}$ m/s	± 12.44%

Experiments were run at room temperature (20°C ± 5°C), constant feed flow rate (1 L/min), and different pressures (0.3-1.5 MPa). The variability on temperature readings reflects the natural variations on room temperature and not measurement errors. Temperature was measured with thermocouples in the feed side liquid in the NF cells. The feed flow rate was such that the effects of concentration polarization were negligible. Every sixth run, a standard experiment was run to monitor changes in membrane performance over time.

Table 5.4 Range and experimental error in operational variables and measurements for system 2.

Variable	Range	Error
Pressure	0.3-0.9 MPa	± 2%
Temperature	20 °C	± 5°C
Feed flow rate	1 L/min	± 1.5%
Soln. Flux MacPF 515	17.96-36.87 x10^{-6} m/s	± 7.81%
Soln. Flux MacPF 508	4.57-10.87 x10^{-6} m/s	± 2.66%
Soln. Flux MacPF 509	6.84-16.45 x10^{-6} m/s	± 3.77%
Soln. Flux MacPF AL7	5.98-14.35 x10^{-6} m/s	± 1.62%

The measured solution flux was corrected to 25°C using eq. (5.1). This empirical equation accounts for temperature effects on the density and viscosity of the solution (Armostrong, 1997). Temperature is given in °C and flux in m/s.

$$J_V(25°C) = J_V(T)\left[-0.575\ln(T) + 2.85\right] \tag{5.1}$$

5.3.3 Experimental Procedure

A total of eight membranes were used in the experiments (7 MacPF, 1 commercial, no duplicates). The membranes were initially stabilized at 0.5 MPa and 25°C in a 250 ppm NaCl solution. The flux and rejection were monitored every 8 hours until both parameters were stabilized (±1%). After stabilization, several experiments were performed. The experimental procedure for each run is described below:

1. Run the system with pure water until steady state is reached (4-8 h)

2. Measurement of the permeate flux and conductivity of permeate solution.
3. Switch the system to a test solution (neutral solutes, electrolytes, etc.).
4. Run the system until steady state is reached (at least 8 h)
5. Measurement of the solution flux, feed flow rate, and feed and permeate concentrations.
6. Run the system with pure water until steady state is reached (at least 8 h).
7. Measurement of pure water flux and conductivity of feed and permeate solutions.

The criterion for steady state was to let approximately 30-40 mL of permeate pass through the lowest flux membrane; approximately 6-8 h. For pure water runs, measurements were made until the permeate conductivity was lower than that of pure water (which was usually after 8 h). The permeate solution flux was measured by collecting permeate in pre-weighted bottles for a period of time.

5.3.4 Experimental Conditions

The experimental plan consisted of four types of experiments: standard experiments, single-salt experiments, mixed-salt experiments, and mixed solutes experiments. All experiments were carried out at room temperature, a feed flow of 1 L/min and an applied pressure of 0.3 to 1.5 MPa for system 1 and 0.3 to 0.9 MPa for system 2. All experiments in each set were randomized (pressure and concentration). The experimental conditions are listed in the following subsections. In all cases, the reported pressures are gauge pressures.

Standard experiments (Table 5.5) were performed every sixth run to monitor the performance (solute rejection and solution flux) of the commercial and MacPF membranes.

Table 5.5 Experimental conditions for Standard Experiment. Systems 1 and 2.

Variable	Settings
Solutes	NaCl
Concentration (ppm)	250
Pressure (MPa)	0.50 (System 1), 0.51 (System 2)

The performance of the membranes was evaluated using single electrolyte solutions. Membrane performance was compared between different solutes (NaCl, Na_2SO_4, or $MgCl_2$) at constant feed concentration and different operating pressures (Table 5.6). Sodium sulfate and magnesium chloride permeation experiments were not performed in the second system.

Table 5.6 Experimental conditions for runs with single electrolyte solutions (constant concentration). Systems 1 and 2.

Variable	Settings
Solute	System 1: NaCl, Na_2SO_4, or $MgCl_2$ System 2: NaCl
Concentration (mol/m^3)	5
Pressure (MPa)	System 1: 0.30, 0.50, 0.70, 0.90, 1.50 System 2: 0.30, 0.51, 0.72, 0.90

The effect of NaCl feed concentration at constant pressure (P = 0.5 MPa) was also analyzed for both NF systems. The conditions for these experiments are listed in Table 5.7.

Additionally, the permeation of mixed solute solutions (lactose and NaCl) was analyzed. The following two cases were considered: the effect of sodium chloride concentration on lactose permeation at constant lactose concentration (Table 5.8); and, the effect of lactose concentration on the permeation of sodium chloride at constant NaCl concentration (Table 5.9). These two sets of experiments were performed at constant pressure (P = 0.5 MPa).

Table 5.7 Experimental conditions for runs with sodium chloride at different concentrations. Systems 1 and 2.

Variable	**Settings**
Solute	NaCl
Concentration (ppm)	250, 500, 1000, 2000, 4000
Pressure (MPa)	0.50

Table 5.8 Experimental conditions for runs with sodium chloride in the presence of lactose. Systems 1 and 2.

Variable	**Settings**
Solute	NaCl and Lactose
Concentration (ppm)	[NaCl] = 250, 500, 1000, 2000, 4000 [Lactose] = 540
Pressure (MPa)	0.50

Table 5.9 Experimental conditions for runs with lactose in the presence of sodium chloride. Systems 1 and 2.

Variable	Settings
Solute	Lactose and NaCl
Concentration (ppm)	[Lactose] = 540 [NaCl] = 250, 500, 1000, 2000, 4000
Pressure (MPa)	0.50

Finally, the permeation of mixed electrolyte solutions was investigated. The effect of common counter-ions and common co-ions was analyzed. The experimental conditions are listed in Table 5.10. These experiments were only performed for system one.

Table 5.10 Experimental conditions for runs with mixed electrolytes solutions System 1.

Variable	Settings
Solutes	NaCl and Na_2SO_4
Concentration (mol/m^3)	$[Cl^-] = 5$ $[SO^=]/[Cl^-] = 1, 3, 6$
Pressure (MPa)	0.30, 0.50, 1.20

Variable	Settings
Solutes	NaCl and $MgCl_2$
Concentration (mol/m^3)	$[Na^+] = 5$ $[Mg^{++}]/[Na^+] = 1, 3, 6$
Pressure (MPa)	0.30, 0.50, 1.20

A total of 110 experiments were performed for system 1 (38 standards, 31 single electrolyte, 11 mixed solutes, and 30 mixed electrolytes) from which 21 were repeats (not including standard experiments). A total of 21 experiments were performed for system 2 (6 standards, 4 single electrolyte, and 11 mixed solutes) from which 2 were repeats (not including standard experiments). The tabulated data for each run are presented in Appendix B. No experiment at the same conditions was repeated in consecutive runs.

Every sixth run, a standard experiment was run to monitor changes in membrane performance over time. If any significant change in performance (flux and/or separation) was noted, then the membranes were regenerated using the following procedure: two hour permeation experiment with HCl (pH 2.0) and salt solution (250 ppm NaCl) at 0.50 MPa and feed flow of 1 L/min (room temperature).

5.3.5 Sample Analysis and Measurements

The concentration of single electrolyte solutions (Table 5.8) was measured using a conductivity meter (Radiometer CDM-210) with a conductivity cell (Radiometer CDC641T) with temperature compensation. The NaCl concentration in the presence of lactose was measured using an Orion 105 Conductivity Meter with an Orion epoxy /platinum conductivity cell with temperature correction.

All conductivity measurements were referenced to 25°C and the conductivity of pure water, on the particular day, was subtracted (about 3-7

μS/cm) from these measurements. Calibration curves were used to relate conductivity measurements to electrolyte concentration. The measurement error was 1.4% for conductivity measurements at 25°C. All measurements were performed at room temperature.

The concentration of lactose was measured with a Rosemount Analytical Dohrmann DC-190 carbon analyzer. The measurement error was 2.5%. Mixed electrolyte solutions were measured using either an ion-coupled adsorption device (ICAP 9000 Analyzer) or an ion chromatograph (Dionex model 4500i). The measurement errors were 1.2%, and 1%, respectively. All samples analyzed with the ICAP 9000 were diluted to less that 300 ppm total concentration. All samples analyzed with the Dionex were diluted to less than 100 ppm total concentration. The ICAP 9000 and Dionex were re-calibrated with standard solutions every time a new batch was analyzed (approximately every 150-200 samples).

5.4 General Safety Considerations

The following precautions were taken when working in the laboratory. Protective eyeware and laboratory coat were worn at all times. Non-latex gloves were worn while handling chemicals. For all chemicals the MSDS were read and understood. High pressures (up to 1.50 MPa) were used during the experiments, however, the fluids under high pressure were an incompressible liquid and a small amount of nitrogen-gas in the accumulator.

The experimental setup was inspected for leaks during operation. The Teflon tubing was checked for leaks, brittleness, and fatigue. All fitting and stainless steel were checked for leaks, salt buildup or rust. Before every experiment it was verified that electrical devices were properly grounded to prevent electric shock hazards. Routinely all electrical equipment was checked for wires in bad conditions (especially in pumps, stirrer, pressure safety device, switches).

Chapter VI

Results and Discussion

An analysis and discussion of the experimental results and model predictions are presented here. The mathematical transport model developed in Chapter IV was used both to fit and to predict the data and to interpret the performance of the membranes used in this investigation. The analysis is performed in a functional, non-chronological order, as follows.

First, the parameter estimation problem is discussed and the parameters (pore radius, pure water permeability, charge density) are estimated for all the membranes (commercial and pore-filled) using the transport model. Second, these same membrane parameters are estimated using the gel conformation model. Third, a comparison between the parameters estimated from the transport and gel models is performed.

Fourth, the experimental performances of the commercial and pore-filled membranes are analyzed using solutions containing different single salts, mixed electrolytes and mixed solutes. Fifth, a comparison between the experimental data and the transport model predictions is made to evaluate the adequacy of the model. Finally, the results are discussed and a general analysis of the advantages and limitations of the transport model is presented.

6.1. Determination of Membrane Parameters

The parameter estimates obtained from the transport and gel models are presented in this section. The parameter estimation procedure is described for both models. The parameter estimates are compared to each other and to parameters found in the literature.

6.1.1 Procedure for Parameter Estimation

The procedure to obtain the membrane parameters is outlined in this section. The parameter estimates are presented in sections 6.1.2 and 6.1.3 for the transport and gel models, respectively. A discussion and interpretation of the significance of the parameter estimates is given in subsequent sections. The membrane parameters for the gel model are estimated as detailed by Mika and Childs (2001) and summarized in section 4.3.3. The estimation procedure for the transport model is as follows.

The pure water permeability (L_P) is obtained by fitting eq. (4.35b) to the measured pure water flux of the membrane at different pressures (see section 6.2.3). The osmotic and streaming potential terms are neglected in eq. (4.35b). In the presence of compaction, eqs. (4.40) and (4.35b) are used to obtain the pure water permeability at zero pressure (L_{PO}) and the compaction coefficient (α_o). These parameter estimates are presented in section 6.1.2 (Table 6.1).

The pore radius (r_P) and the surface charge density (q_w) are obtained simultaneously by fitting the transport model to data (see section 6.2.5.1) from

mixed-solute systems (Lactose and NaCl). The ratio of effective membrane thickness to water content (λ/E) is obtained from the Hagen-Poiseuille (eq. 3.11). These parameter estimates are presented in section 6.1.2 (Table 6.2).

The dependency of the surface charge density on ionic strength is estimated from the same data set (mixed-solute system). The commercial membrane is fitted with a linear model (eq. 4.41a) and the MacPF membranes are fitted with a Langmuir-type isotherm (eq. 4.41b). These parameter estimates are presented in section 6.1.2 (Table 6.3). Model calculations and experimental data for this specific dependency are presented in Appendix D.

The effect of concentration polarization was investigated and found to be negligible, as discussed in section 6.2.1. Thus, for this dissertation, concentration polarization effects are assumed to be negligible. The membrane parameters in all cases are obtained under this assumption.

6.1.2 Membrane Parameters Obtained from the Transport Model

The parameter estimates for the commercial and MacPF membranes are presented in Tables 6.1-6.3. The model parameters are consistent with the data as indicated by the narrow 95% confidence intervals of the parameter estimates (Tables 6.1-6.3).

The permeability of the MacPF membranes (508, 509, AL7) prepared with PP substrates is almost linear throughout the pressure range. On the other hand the permeability of the MacPF membranes (352, 324, 382) prepared with PE

substrates is a strong function of pressure. The degree of compaction of the membranes, α_o, prepared with a PP substrate is 2-3 times smaller (Table 6.1) than the degree of compaction of the PE membranes, which agrees with experimental observations (section 6.2.3).

Table 6.1 Transport model parameter estimates for the pure water permeability and 95% confidence intervals for the linear permeability model (L_P) and the exponential permeability model (L_{PO}, α_O).

Membrane	Linear	Exponential	
	$L_P \times 10^9$ m/(kPa s)	$L_{PO} \times 10^9$ m/(kPa s)	$\alpha_O \times 10^3$ (-)
HN-7450	8.494 ± 0.52	N/A	N/A
MacPF 352	1.944 ± 0.75	2.983 ± 0.26	0.519 ± 0.12
MacPF 324	3.251 ± 0.41	4.1248 ± 0.34	0.539 ± 0.01
MacPF 382	13.223 ± 1.95	17.745 ± 5.71	0.349 ± 0.30
MacPF 515	44.156 ± 0.62	73.815 ± 1.23	0.694 ± 0.71
MacPF 508	12.145 ± 0.04	13.761 ± 0.62	0.166 ± 0.24
MacPF 509	18.538 ± 0.12	21.043 ± 1.58	0.169 ±0.32
MacPF AL7	16.199 ± 0.02	17.803 ± 0.94	0.126 ± 0.45

The pure water permeabilities estimated (Table 6.1) here for the MacPF membranes (352, 324, 382) agree with the physicochemical properties listed in Table 5.1. Membrane permeability increases (1.94, 3.25, 13.22) with decreasing mass gain (188, 185, 57.7%) and decreasing membrane thickness (158, 108, 78 μm), as expected. The compressibility (or degree of compaction) of these

membranes is correlated to the mass gain of each membrane. However, the degree of cross-linking of the polyelectrolyte has no obvious effect on the compressibility of the membranes prepared with PE or PP substrates (Table 5.1 and Table 6.1).

The compressibility of the MacPF membranes is dependent on both the substrate and the pore-filling polyelectrolyte. However, from the experimental data and parameter estimates, the type of substrate seems to be the determining factor in pressure-induced compaction.

Table 6.2 Transport model parameter estimates and 95% confidence intervals for the commercial and MacPF membranes: pure water permeability (L_P), pore radius (r_P), surface charge density * (q_w) and ratio of effective membrane thickness to water content (λ/E).

Membrane	**L_P x 10^9 m/(kPa s)**	**r_P (nm)**	**q_w (mC/m^2)**	**λ/E (μm)**
HN-7450	8.494 ± 0.52	0.565 ± 0.08	-11.18	5.26
MacPF 352	1.944 ± 0.75	3.482 ± 0.94	10.01	568.49
MacPF 324	3.251 ± 0.41	4.551 ± 1.05	12.74	1006.08
MacPF 382	13.223 ± 1.95	3.562 ± 0.62	0.34	100.00
MacPF 515	44.156 ± 0.62	3.524 ± 1.25	0.46	39.33
MacPF 508	12.145 ± 0.04	3.253 ± 0.79	1.19	121.89
MacPF 509	18.538 ± 0.12	7.451 ± 2.31	4.96	418.92
MacPF AL7	16.199 ± 0.02	5.648 ± 0.45	10.71	275.44

* The surface charge density was calculated using the parameters from Table 6.3 and a NaCl solution (5 mol/m^3).

For all membranes, the transport model parameters (Table 6.2) are in the range normally found for NF membranes. The pore radius is small for the commercial membrane (r_P = 0.56 nm) and larger for the MacPF membranes (r_P = 3 to 6 nm). The effective thickness of the MacPF membranes is in agreement with the experimental measurements presented in Table 5.1 (λ > 100 μm). The parameter estimates of the membrane HN-7450 are comparable to those of the membrane Nitto Denko NTR-7450 (r_P = 0.70 nm, λ/E = 0.74 μm, L_P = 8.68 x 10^9 m/s kPa), which is an optimized version of the former (Wang et al., 1995b).

Table 6.3 Transport model parameter estimates and 95% confidence intervals for the commercial and MacPF membranes for the charge density dependency on concentration*.

Membrane	**A x 10^5 mol m/mC**	**B x 10^2 (m^3/mol)**	**q_w (mC/m^2)**	**C_X (mol/m^3)**
HN-7450	-0.15 ± 0.01	-9.68 ± 1.23	-11.18	-410.16
MacPF 352	23.5 ± 4.12	13.5 ± 5.35	10.01	59.52
MacPF 324	36.2 ± 7.95	18.4 ± 10.23	12.74	58.05
MacPF 382	0.36 ± 0.24	0.57 ± 0.42	0.34	1.98
MacPF 515	0.51 ± 0.16	0.95 ± 0.45	0.46	2.73
MacPF 508	1.52 ± 0.78	2.7 ± 0.12	1.19	7.62
MacPF 509	0.41 ± 0.53	0.43 ± 0.85	4.96	13.81
MacPF AL7	18.24 ± 3.97	7.02 ± 2.34	10.71	39.33

* Constants A and B and estimates of the surface charge density (q_w) and volumetric charge density (C_X) for a NaCl solution (5 mol/m^3).

The surface charge densities (q_w) of the highly charged MacPF membranes (352, 324, 509 and AL7) are comparable to that of the commercial membrane (Table 6.3 and Appendix D). However, the effective volumetric charge density (C_X) of the MacPF membranes is one order of magnitude lower compared to the commercial membrane and opposite in sign. The difference in charge densities is proportional to the larger pore radius of the MacPF membrane compared to the commercial membrane.

Overall, parameter estimates are independent of starting guesses as long as these guesses are physically reasonable. Parameter estimates are relatively insensitive to the number of data points used in the estimation procedure. The parameter estimates are more dependent on the quality than on the quantity of data, which agree with previous findings (Garcia-Aleman, 1998). As the number of data point decreases the 95% confidence intervals increase, but the parameter estimates are statistically equal to those estimates obtained with a whole data set (i.e., within 95% confidence intervals).

6.1.3 Membrane Parameters Obtained from the Gel Model

The parameter estimates obtained independently from the gel model (see section 4.3.3) for the MacPF membranes 515, 508, 509 and AL7 are presented in Table 6.4. The membrane parameters are adjusted according to the conversion factors presented in Table 4.1. The parameter estimates for the membranes with the PP substrate are obtained assuming that the polymer volume fraction, and

hence permeability, of the polyelectrolyte gel is nearly constant with applied pressure within the pressure range studied here. This assumption is valid, as demonstrated in section 6.2.3 and Mika et al. (2001).

The permeability of the MacPF 352, 324 and 382, and hence the polymer volume fraction, vary with pressure. A constant polymer volume fraction is a prerequisite to predict the membrane parameters using the gel model. Therefore, no gel model parameter estimates are provided for the MacPF membranes 352, 324 and 382.

Table 6.4 Gel model parameter estimates for the MacPF membranes: pure water permeability (L_P), pore radius (r_P), surface charge density (q_w) membrane thickness (Δx) and the ratio of effective membrane thickness to water content (λ/E) *.

Membrane	**L_P x 10^9 (m/(kPa s))**	**r_P (nm)**	**q_W (mC/m^2)**	**Δx (μm)**	**λ/E (μm)**
MacPF 515	16.27	2.46	18.01	129	51.69
MacPF 508	27.27	2.78	17.8	124	39.53
MacPF 509	45.77	3.15	17.67	119	30.25
MacPF AL7	17.02	2.45	18.01	122	49.01

* The ratio of effective membrane thickness to water content is calculated from the Hagen-Poiseuille and the gel model estimates of L_P and r_P. The membrane thickness is measured, as discussed in section 5.2.

The pure water permeabilities (L_P) and pore radii (r_P) obtained from the gel model are inversely proportional to the degree of DBX cross-linking as shown in

Table 5.1. This suggests that the polyelectrolyte gel either partially collapses into the pore wall or into other polyelectrolyte chains as the degree of cross-linking increases and the polymer chains stiffen. The estimates of the pore radius are in the range expected for the MacPF membranes (> 2 nm).

The ratio of effective membrane thickness to water content shown in Table 6.4 is calculated from the Hagen-Poiseuille using the gel transport estimates for the pore radius and pure water permeability. The ratio of effective membrane thickness to water content obtained here (λ/E) is 50-60% smaller than the measured thickness (Δx) of the membrane, which is not realistic. The effective thickness takes into account the porosity and tortuosity of the membrane, and therefore, should be larger than the thickness of the membrane or substrate. This contradiction may be due to the assumption that fully developed, parabolic flow exists. While the real membranes have complex flow around networks of polymer chains.

On the other hand, the ratio of effective membrane thickness to water content can also be obtained from the thickness of the membrane if the porosity and tortuosity of the membrane are known. From Mika and Childs (2001) the porosity and tortuosity of these membranes are assumed to be 84% and 2.5, respectively. Therefore, the effective thickness for the membranes 515, 508, 509, and AL7 are 384, 363, 354, and 363 μm, respectively. Then, from the Hagen-Poiseuille, the pore radii for these membranes are calculated as 6.69, 8.49, 10.78, and 6.65 nm, respectively. The effective membrane thicknesses and pore radii

obtained by this approach are more realistic (λ/E >100 μm, r_P > 1-2 nm) and have better agreement with the estimates obtained from the transport model, as discussed below.

6.1.4 Discussion and Comparison of Model Parameters

The parameter estimates from the transport (TM) and gel (GM) models are compared and discussed in this section. This comparison is necessary as outlined in section (1.9). The theoretical design and true tailor making of the MacPF membrane relies on the assumption that the membrane parameters can be predicted using the gel model. Then these parameters can be used with the transport model to predict membrane performance. Therefore, it is necessary to compare the membrane performance predicted exclusively from theory (gel model plus transport model) and that predicted by extrapolation (transport model fitted with experimental data).

From Tables 6.2 and 6.4, we can observe that the parameter estimates between both models are within an order of magnitude. However, most estimates are statistically different, except for the permeability of the membrane AL7.

The parameters obtained from measurements of the membrane thickness are comparable (20-50%) to the transport model parameter estimates, especially for the membranes 509 and AL7. At first, this seems like a large variation. However, when the predicted performance of both models is compared to the experimental data (Figs 6.1-6.2), the model predictions for rejection deviate 10-

12% on average. Solution flux predictions for the membrane 509 are within 3% for the transport model and above 100% error for the gel model (Fig. 6.1b). Solution flux predictions for the membrane AL7 are within 2% for both models (Fig. 6.2b).

The predicted rejection of both models is similar because of the trade off between steric and electrostatic contributions to solute rejection by the membrane. Some of the deviations encountered are explained by changes in the physicochemical parameters of the membranes, especially the MacPF 509. See section 6.2.2 for details.

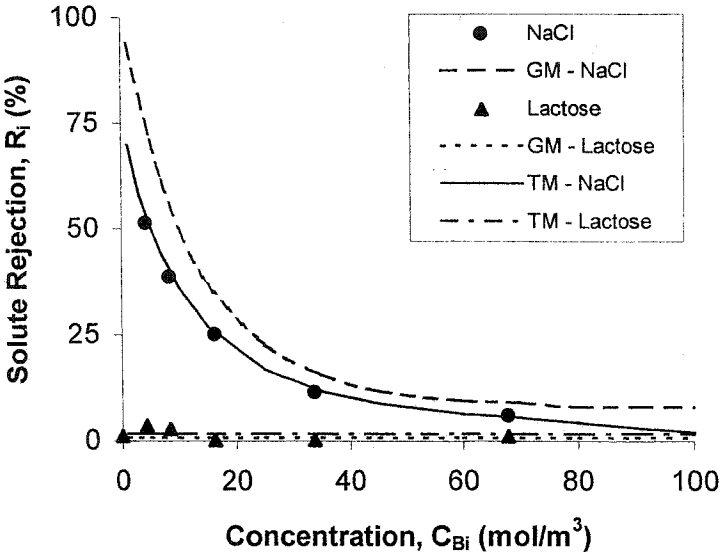

(a)

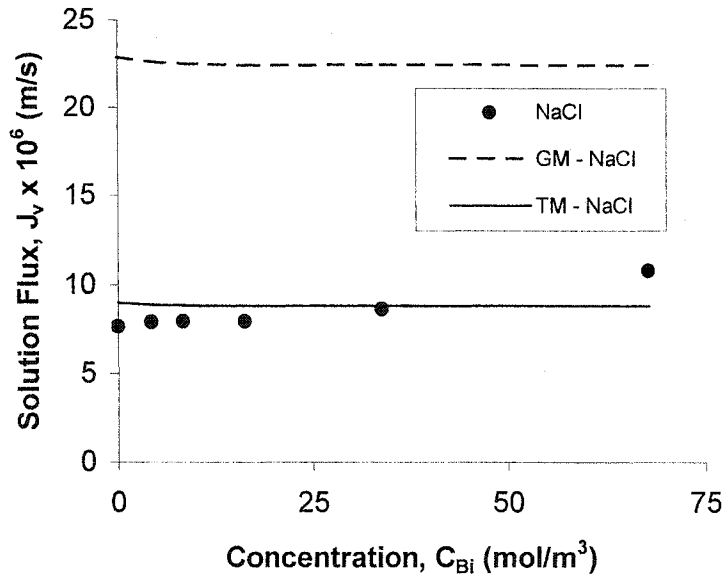

(b)

Figure 6.1 Comparison of the experimental and modeled performance of the MacPF membrane 509 for a NaCl:lactose solution as a function of NaCl feed concentration (0-4000 ppm) at constant lactose concentration (500 ppm) and constant applied pressure (ΔP = 0.5 MPa). Points are experimental data. Lines are TM calculations or GM predictions. a) rejection, b) solution flux.

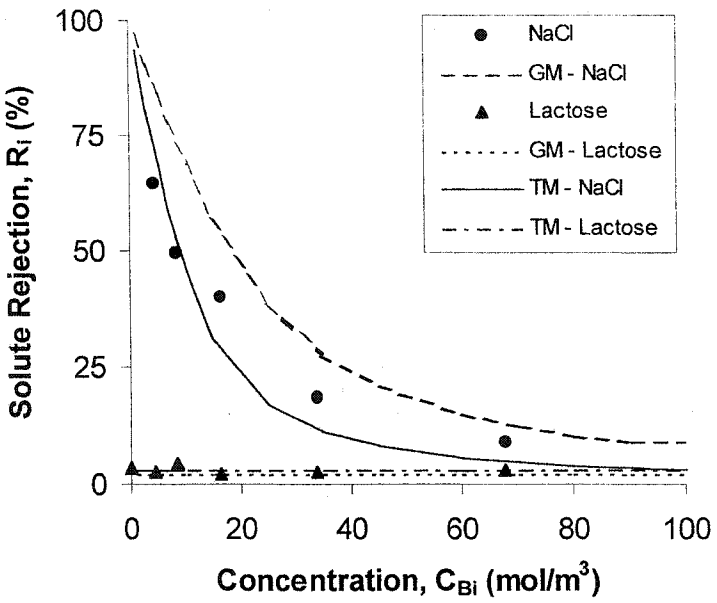

(a)

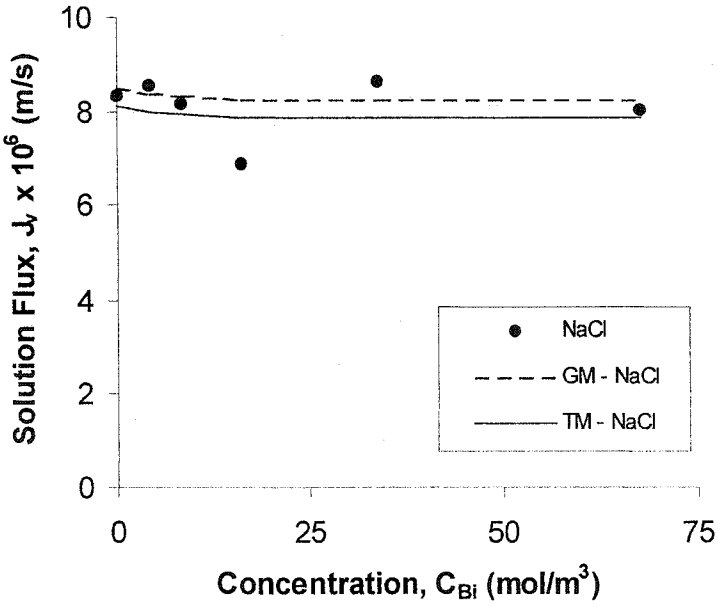

(b)

Figure 6.2 Comparison of the experimental and modeled performance of the MacPF membrane AL7 for a NaCl:lactose solution as a function of NaCl feed concentration (0-4000 ppm) at constant lactose concentration (500 ppm) and constant applied pressure (ΔP = 0.5 MPa). Points are experimental data. Lines are TM calculations or gel model GM predictions. a) rejection, b) solution flux.

6.2 Membrane Performance: Interpretation of Experimental and Modeled Results

The experimental and modeled results are presented and discussed in the following sections. The experimental data are presented in the following order: standard experiments (section 6.2.2), pure water flux as a function of pressure; (section 6.2.3); membrane performance using single electrolytes as a function of pressure (section 6.2.4.1) and concentration (section 6.2.4.2); membrane performance using mixed solutes (section 6.2.5); and, membrane performance using mixed electrolytes with a common counter-ion (section 6.2.6.1) and a common co-ion (section 6.2.6.2-6.2.6.3). For all figures containing experimental data, lines are model calculations or predictions and points are experimental data.

6.2.1 Concentration Polarization

Concentration polarization effects are assumed to be negligible for the operating conditions and experimental setup used in this investigation. Garcia-Aleman (1998) calculated the mass transfer coefficient using film theory and the Kimura-Sourirajan Analysis, as proposed by Mehdizadeh (1990). Results indicate that the concentration in the bulk solution and in the feed side of the membrane differ by less than 2-3%. Therefore, the concentrations in the feed side of the membrane and in the feed solutions are considered to be essentially the same.

6.2.2 Standard Experiments

Every sixth run, a standard experiment was run to monitor changes in membrane performance (solution flux and separation) over time. The standard experiment consisted of a 250 ppm NaCl solution at room temperature and 0.50 and 0.51 MPa for systems one and two, respectively. The results of the standard experiments for all the membranes are presented in Figure 6.3. Outliers and data obtained when the membranes required regeneration are included in the figure, but eliminated for calculating the average results and deviations, as presented in Table 6.5.

Table 6.5 Average rejection and solution flux for standard experiments. Outliers were eliminated from the calculations.

Membrane	**Rejection** R_i **(%)**	**Solution Flux** $Jv \times 10^6$ $m^3/(m^2s)$
HN-7450	79.51 ± 3.98	1.19 ± 0.12
MacPF 352	81.37 ± 4.07	1.43 ± 0.14
MacPF 382	73.61 ± 3.68	3.93 ± 0.39
MacPF 324	10.61 ± 0.53	6.87 ± 1.53
MacPF 515	11.22 ± 3.12	20.23 ± 9.52
MacPF 508	75.05 ± 15.75	9.31 ± 0.93
MacPF 509	43.93 ± 2.19	21.06 ± 2.12
MacPF AL7	66.72 ± 3.34	8.26 ± 0.83

The general trend for the commercial membrane was an increase in solution flux over the course of this investigation (Fig. 6.3a). Rejection decreased

periodically until the membrane was regenerated. The standard performance of the MacPF membranes 352 and 324 were stable throughout the experiments (Figs. 6.3b and 6.3c, respectively), except from the period in which the membrane 324 required regeneration (Fig. 6.3c). Membrane performance stabilized after the regeneration was performed. The rejection of the membrane 382 decreased considerably during the course of the experiments (Fig. 6.3d). However, the flux remained constant. Membrane regeneration had no effect on the standard performance of this membrane (MacPF 382).

The standard performance of the MacPF membranes 515, 508 and 509 was statistically constant during the first 10 standard experiments (Figs. 6.3e-g). However, rejection increased and solution flux decreased on later experiments.

The standard performance of the MacPF membrane AL7 was statistically constant throughout this investigation (Fig. 6.3h). Regeneration had only a small effect on the performance of this membrane (AL7).

In summary, the performance of the commercial and MacPF membrane is relatively stable during the course of this investigation. The MacPF membranes made by photografting (352, 324, 382) proved to be more stable than the membranes made by *in situ* cross-linking (515, 508, 509, AL7), as shown in Fig. 6.3. The performance of the commercial (HN-7450) and MacPF membranes (352, 324, 382) remain fairly constant during the 5-year long test period. The performance of the MacPF membranes (515, 508, 509, AL7) slowly changed with time during the 2.5-year long test period, except for the membrane AL7.

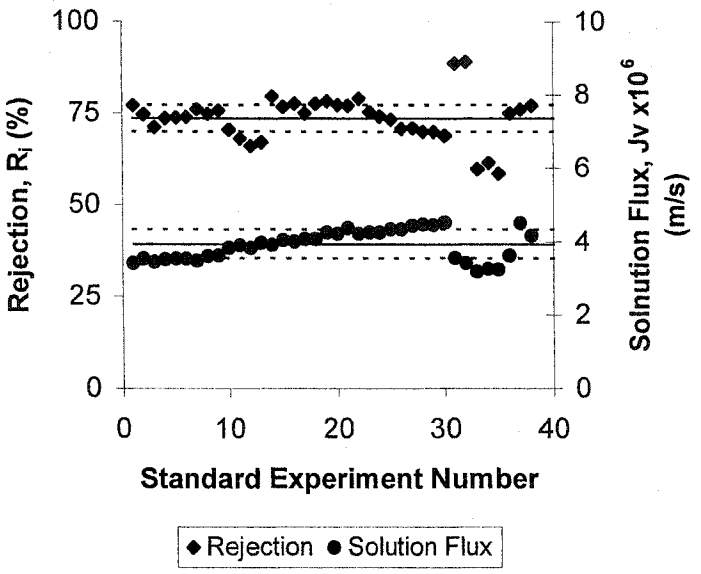

(a) HN-7450

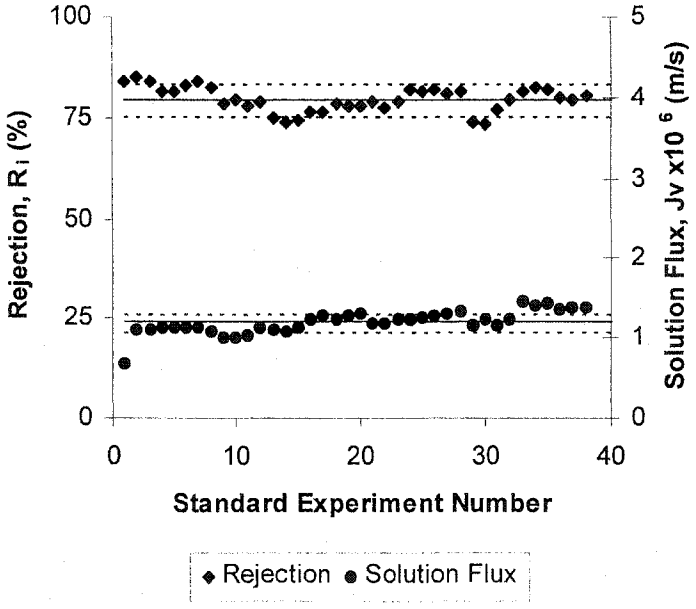

(b) MacPF 352

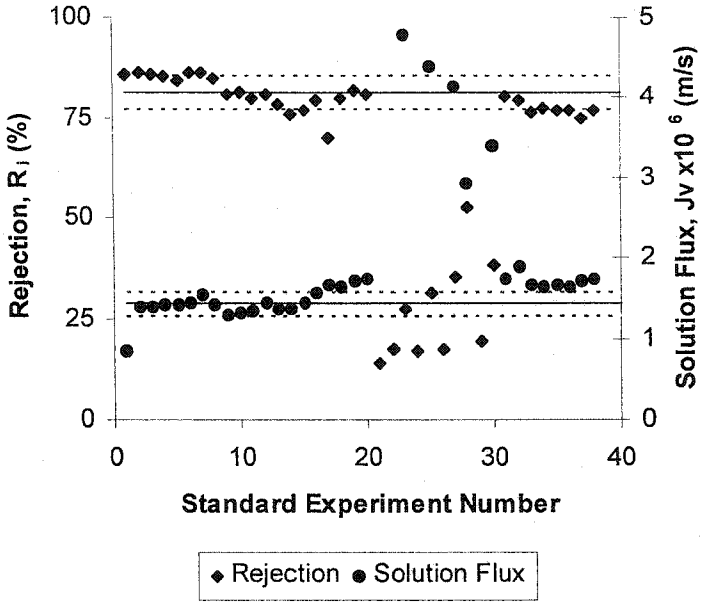

(c) MacPF 324

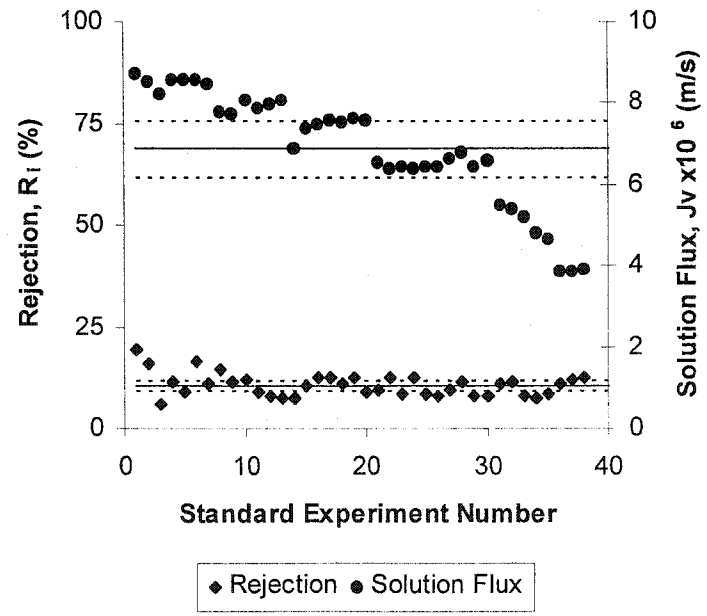

(d) MacPF 382

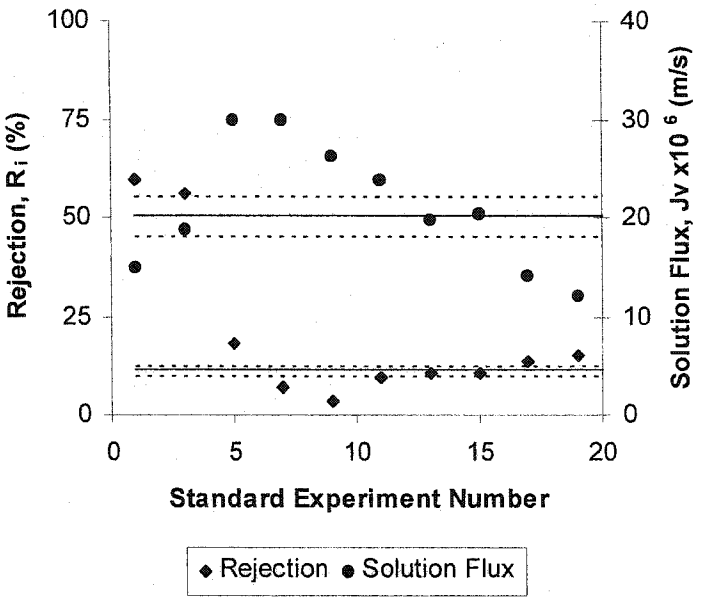

(e) MacPF 515

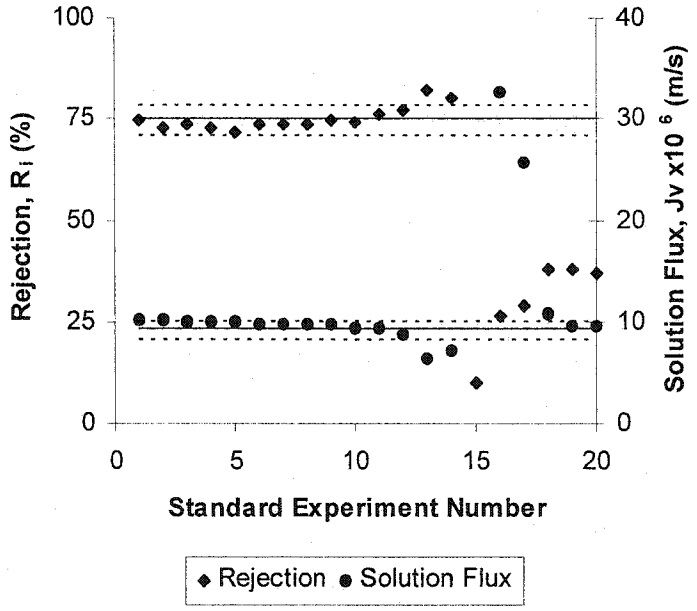

(f) MacPF 508

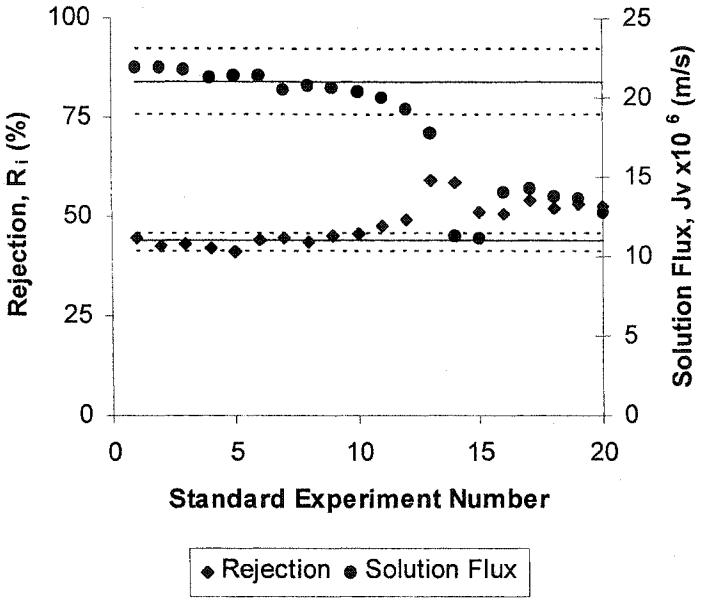

(g) MacPF 509

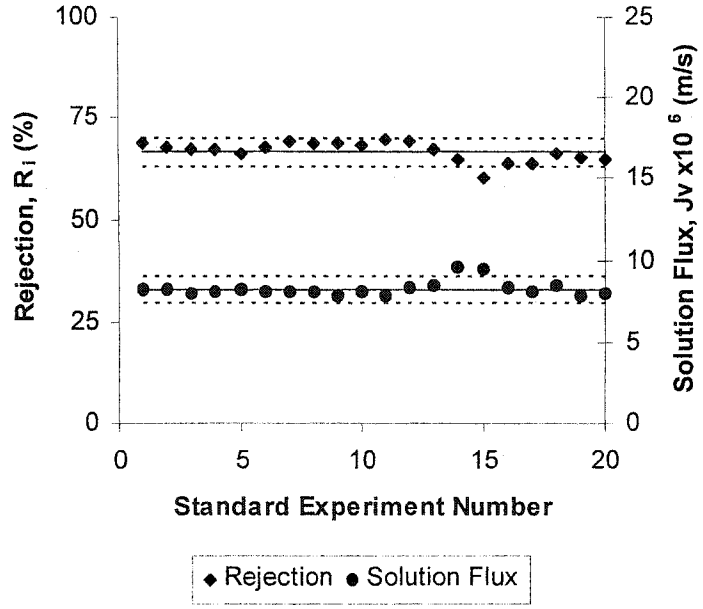

(h) MacPF AL7

Figure 6.3 Membrane performance vs. standard experiment number ([NaCl] = 250 ppm, ΔP = 0.5 MPa). Points are experimental data. Lines are the mean value (-) and 95% confidence intervals (--). Membranes: a) HN-7450 and MacPF b) 352, c) 324, d) 382, e) 515, f) 508, g) 509, and h) AL7.

6.2.3 Permeation Experiments with Pure Water Solutions

The effect of applied pressure on membrane flux and permeability is analyzed in this section. Experiments with de-ionized (pure) water were conducted at different applied pressures (ΔP = 0.3-1.5 MPa). The experimental data and model calculations are presented in Figure 6.4. The pure water permeability for all membranes was calculated as described earlier (section 6.1.1).

In the absence of compaction or fouling, the pure water flux should increase linearly with pressure (i.e., constant permeability). The relationship between flux and pressure is linear for the commercial membrane (Fig 6.4a). The MacPF membranes with a polyethylene (PE) substrate have a nonlinear pressure-flux relationship (Figs. 6.4b-d) at higher pressures ($\Delta P > 0.5$ MPa) caused by pressure-induced compaction of the substrate, as discussed earlier (section 6.1.2). This relationship is nearly linear at low pressures ($\Delta P < 0.5$ MPa). The pressure-flux relationship is nearly linear for the MacPF membranes made with a polypropylene (PP) substrate (Figs. 6.4e-h).

From Figures 6.4b and 6.4d we can observe that membrane permeability (PE substrate) is nearly linear until a critical pressure is reached (ΔP = 0.7-0.8 MPa). Above this pressure, the permeability of the membrane has an exponential decay proportional to the operating pressure and the degree of compaction. Parameters for fitting these data are presented already in Table 6.1.

Model predictions for solution flux are in agreement with experimental data within ±0.05 m/s (HN-7450) and ±0.10-0.13 m/s (MacPF).

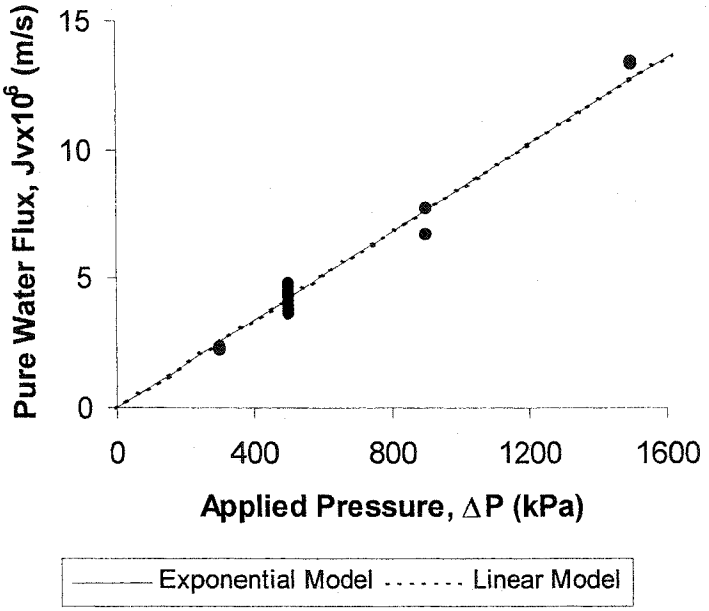

(a) HN-7450

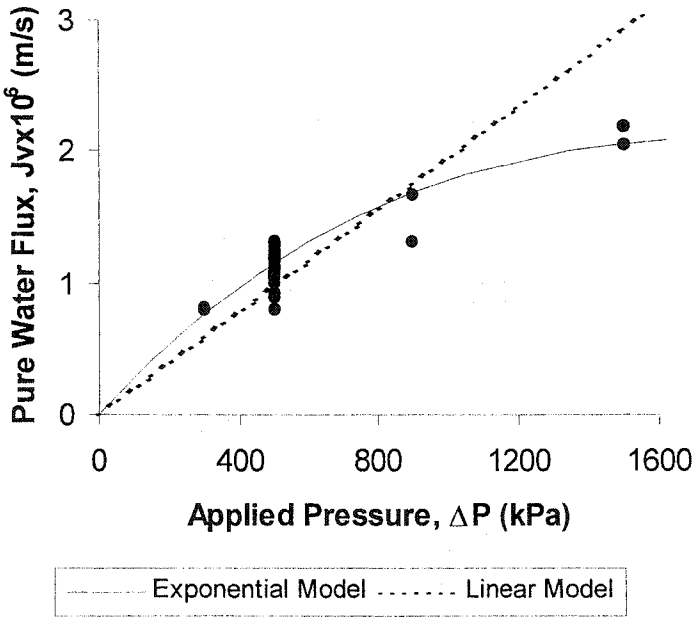

(b) MacPF 352

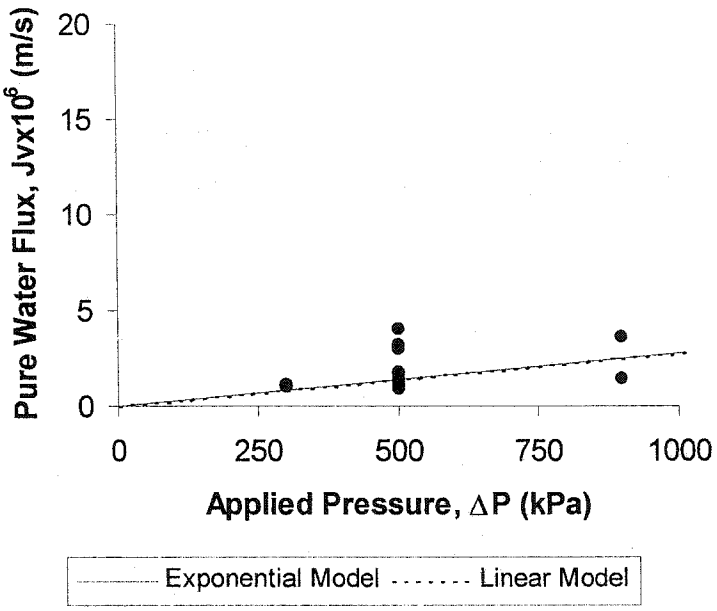

(c) MacPF 324

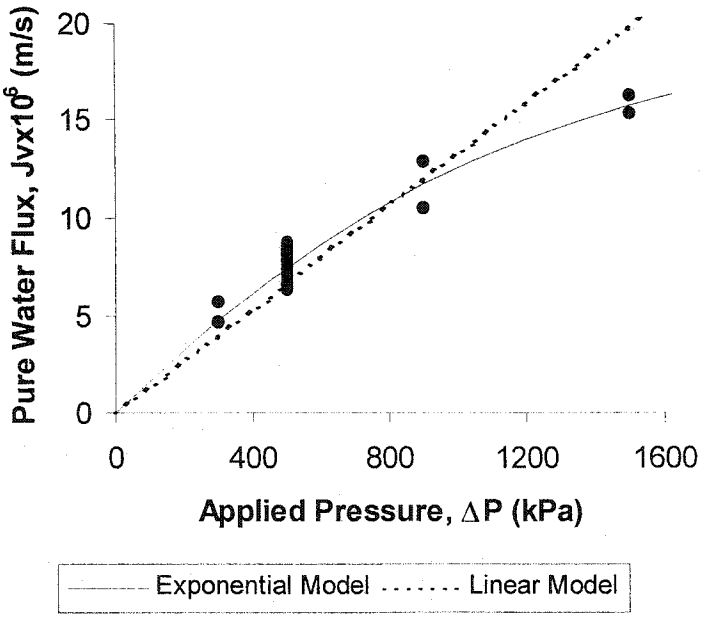

(d) MacPF 382

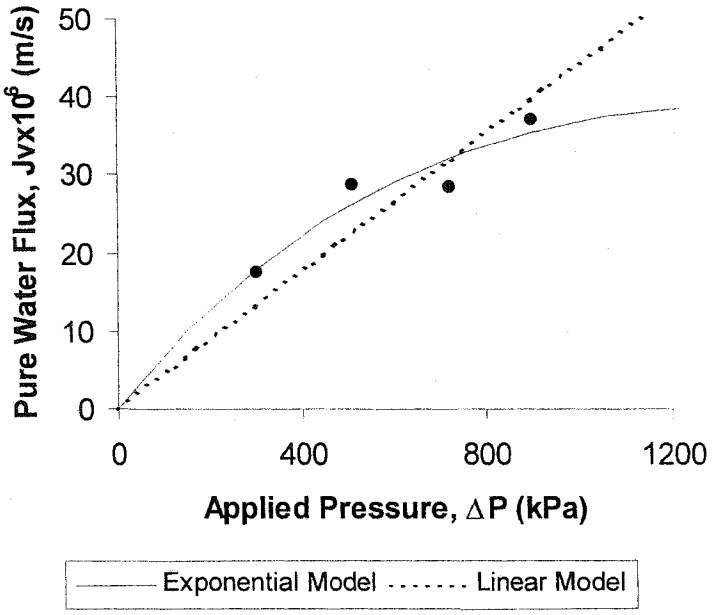

(e) MacPF 515

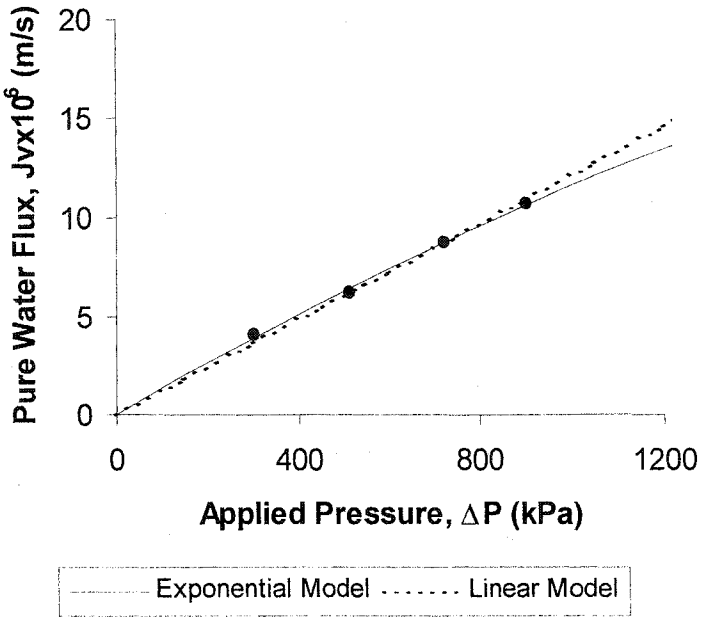

(f) MacPF 508

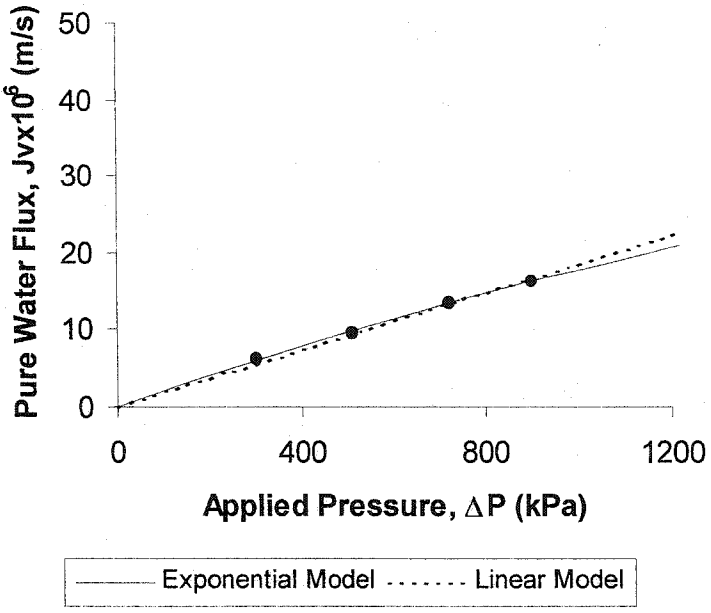

(g) MacPF 509

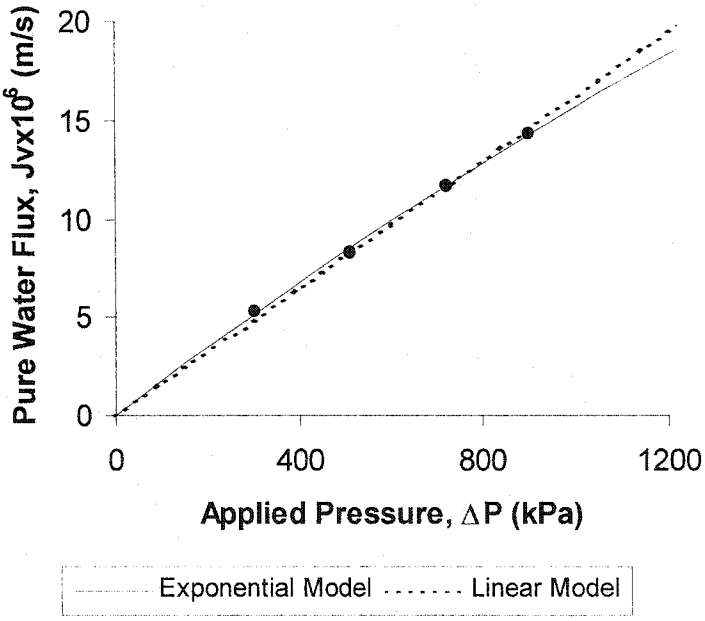

(h) MacPF AL7

Figure 6.4 Pure water flux as a function of applied pressure (ΔP = 0.3-1.5 MPa). Points are experimental data. Lines are obtained from eq. (4.35) assuming constant (--) permeability and from eq. 4.40 assuming varying (—) permeability. Membranes: a) HN-7450 and MacPF b) 352, c) 324, d) 382, e) 515, f) 508, g) 509, and h) AL7.

6.2.4 Permeation Experiments with Single Electrolytes

Experimental results for single salts are presented in this section. The effect of salt type, concentration and pressure on membrane performance is analyzed. Model predictions are presented and discussed.

6.2.4.1 Permeation Experiments with NaCl, $MgCl_2$ and Na_2SO_4 at Constant Concentration

The permeation of NaCl, $MgCl_2$ and Na_2SO_4, as single salts, is analyzed in this section. Magnesium chloride and sodium sulfate experiments were conducted only for the commercial membrane (HN-7450) and the MacPF membranes 352, 324 and 382. Salt feed concentration is kept constant (5 mol/m^3) and pressure is varied (ΔP = 0.3-1.5 MPa). The experimental and predicted performances are presented in Figs. 6.5 to 6.14.

Salt rejection increases with increasing solution flux, as expected. Rejection increases with increasing pressure because more water permeates through the membrane, while the concentration driving force for the solute remains essentially constant. Thus, the permeate stream is further diluted as pressure increases. At higher pressures, rejection plateaus at a maximum rejection that, in theory, is proportional to $1-\sigma_i$ (Stavermann, 1951). This qualitative behavior is observed in all the membranes analyzed here (Figs. 6.5-6.14). The quantitative differences arise from the different physicochemical parameters of each membrane.

The MacPF membranes 352 and 324 have nearly identical rejection (± 4%) between each of the three single salts (Figs 6.7a and 6.9a). However, the membrane 324 produces 30% more permeate, on average, than the membrane 352 (Figs. 6.7b and 6.9b). For these membranes steric effects are relatively unimportant and rejection follows the Donnan exclusion mechanism. The rejection of the divalent co-ion (Mg^{++}) is high (≈90+%), of the monovalent co-ion (Na^{+}) is intermediate (75%), and of the divalent counter-ion ($SO_4^{=}$) is low (20%).

The membrane 382 has a lower charge density, thus, salt rejection is low (< 25%) in the absence of steric effects (Fig. 6.10a). One interesting aspect of this membrane is that the rejection of Na_2SO_4, as a single salt, is considerably larger than the rejection of $MgCl_2$ and NaCl. The causes of this behavior are discussed later (section 6.2.2). The membrane 515 has a low charge density too, thus salt rejection is low (<10%), as observed in Figure 6.11a.

The MacPF membranes 508, 509 and AL7 have a similar NaCl rejections (R_{NaCl} = 50-75%) (Figs. 6.12a-6.14a), but significantly different fluxes (Figs. 6.12b-614b). These experimental findings suggest that NF membranes with different characteristics can achieve a similar performance, which agree with previous findings (Garcia-Aleman, 1998). The similar performance occurs because of the trade-off between steric and electrostatic contributions to ion rejection by the membrane.

The same selectivity mechanism (Donnan) is observed in the commercial membrane as in the highly charged MacPF membranes (Fig. 6.5). The divalent

($SO_4^{=}$) and monovalent (Cl^-) co-ions are highly rejected (70-95%). However, the rejection of the divalent counter-ion (Mg^{++}) is also high (90%), which contradicts Donnan exclusion theory. The negatively charged membrane is highly attracted to the divalent counter-ion (Mg^{++}), however, due to high steric effects, magnesium ions are retained by the membrane. Another consideration to the unusual multivalent counter-ion permeation is the absorption of the counter-ion by the membrane, and subsequent charge inversion. See section 6.2.2 for details.

The solution flux of the commercial membrane follows the expected linear behavior with increasing applied pressure. The MacPF membranes follow the nonlinear behavior (Fig. 6.7b, 6.9b-6.14b) already discussed in section 6.2.3. Solution flux can be affected by the concentration and type of the ions permeating through the membrane. However, due to the dilute nature of the solutions used here this effect is small (Fig. 6.5b-6.14b). From Figs. 6.7b and 6.9b-6.10b there appears to be a trend of decreasing flux with increasing valence of the counter-ion. However, this effect cannot be accurately quantified due to experimental error.

Model calculations of the concentration profile inside the commercial and MacPF 352 membranes are presented in Fig 6.6 and 6.8, respectively. The rejection mechanisms for single salt solutions are qualitatively the same for the commercial (Fig. 6.6) and the MacPF membranes (Fig. 6.8). Ions are transported by the same mechanisms and the quantitative differences in concentration originate from the steric and electrostatic contributions of each membrane.

From Fig. 6.8 we can observe that the concentration profile inside the membrane is nearly linear at low pressures. This behavior indicates that diffusion is the main transport mechanism at low pressures. As applied pressure increases, the concentration profile becomes non-linear due to the contribution of convective transport to overall ion transport. In the presence of convection, the concentration gradient is initially nearly independent of axial position. In the latter sections of the membrane, the concentration gradient increases significantly according to the nonlinear model.

Model predictions for salt rejection are in qualitative and quantitative agreement with experimental data (NaCl and $MgCl_2$) within ±4.5% (HN-7450) and ±2.7% (MacPF), except for Na_2SO_4 predictions where the deviation grows to a maximum of ±6.2% for the MacPF membranes.

Model predictions for solution flux are in agreement with experimental data (NaCl and $MgCl_2$) within ±0.41 m/s (HN-7450) and ±0.17 m/s (MacPF), except for Na_2SO_4 predictions where the deviation grows to a maximum of ±0.53 m/s for the MacPF membranes.

The transport model predicts accurately the solution flux of the membrane 508 (Fig. 6.12b). However, rejection is predicted poorly. This implies that the changes observed in this membrane throughout this investigation are caused by a decrease in the effective charge density of the membrane and not on a change in membrane permeability.

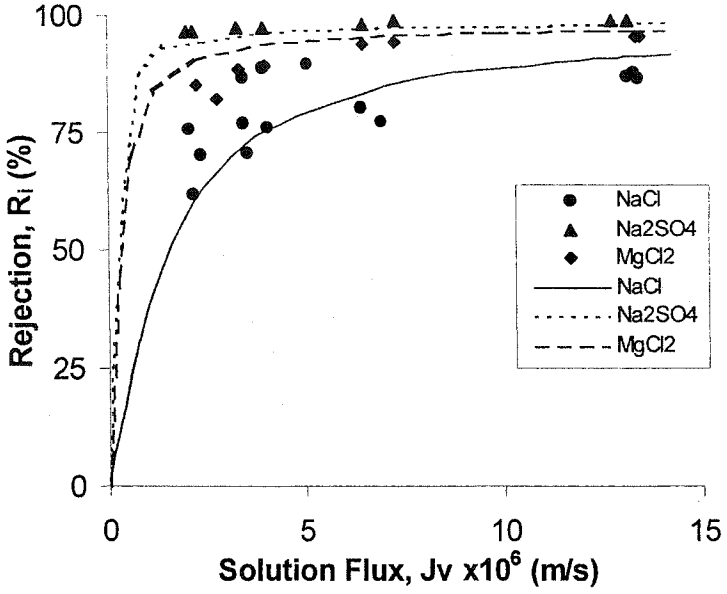

(a)

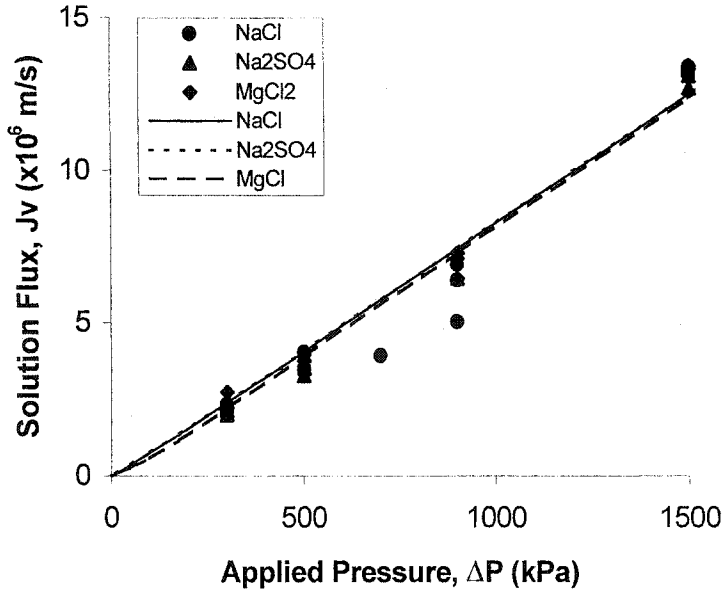

(b)

Figure 6.5 Membrane performance (HN-7450) for single salt solutions (NaCl, Na_2SO_4, and $MgCl_2$) as a function of applied pressure (ΔP = 0.3-1.5 MPa) and constant feed concentration (5 mol/m^3). Points are experimental data. Lines are model predictions. a) salt rejection vs. solution flux and b) solution flux vs. applied pressure.

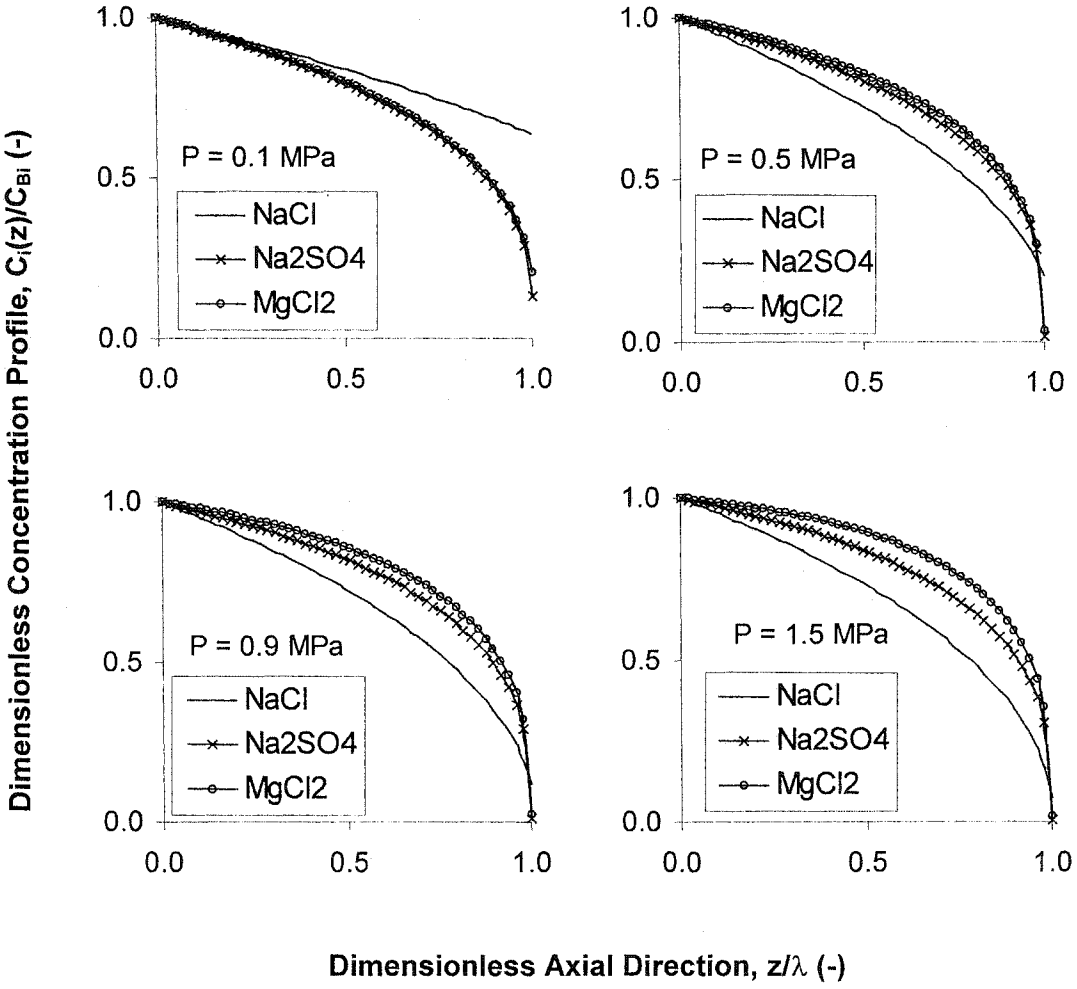

Figure 6.6 For membrane HN-7450, dimensionless concentration profile vs. dimensionless axial direction for NaCl, Na_2SO_4, and $MgCl_2$ as single salts (feed concentration = 5 mol/m^3) at different applied pressures.

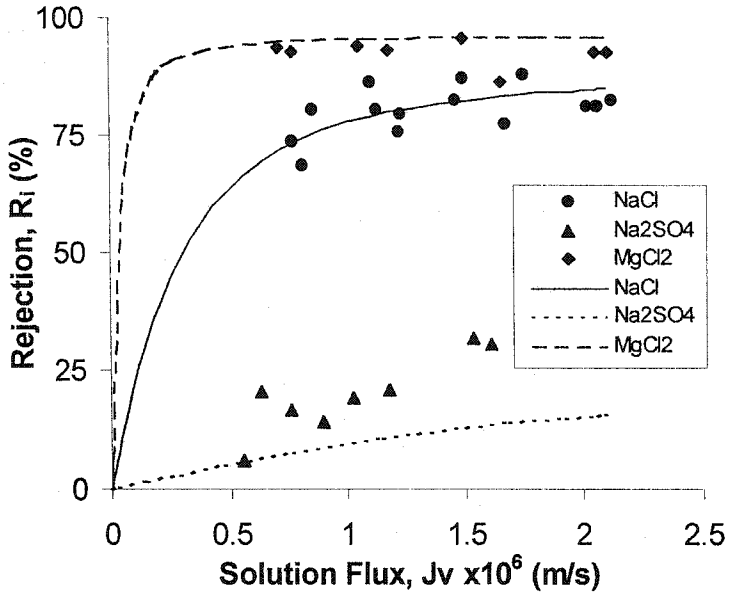

(a)

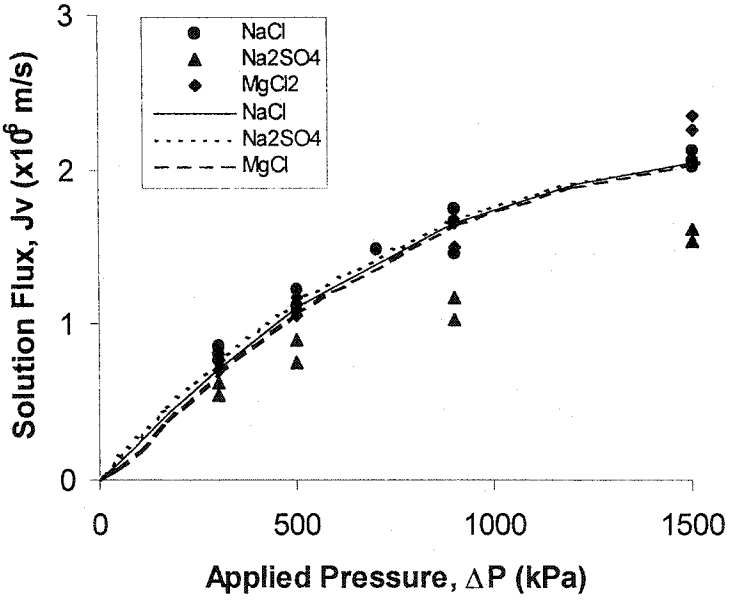

(b)

Figure 6.7 Membrane performance (MacPF 352) for single salt solutions (NaCl, Na_2SO_4, and $MgCl_2$) as a function of applied pressure (ΔP = 0.3-1.5 MPa) and constant feed concentration (5 mol/m^3). Points are experimental data. Lines are model predictions. a) salt rejection vs. solution flux and b) solution flux vs. applied pressure.

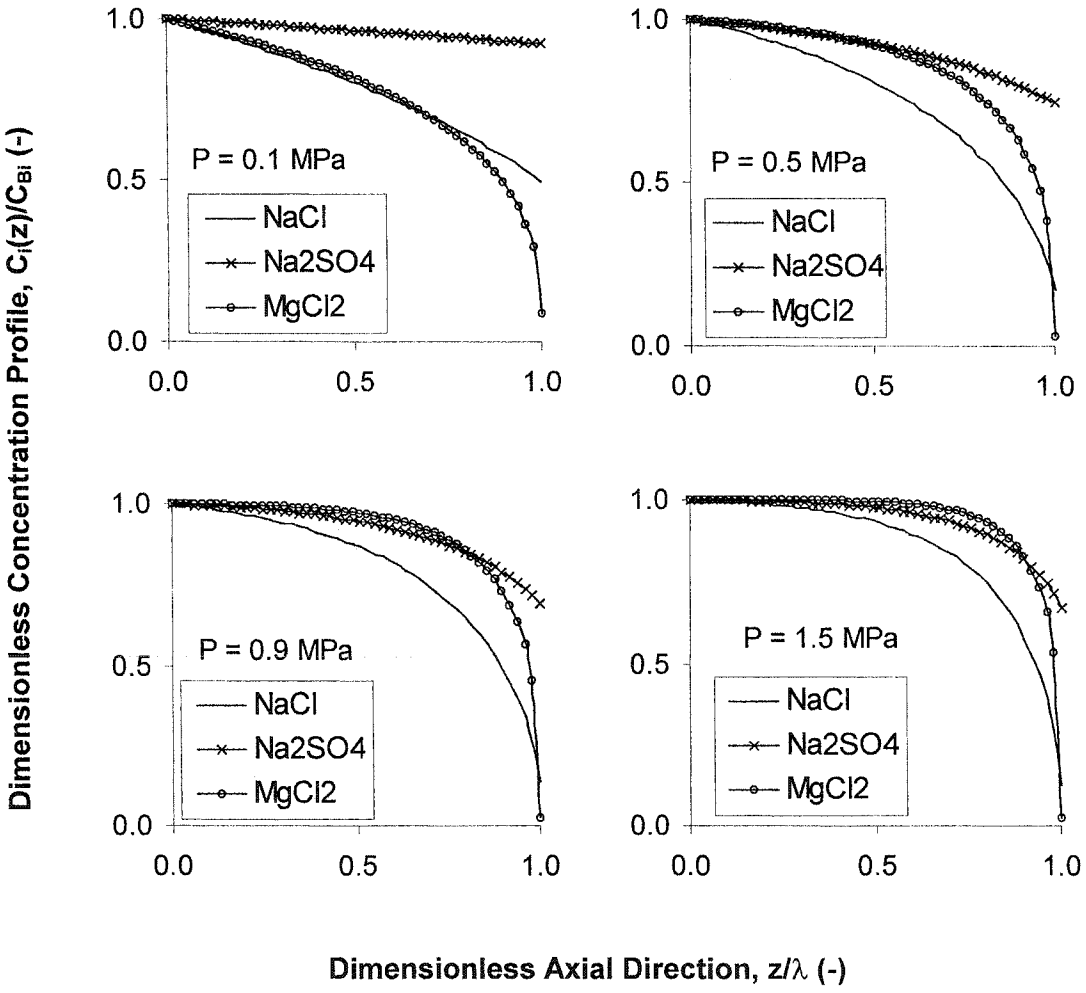

Figure 6.8 For membrane MacPF 352, dimensionless concentration profile vs. dimensionless axial direction for NaCl, Na_2SO_4, and $MgCl_2$ as single salts (feed concentration = 5 mol/m^3) at different applied pressures.

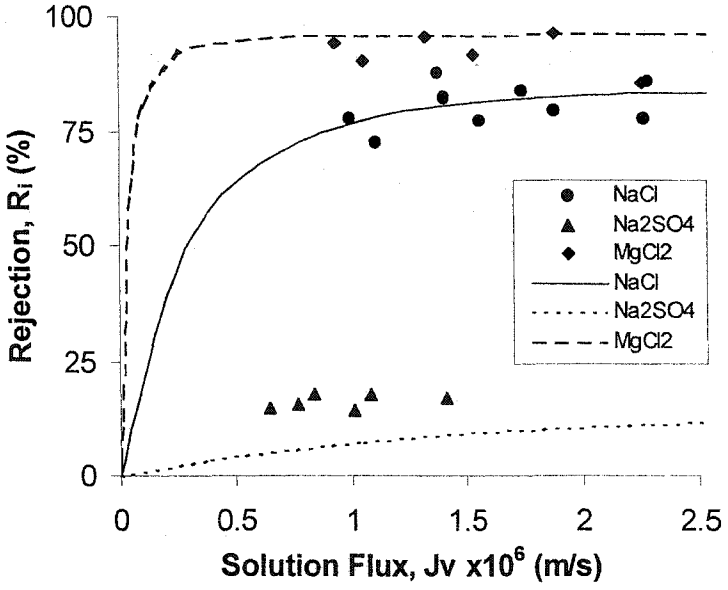

(a)

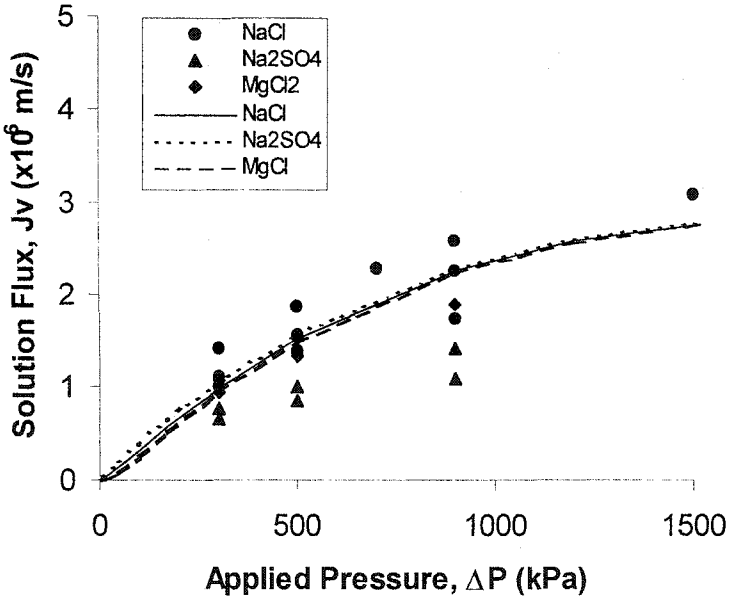

(b)

Figure 6.9 Membrane performance (MacPF 324) for single salt solutions (NaCl, Na_2SO_4, and $MgCl_2$) as a function of applied pressure (ΔP = 0.3-1.5 MPa) and constant feed concentration (5 mol/m^3). Points are experimental data. Lines are model predictions. a) salt rejection vs. solution flux and b) solution flux vs. applied pressure.

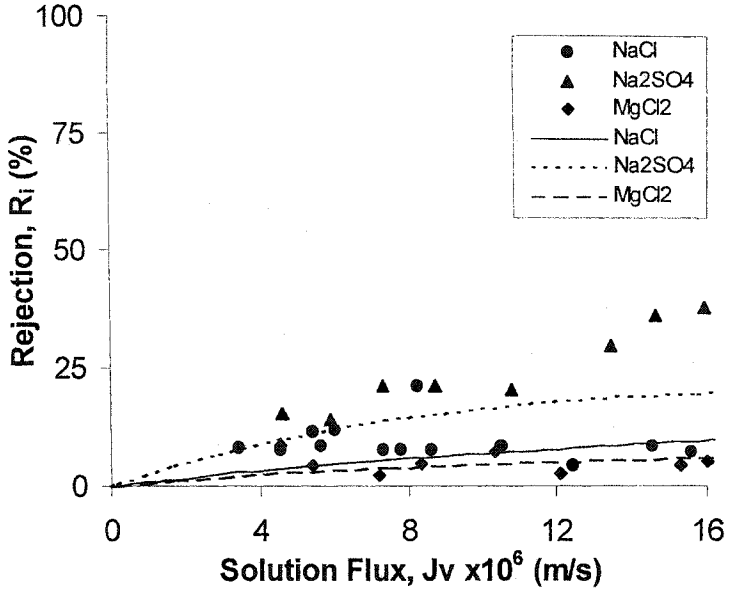

(a)

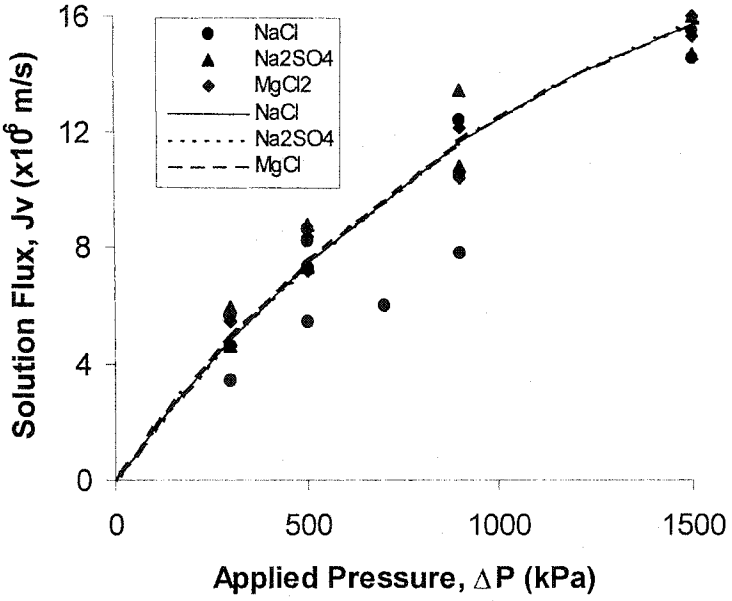

(b)

Figure 6.10 Membrane performance (MacPF 382) for single salt solutions (NaCl, Na_2SO_4, and $MgCl_2$) as a function of applied pressure (ΔP = 0.3-1.5 MPa) and constant feed concentration (5 mol/m^3). Points are experimental data. Lines are model predictions. a) salt rejection vs. solution flux and b) solution flux vs. applied pressure.

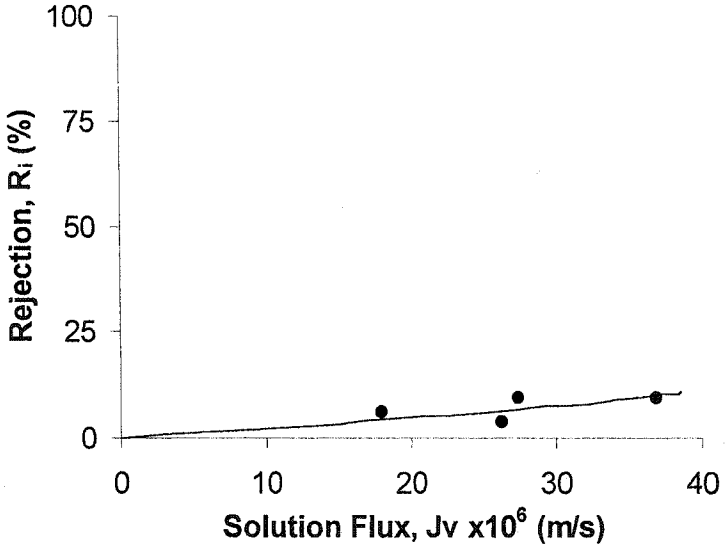

(a)

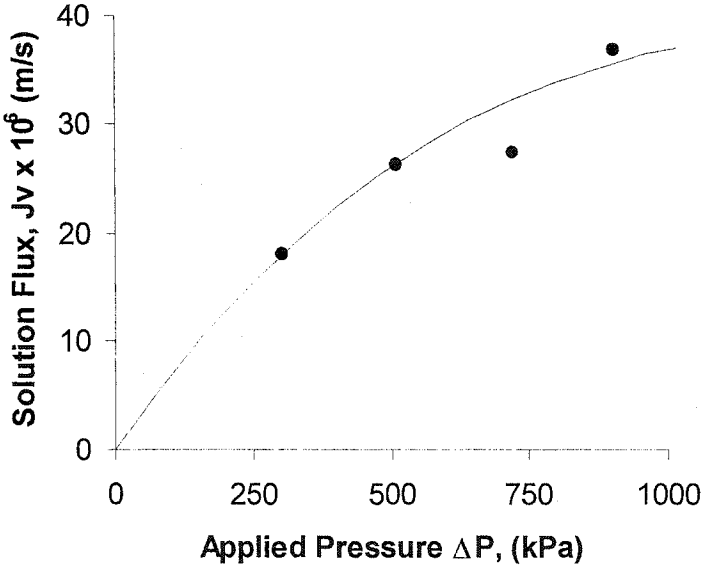

(b)

Figure 6.11 Membrane performance (MacPF 515) for single salt solutions (NaCl) as a function of applied pressure (ΔP = 0.3-0.9 MPa) and constant feed concentration (5 mol/m^3). Points are experimental data. Lines are model predictions. a) salt rejection vs. solution flux and b) solution flux vs. applied pressure.

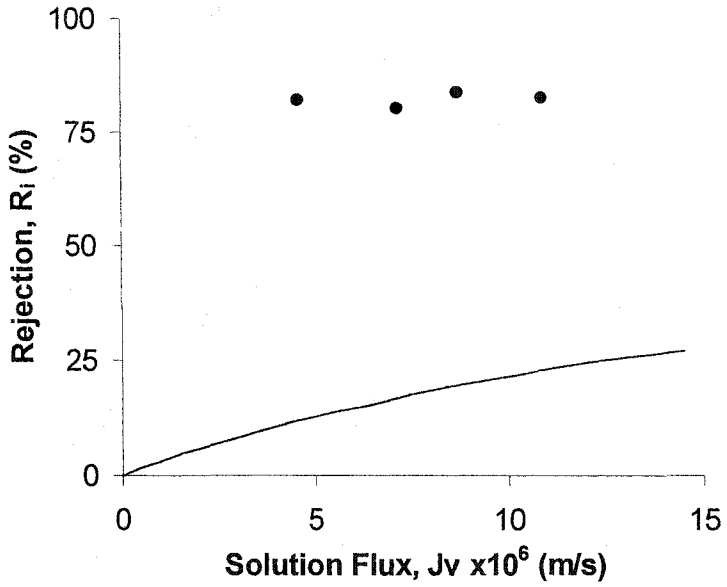

(a)

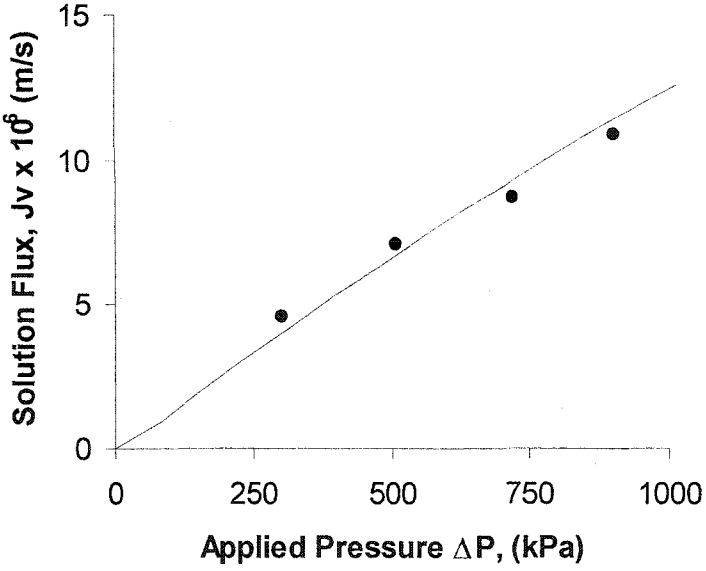

(b)

Figure 6.12 Membrane performance (MacPF 508) for single salt solutions (NaCl) as a function of applied pressure (ΔP = 0.3-0.9 MPa) and constant feed concentration (5 mol/m^3). Points are experimental data. Lines are model predictions. a) salt rejection vs. solution flux and b) solution flux vs. applied pressure.

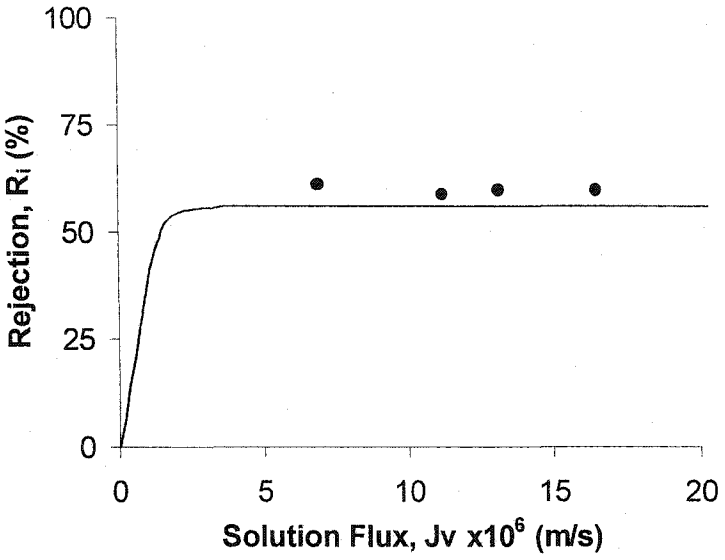

(a)

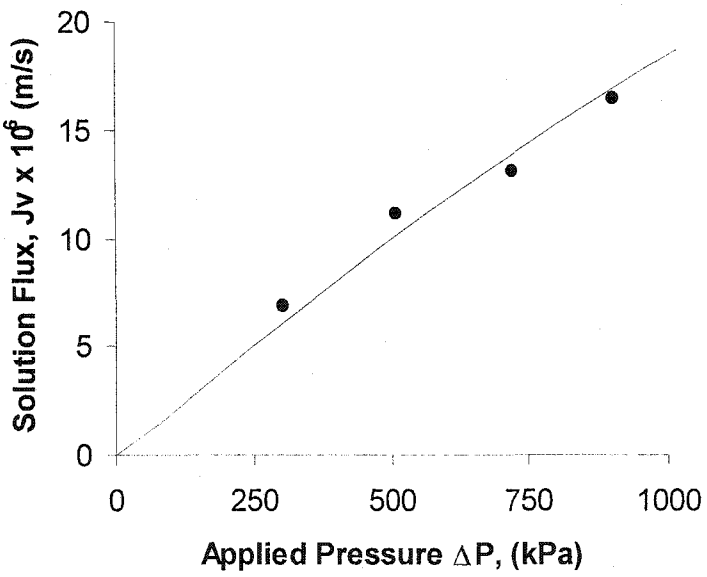

(b)

Figure 6.13 Membrane performance (MacPF 509) for single salt solutions (NaCl) as a function of applied pressure (ΔP = 0.3-0.9 MPa) and constant feed concentration (5 mol/m^3). Points are experimental data. Lines are model predictions. a) salt rejection vs. solution flux and b) solution flux vs. applied pressure.

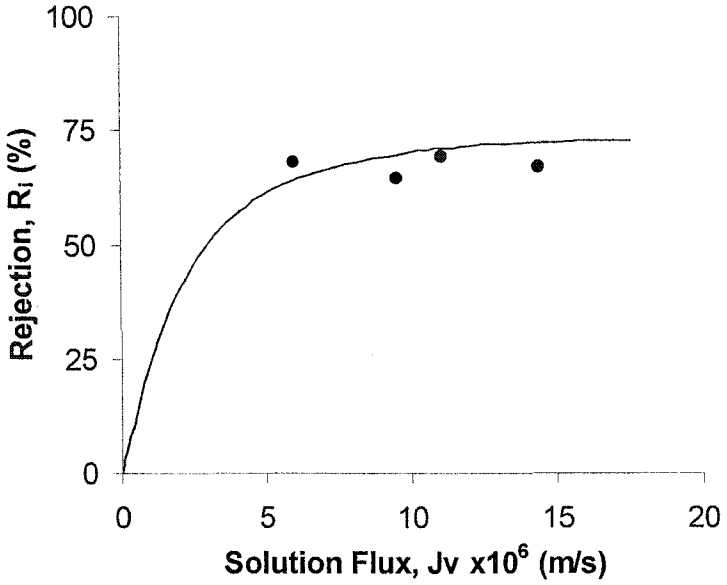

(a)

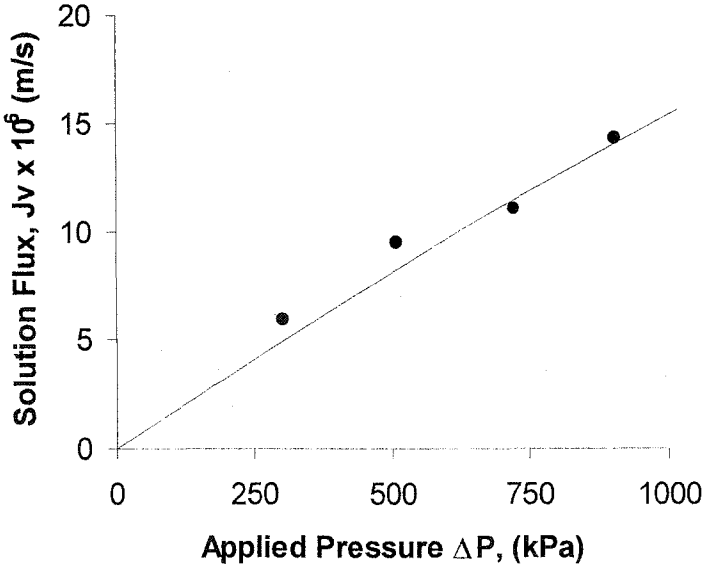

(b)

Figure 6.14 Membrane performance (MacPF AL7) for single salt solutions (NaCl) as a function of applied pressure (ΔP = 0.3-0.9 MPa) and constant feed concentration (5 mol/m^3). Points are experimental data. Lines are model predictions. a) salt rejection vs. solution flux and b) solution flux vs. applied pressure.

6.2.4.2 Permeation Experiments with NaCl: Effect of Salt Concentration on Membrane Performance

The effect of sodium chloride feed concentration on rejection at constant operating pressure is analyzed in this section. Sodium chloride feed concentration is increased from 4-70 mol/m^3 (250-4000 ppm) at constant operating pressure (0.5 MPa). The experimental results and model predictions are presented in Fig. 6.15.

All membranes present the same qualitative behavior. Salt rejection and solution flux decrease with increasing feed solution concentration (Fig 6.15). As feed concentration increases, more counter-ions are available to shield the effective charge of the membrane, thus decreasing the charge density in the membrane and salt rejection. Additionally, increasing feed concentration increases the effective osmotic pressure in the system, thus reducing the effective pressure driving force. However, at low concentrations, as the ones used here, the contribution of osmotic pressure is small (less than 6%).

The membranes HN-7450, 352, 324 and AL7 have similar performance ($R_{NaCl} \approx$ 65-75%) at low feed concentrations (5-10 mol/m^3). Rejection decreases with concentration. However, the rejection of the MacPF membranes (Figs. 6.15b, c, h) is more dependent on feed concentration compared to the membrane HN-7450 (Fig. 6.15a). The rejection of the commercial membrane appears to plateaus ($R \approx$ 25%) at high feed concentrations, while the rejection of the MacPF membranes keeps decreasing with increasing concentration (below $R \approx$ 10-15%). The rejection of both membranes decreases with concentration, however the rate

of change is larger in the MacPF membranes compared to the commercial membrane.

The membrane 509 has a lower rejection (~10% less) compared to the highly charged MacPF membranes (352, 324 and AL7). However, the dependency of rejection on concentration (Fig. 6.15g) is qualitatively the same as the other membranes, especially MacPF AL7.

The MacPF membranes with low charge densities (382, 515 and 508) have the same qualitative behavior as the other MacPF membranes. However, from Figs. 6.15d-f, rejection appears to be nearly independent of concentration. In reality, rejection still is a strong function of concentration, however, the changes are not appreciable because of the low rejection of these membranes.

The MacPF membrane 508 has a stronger concentration dependency than the other lowly charged membranes. However, rejection is still less dependent on concentration at concentrations higher than 20 mol/m^3. As mentioned before, the performance of the membrane 508 changed throughout the course of this investigation. Originally, this membrane had intermediate NaCl rejection (60-75%) at low concentrations (5 mol/m^3) (Fig. 6.12a).

Model predictions for salt rejection are in qualitative and quantitative agreement with experimental data within ±4.5% (HN-7450) and ± 2-8% (MacPF) throughout the concentration range. The largest deviations were observed for the membranes with low rejection, especially at low feed concentrations.

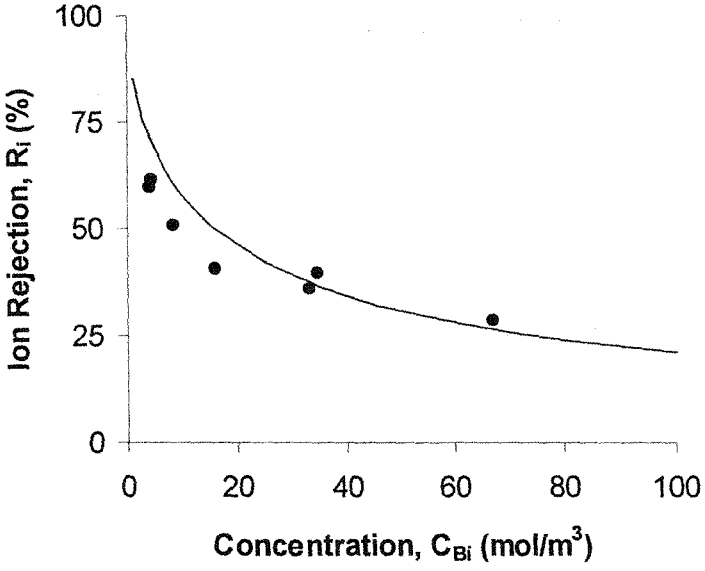

(a) HN-7450

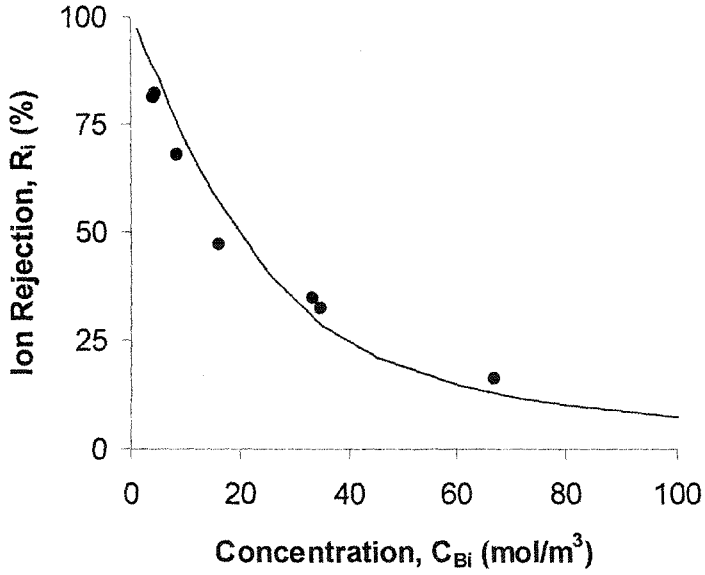

(b) MacPF 352

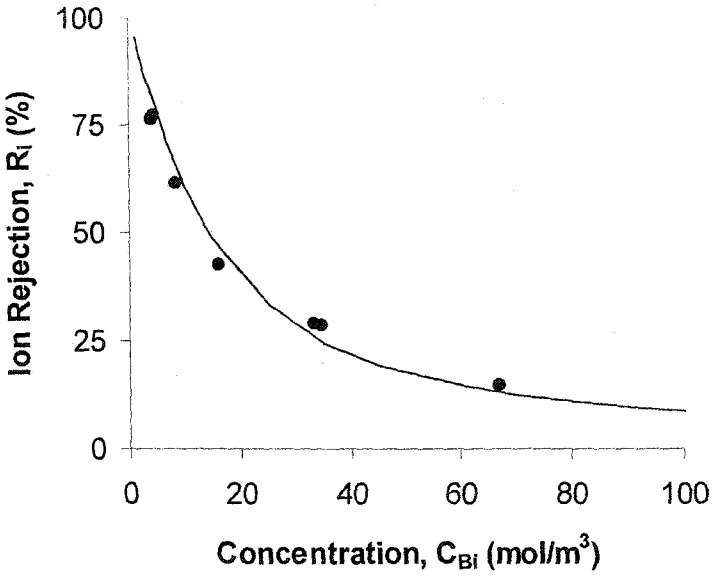

(c) MacPF 324

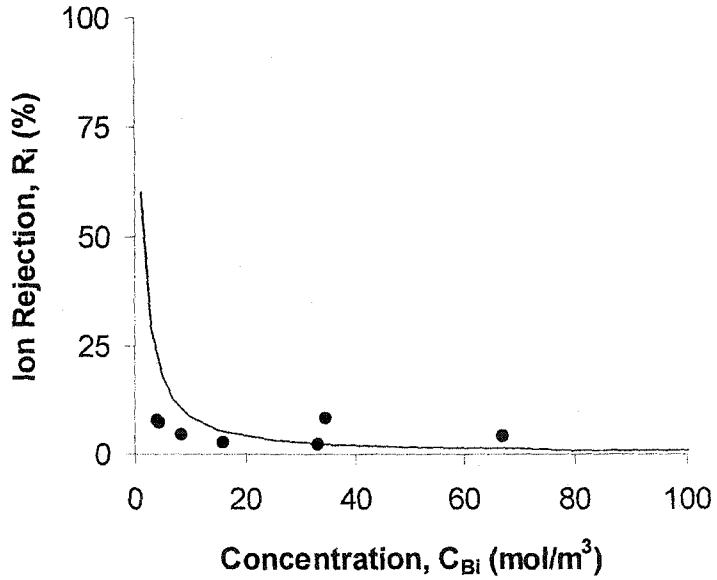

(d) MacPF 382

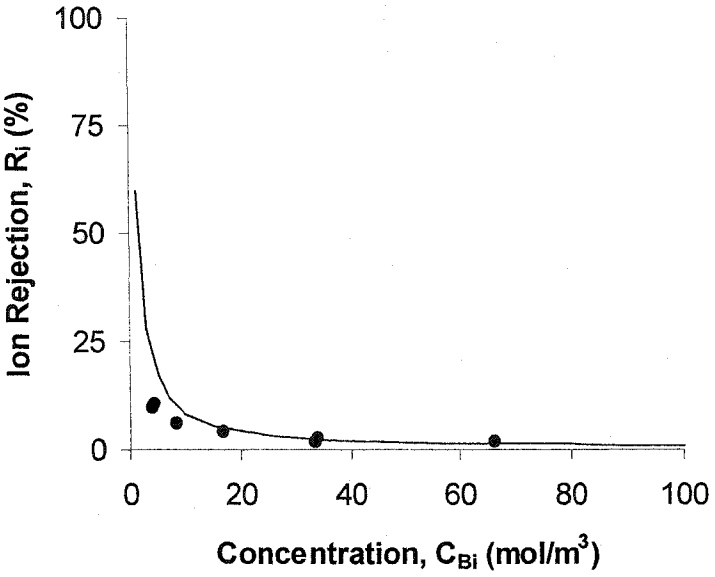

(e) MacPF 515

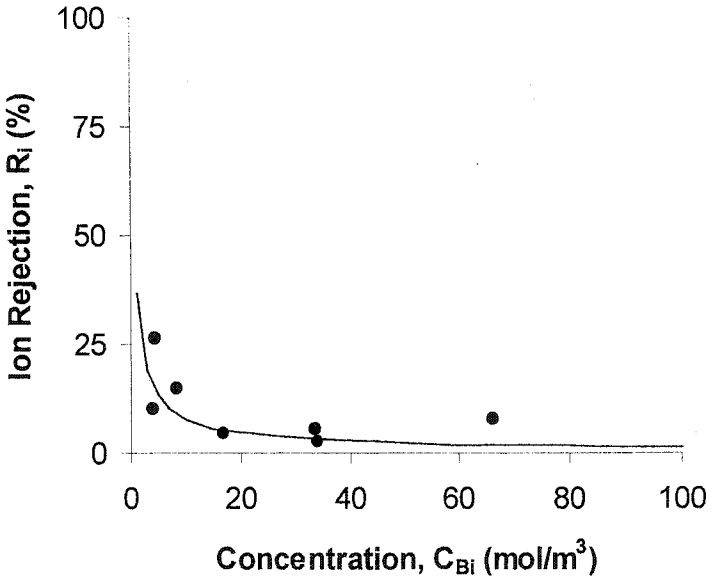

(f) MacPF 508

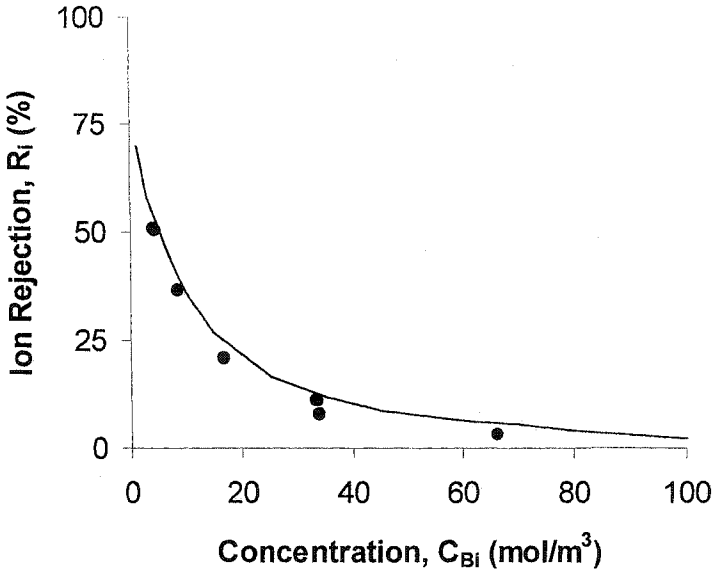

(g) MacPF 509

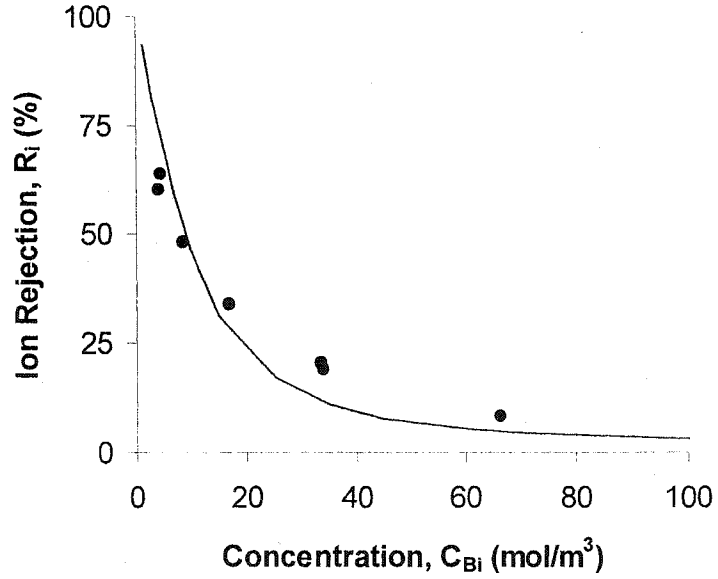

(h) MacPF AL7

Figure 6.15 Salt rejection vs. feed concentration for a NaCl solution as a function of feed concentration (250-4000 ppm) at constant applied pressure (ΔP = 0.5 MPa). Points are experimental data. Lines are model predictions. Membranes: a) HN-7450 and MacPF b) 352, c) 324, d) 382, e) 515, f) 508, g) 509, and h) AL7.

6.2.5 Permeation Experiments with Mixed Solutes (Lactose and NaCl)

Membrane performance with mixed electrolyte and neutral organic solutions is analyzed in this section. Solutions with different concentrations of sodium chloride and lactose are used for this purpose. The operating pressure (ΔP = 0.5 MPa) is kept constant.

The effect of NaCl concentration (0-70 mol/m^3, 0-4000 ppm) on membrane performance at constant lactose concentration (1.6 mol/m^3, 500 ppm) is analyzed in section 6.2.5.1. The effect of lactose concentration (0-12 mol/m^3, 0-4000 ppm) on membrane performance at constant NaCl concentration (35 mol/m^3, 2000 ppm) is analyzed in section 6.2.5.2.

6.2.5.1 Effect of NaCl Concentration on Membrane Performance

The experimental data presented in this section were used to estimate the parameters of the transport model. Modelled results presented in this section are calculations and not predictions. Solution flux calculations are not shown or discussed because the data were collected at constant operating pressure.

Sodium chloride rejection follows the qualitative behavior described in section 6.2.4.2. Sodium chloride rejection decreases as NaCl feed concentration increases at constant operating pressure. Lactose rejection is nearly independent of NaCl concentration (Fig. 6.16). Sodium chloride rejection is essentially unaffected by the presence of lactose, at low lactose concentrations (compare Figs. 6.15 and 6.16). Vellenga et al. (1998) reported no coupling between the

retention of sucrose and NaCl in commercial membranes at low sucrose feed concentrations.

Sodium chloride rejection is similar between the MacPF membranes 352, 324, 509 and AL7 (Fig. 6.16b-c, g-h) and the commercial membrane (Fig. 6.16a). However, lactose rejection is significantly different ($R_{comm} \approx 100\%$, $R_{MacPF} \approx 3$-8%). This is in agreement with previous findings (Garcia-Aleman, 1998), where it was concluded that both steric effects and charge repulsion had important contributions in the partitioning of solutes into the membrane and their transport through commercial NF membranes. Therefore, rejection of uncharged organics and electrolytes is high (50–99%) in commercial membranes. These results are well described by the transport model with the parameters estimated earlier (see Table 6.2).

The membrane HN-7450 is highly charged (see Table 6.3), thus salt rejection is high. Lactose rejection is high due to the relative size of the solute compared to the pore radius ($r_{Lac} = 0.49$ nm vs $r_P = 0.57$ nm, $K_{LAC} \approx 0.02$). The partition coefficient (K_{LAC}) calculated from eq. 4.21 shows that less than 2% (concentration-wise) of the lactose in the feed is available to enter the membrane. On the other hand, the MacPF membranes (352, 324, 509 AL7 rely almost exclusively on Donnan exclusion as the main rejection mechanism. Sodium chloride is highly rejected due to the charge density of the membrane (Donnan exclusion), however lactose is very permeable due to the absence of strong steric effects ($r_{Lac} = 0.49$ nm vs $r_P = 3.71$-7.41 nm, $K_{LAC} \approx 0.70$-0.9).

The NaCl rejection on both types of membranes is similar because of the interplay between membrane permeability, pore radius, and volumetric charge density. These three parameters are different in both types of membranes, but the net contribution to NaCl transport is equivalent at the given operating conditions (pressure and concentration).

As mentioned before, salt rejection is nearly independent of concentration for the membrane with low charge density (MacPF 382, 515 and 508) (Figs. 6.16d-f). Lactose rejection is low (> 20%) in the absence of strong steric effects. The MacPF membrane 382 has the highest lactose rejection (15%) of the pore-filled membrane due to the small pore radius.

Model calculations are in qualitative and quantitative agreement with experimental data within ±5% (HN-7450) and ±2-8% (MacPF) throughout the concentration range. The largest deviations were observed for the membranes with low NaCl rejection, especially at low feed concentrations. Lactose rejection is calculated within ±0.5% (HN-7450) and ±2% (MacPF).

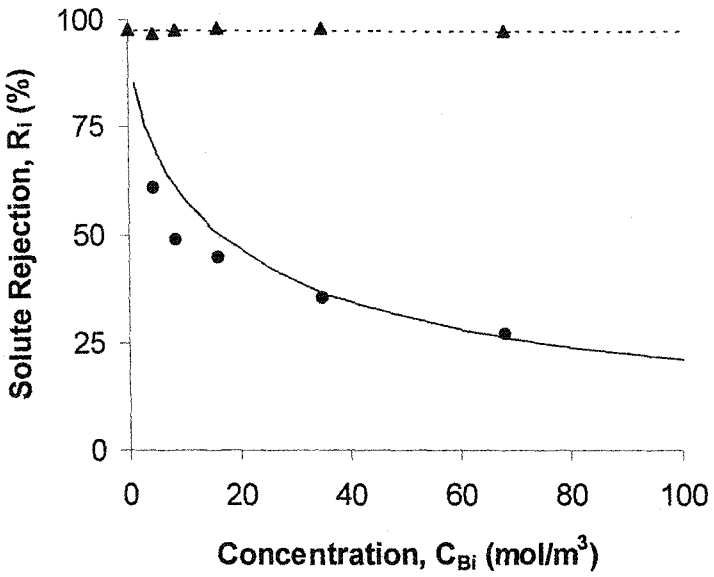

(a) HN-7450

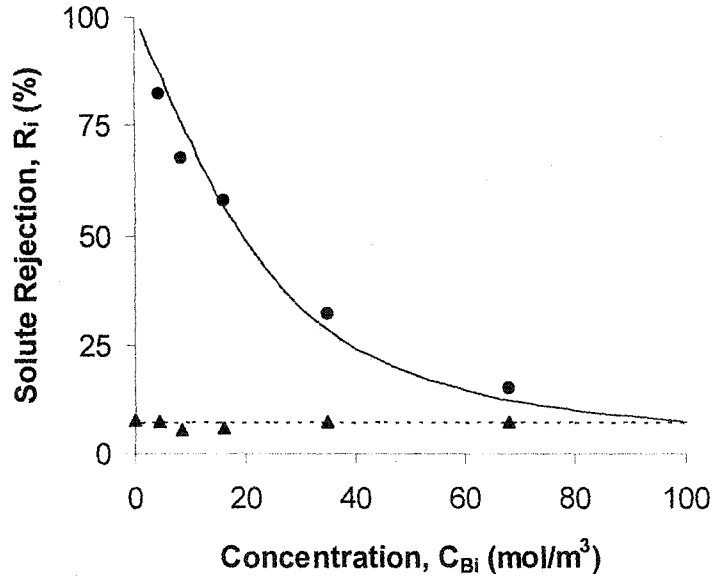

(b) MacPF 352

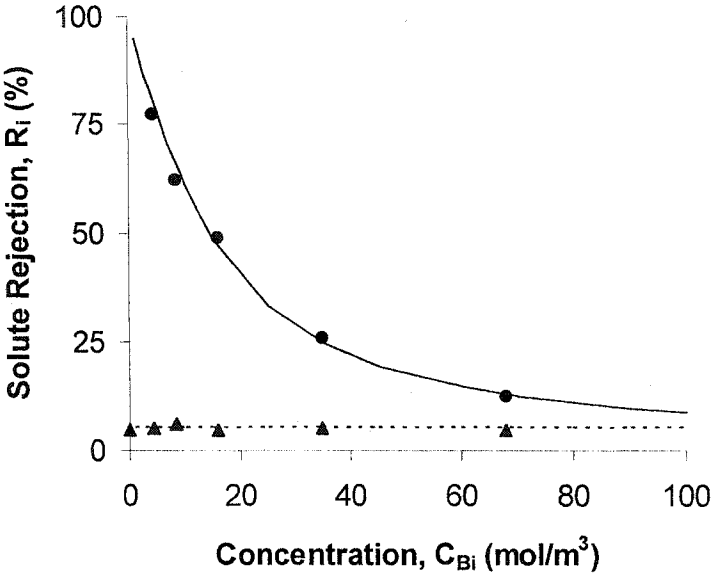

(c) MacPF 324

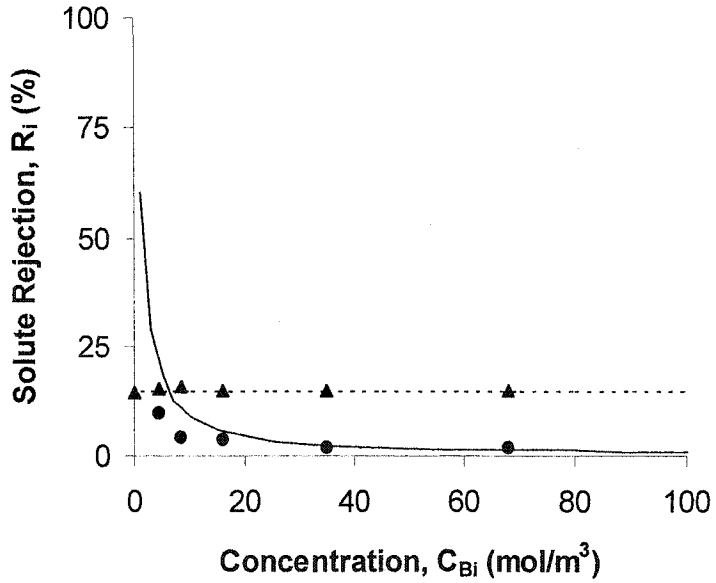

(d) MacPF 382

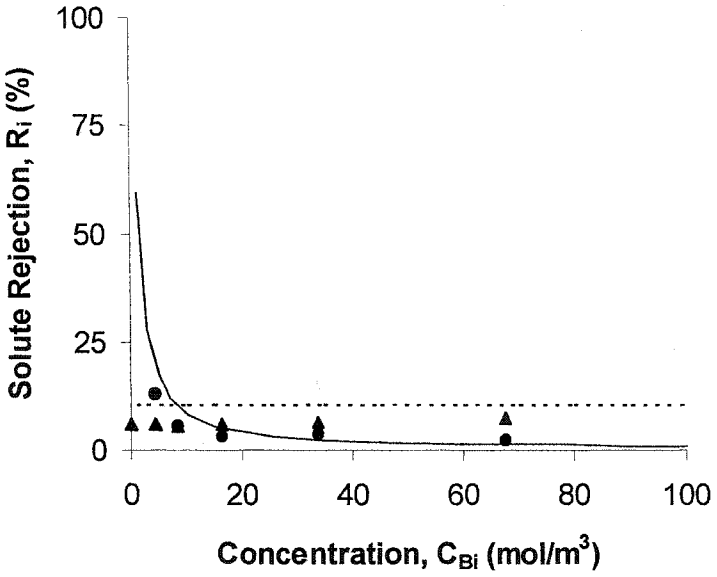

(e) MacPF 515

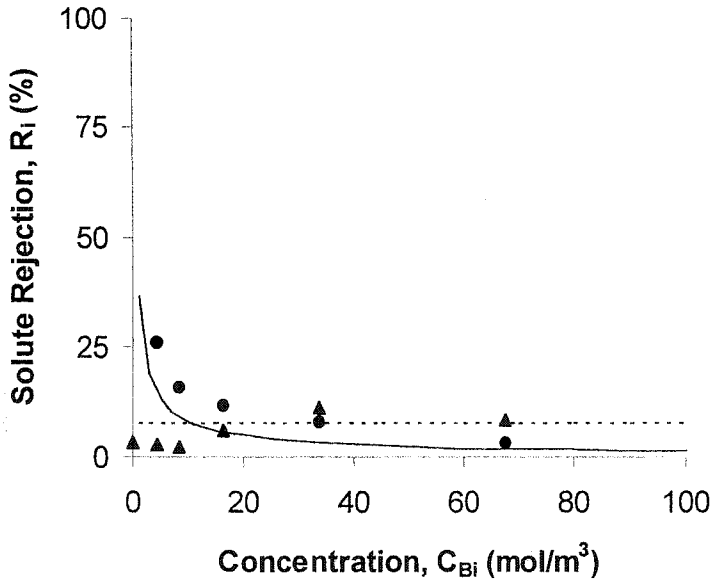

(f) MacPF 508

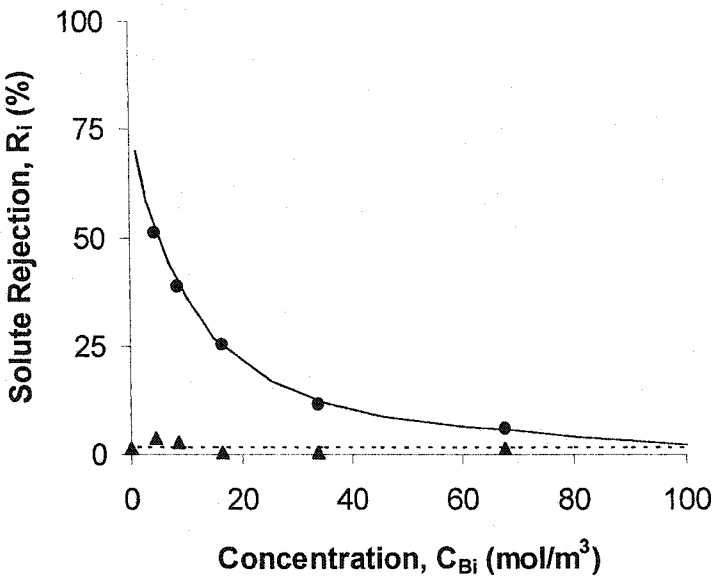

(g) MacPF 509

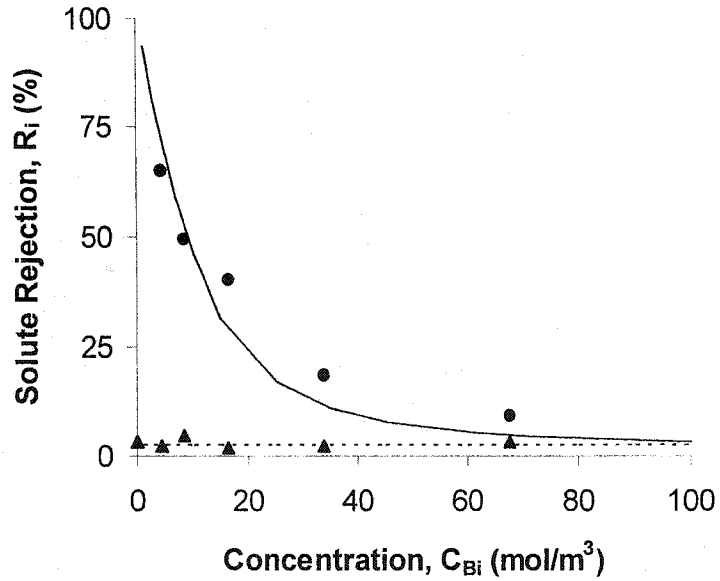

(h) MacPF AL7

Figure 6.16 Solute rejection vs. feed concentration for a NaCl:lactose solution as a function of NaCl feed concentration (0-4000 ppm) at constant lactose concentration (500 ppm) and constant applied pressure (ΔP = 0.5 MPa). Points are experimental data. Lines are model calculations. NaCl (●,—) and Lactose (▲,---). Membranes: a) HN-7450 and MacPF b) 352, c) 324, d) 382, e) 515, f) 508, g) 509, and h) AL7.

6.2.5.2 Effect of Lactose Concentration on Membrane Performance

Sodium chloride rejection and lactose rejection both are nearly independent of lactose concentration over the concentration range (0-4000 ppm) studied here (Fig. 6.17). The membranes HN-7450 and MacPF 352 have nearly identical NaCl rejection (35%) (Figs. 6.15a-b). The MacPF membranes 324, 509 and AL7 have a lower NaCl rejection (15-25%) compared to the other two membranes (Fig. 6.17c, g-h). Such performance is in accordance with the findings in section 6.2.5.4.

The membranes 382, 515 and 508 do not discriminate effectively between lactose and NaCl, which makes these membranes a poor choice for fractionation of mixed-salt-neutral-organic solutions (Figs. 6.17d-f).

Lactose rejection follows the behavior described in section 6.2.5.1. Lactose is completely rejected ($R_{LAC} \approx 99\%$) by the commercial membrane and poorly rejected ($R_{LAC} \approx 3\text{-}10\%$) by the MacPF membranes.

Model calculations are in qualitative and quantitative agreement with experimental data throughout the concentration range. Sodium chloride rejection is calculated within ±2% (HN-7450) and ±1.5% (MacPF). Lactose rejection is calculated within ±1% (HN-7450) and ±2% (MacPF).

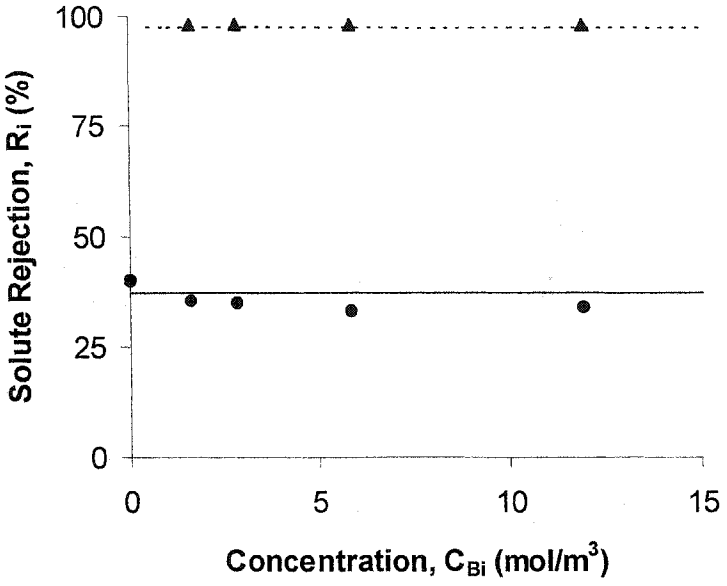

(a) HN-7450

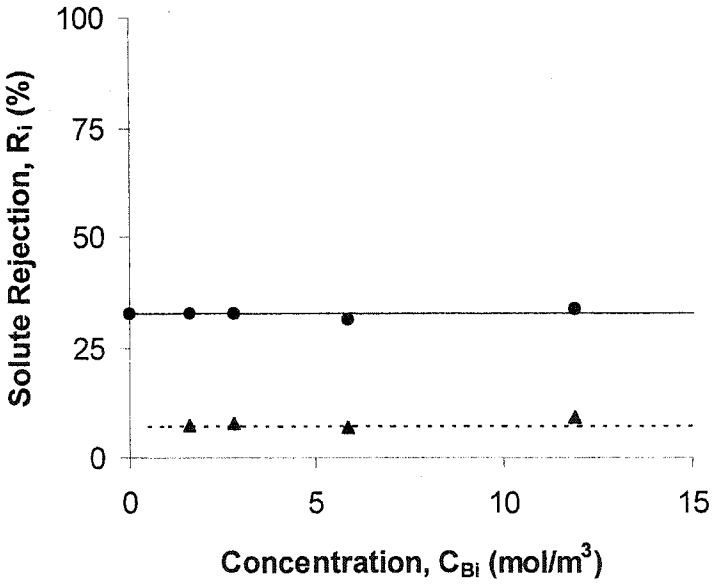

(b) MacPF 352

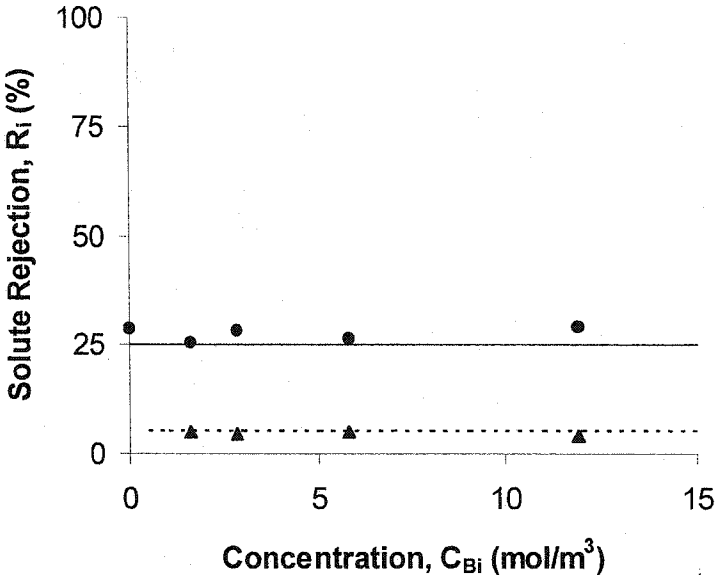

(c) MacPF 324

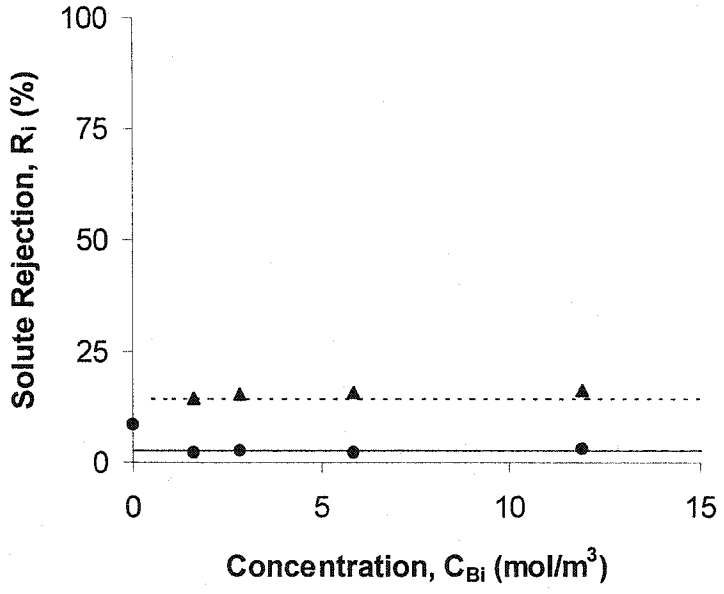

(d) MacPF 382

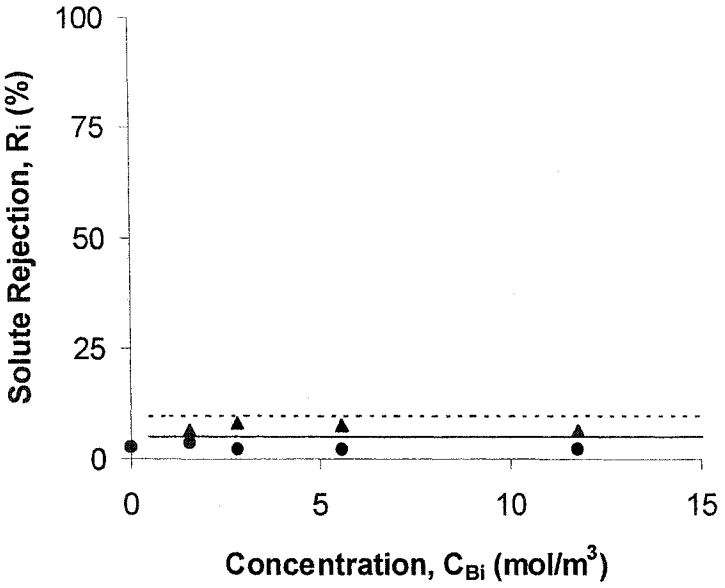

(e) MacPF 515

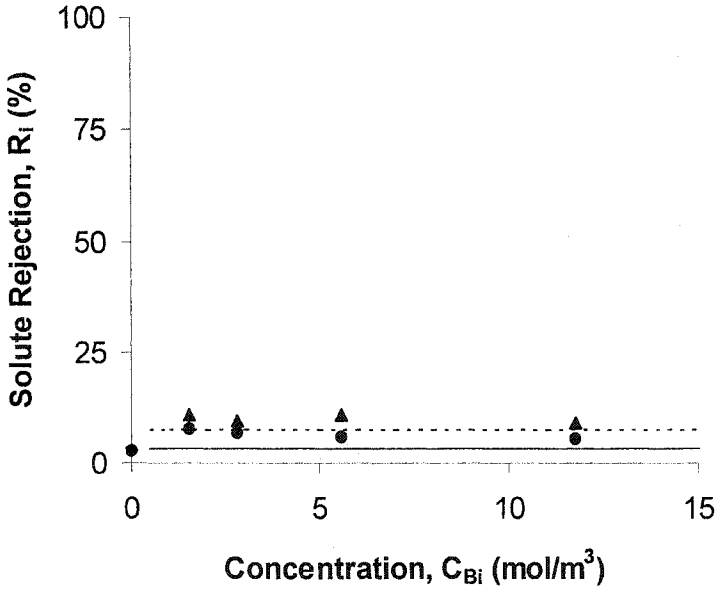

(f) MacPF 508

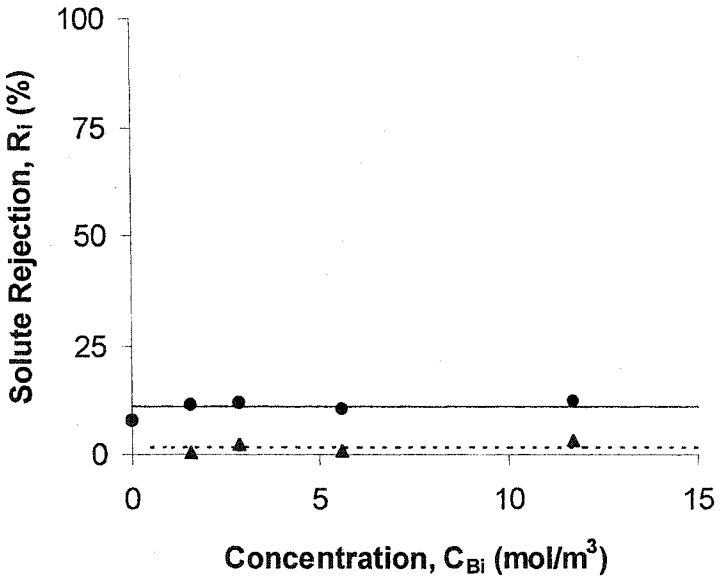

(g) MacPF 509

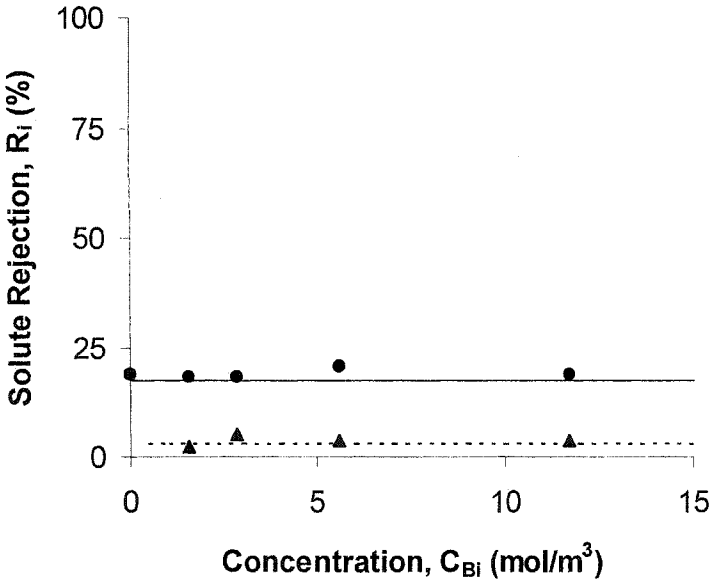

(h) MacPF AL7

Figure 6.17 Solute rejection vs. feed concentration for a NaCl:lactose solution as a function of lactose feed concentration (0-4000ppm) at constant NaCl concentration (2000 ppm) and constant applied pressure (ΔP = 0.5 MPa). Points are experimental data. Lines are model predictions. NaCl (●,—) and Lactose (▲,- - -). Membranes: a) HN-7450 and MacPF b) 352, c) 324, d) 382, e) 515, f) 508, g) 509, and h) AL7.

6.2.6 Permeation Experiments with Mixed Electrolytes

Membrane performance with mixed-electrolyte solutions is analyzed in this section. Solutions with common counter-ions and with common co-ions are studied here ($NaCl:MgCl_2$ and $NaCl:Na_2SO_4$). The effect of pressure (ΔP = 0.3-1.5 MPa) and the concentration of the common co- or counter-ion on membrane performance are investigated. The solutions are used at constant feed concentration of NaCl (5 mol/m^3) and different feed molar ratios (FR = 1, 3, 6). The feed molar ratio is the ratio of feed concentrations of the multivalent ion to the monovalent ion.

Note again that the MacPF membranes are positively charged while the commercial membrane is negatively charged. Therefore, a solution containing a common counter-ion consists of $NaCl:MgCl_2$ for the pore-filled membrane and $NaCl:Na_2SO_4$ for the commercial membranes. The opposite applies for solutions with a common co-ion. Solutions containing $NaCl:Na_2SO_4$ and $NaCl:MgCl_2$ are used for the pore-filled and commercial membranes, respectively.

Model predictions and experimental data are presented in sections 6.2.6.1 and 6.2.6.2 - 6.2.6.3 for solutions containing common counter- and co-ions, respectively. Only the membranes HN-7450 and MacPF 352, 324, and 382 were used in this phase of the investigation.

6.2.6.1 Effect of Common Counter-ion on Membrane Performance

Membrane performance with mixed-electrolyte solutions containing a common counter-ion is analyzed in this section. The experimental data and model predictions for these solutions are presented in Figs. 6.18 to 6.23.

Membrane performance is significantly different between single and mixed electrolytes. For example, compare Figs. 6.5a and 6.18a. In single-salt solutions, rejection generally increases with increasing solution flux (Fig. 6.5a). However, with mixed electrolyte solutions, the rejection of the monovalent co-ion first decreases with increasing flux (Fig 6.18a) due to the Donnan effect, as discussed below. However, when rejection reaches a minimum the contribution of increasing water flux becomes important, thus rejection increases with increasing pressure (solution flux).

Both commercial and MacPF membranes follow the same qualitative behavior, as described by Donnan exclusion theory. In a mixture of electrolytes, the counter-ion permeates through the membrane, and co-ions are rejected due to electrostatic repulsion (Figs. 6.18-6.23). Due to the condition of electroneutrality one of the co-ions has to permeate together with the counter-ion.

The monovalent co-ion permeates preferentially compared to the divalent co-ion because it has a lower valence. Thus, the rejection of the monovalent co-ion decreases (increases negatively) as more divalent co-ion is added to the feed solution (Figs. 6.18a-c, for example). The degree of fractionation (see eq. 2.6) is normally at a maximum when the minimum rejection of monovalent co-ion is

reached and it decreases as the solution flux increases, until the limiting rejection is reached.

However, there are quantitative differences between both types of membranes. The degree of fractionation is 25% greater, at high flux, in the commercial membrane (Fig. 6.18a) compared to the MacPF membranes 352 (Fig. 6.20a) and 324 (Fig. 6.22a). Comparing these two membranes, the commercial membrane has a higher charge density (see Table 6.1) and the Donnan exclusion effect, thus fractionation, is higher. For example, the degree of fractionation in the commercial membrane increases (150-300%) with increasing divalent co-ion (sulfate) concentration (Figs. 6.18a-c). On the other hand, the degree of fractionation is nearly constant for the membrane 352 (100%) (Figs. 6.20a-c) and decreases slightly with increasing magnesium chloride concentration for the membrane 324 (110-80%) (Figs. 6.22a-c).

The membrane 382 (Fig. 6.23) does not fractionate effectively mixed-electrolytes due to the low charge of the membrane. Rejection and fractionation are low (0-5%) and are independent of divalent co-ion concentration (Fig. 6.23a-c). Due to low ion rejection the solution flux is similar to that of pure water.

The solution flux (Fig 6.18d) of the commercial membrane follows the expected linear behavior with increasing applied pressure. The MacPF membranes follow the nonlinear behavior (Fig. 6.20d, 6.22d-6.23d) already discussed in section 6.2.3. The effect of concentration on solution flux cannot be accurately assessed from the data due to the dilute nature of the solutions.

Model calculations of the concentration profile inside the commercial and MacPF 352 membranes are presented in Figs. 6.19 and 6.21, respectively. The rejection mechanisms for mixed-electrolyte solutions are qualitatively the same for the commercial (Fig. 6.19) and the MacPF membranes (Fig. 6.21). Ions are transported by the same mechanisms and the quantitative differences in concentration originate from the relative importance of steric and electrostatic contributions of each membrane.

An interested behavior is observed in both types of membranes (Figs. 6.19 and 6.21). The concentration of divalent co-ion and counter-ion decreases as they are transported through the membrane, regardless of the operating pressure, which agrees with single salt behavior. The concentration of monovalent co-ion increases as is transported through the membrane at low pressures, which is consistent with Donnan exclusion theory. As the operating pressure increases, the monovalent co-ion is initially depleted by the membrane. However, as the co-ion reaches the permeate side of the membrane it is partially enriched, in order to comply with the electroneutrality condition at the permeate side of the membrane.

Model predictions for salt rejection are in qualitative and quantitative agreement with experimental data within ±15.7% (Na^+) and ±7.8% (Mg^{++}) for the commercial membrane; and, ±3.3-6.1% (Na^+) and ±2.6-4.1% (Mg^{++}) for the MacPF membranes. Model predictions for solution flux are in agreement with experimental data within ±0.42 m/s (HN-7450) and ±0.08-0.44 m/s (MacPF).

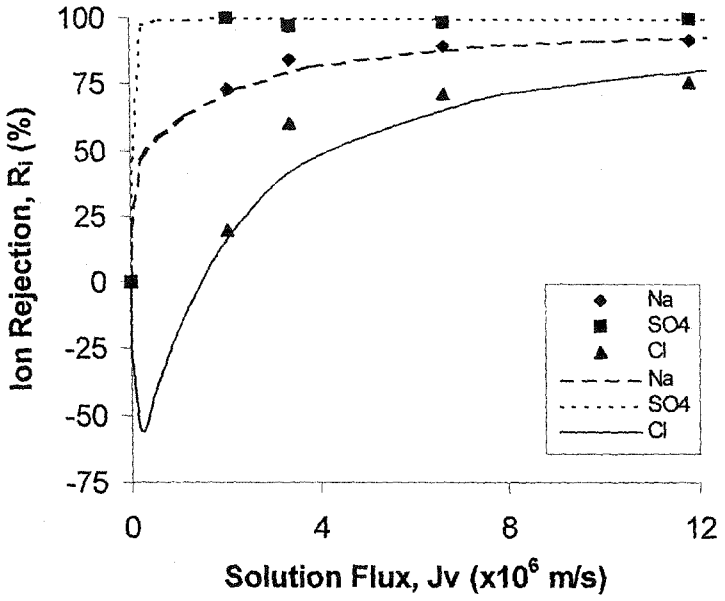

(a) $[SO_4^{=}]/[Cl^-] = 1$

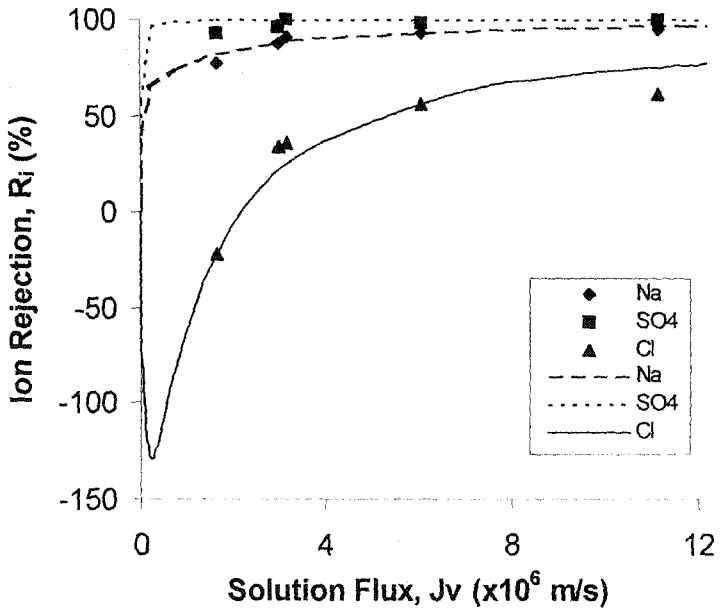

(b) $[SO_4^{=}]/[Cl^-] = 3$

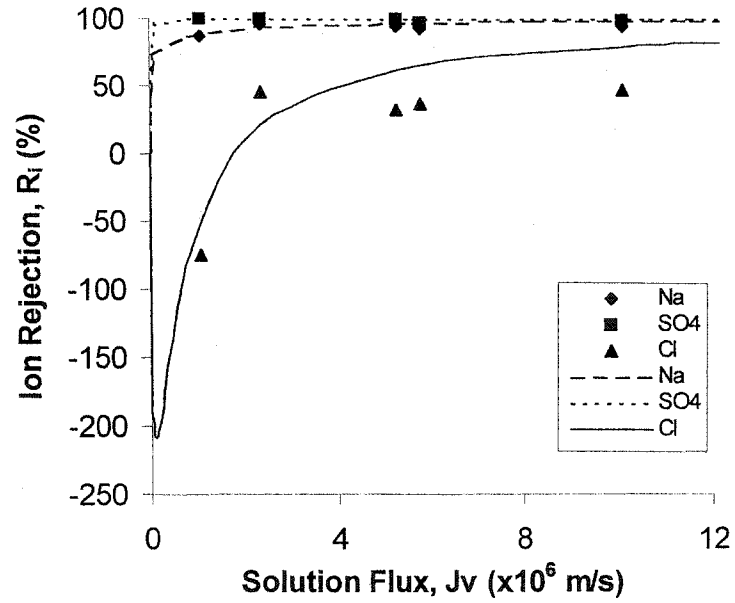

(c) $[SO_4^{=}]/[Cl^-] = 6$

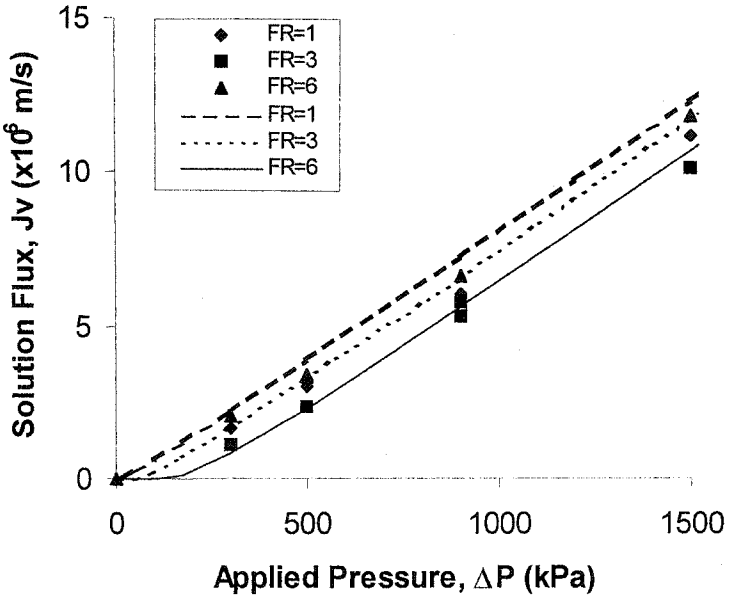

(d)

Figure 6.18 Membrane performance (HN-7450) for mixed-electrolyte solutions (NaCl: Na_2SO_4) as a function of applied pressure (ΔP = 0.3-1.5 MPa) and feed molar ratio ($[Cl^-]$ = 5 mol/m^3, FR = $[SO_4^{=}]/[Cl^-]$ = 1-6) Points are experimental data. Lines are model predictions. Ion rejection vs. solution flux at a) FR = 1, b) FR = 3, c) FR = 6 and d) solution flux vs. applied pressure.

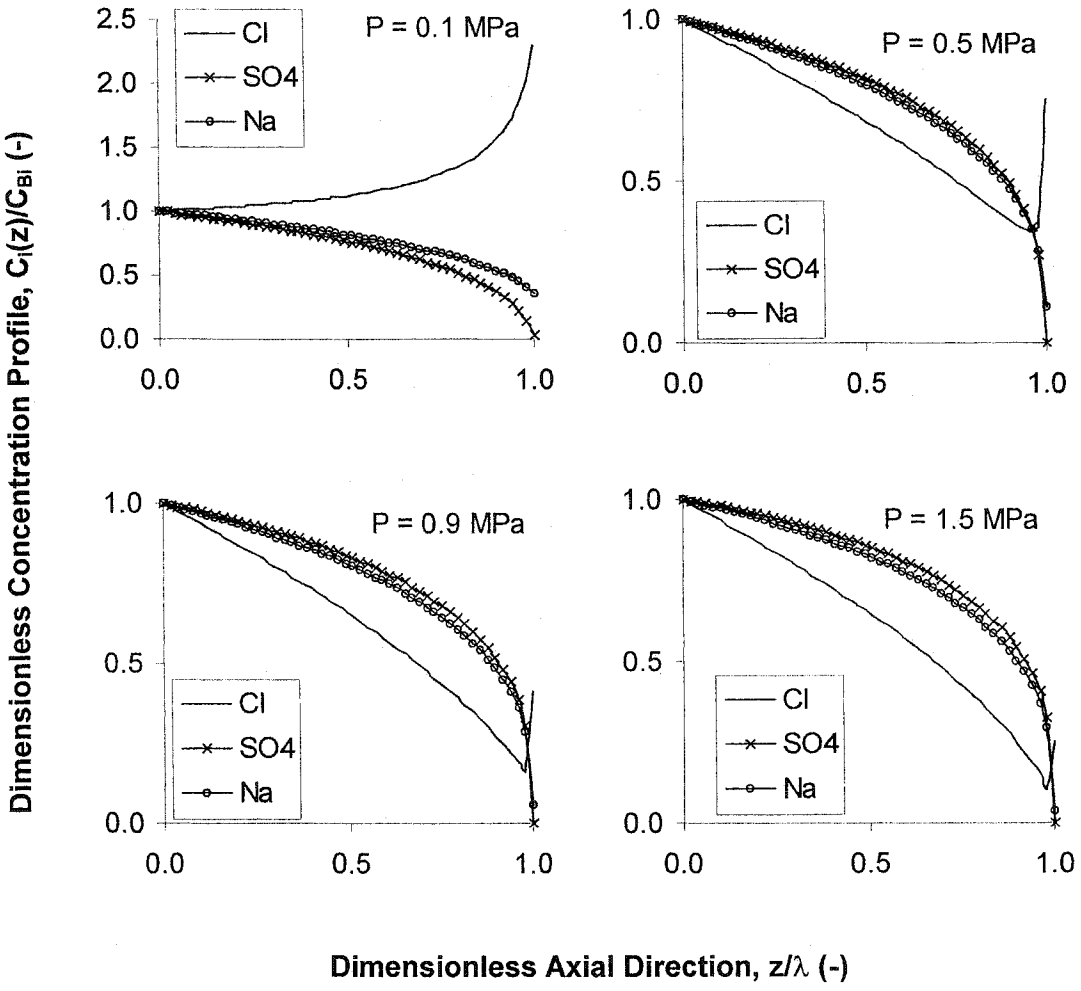

Figure 6.19 For membrane HN-7450, dimensionless concentration profile vs. dimensionless axial direction for a mixed electrolyte solution containing a common counter-ion $NaCl:Na_2SO_4$ ($[Cl^-] = 5$ mol/m^3, $[SO_4^{=}]/[Cl^-] = 3$).

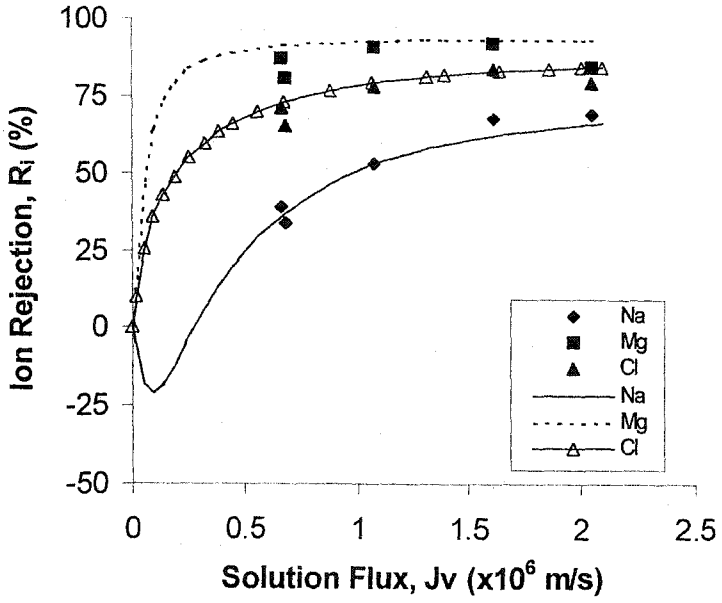

(a) $[Mg^{++}]/[Na^{+}] = 1$

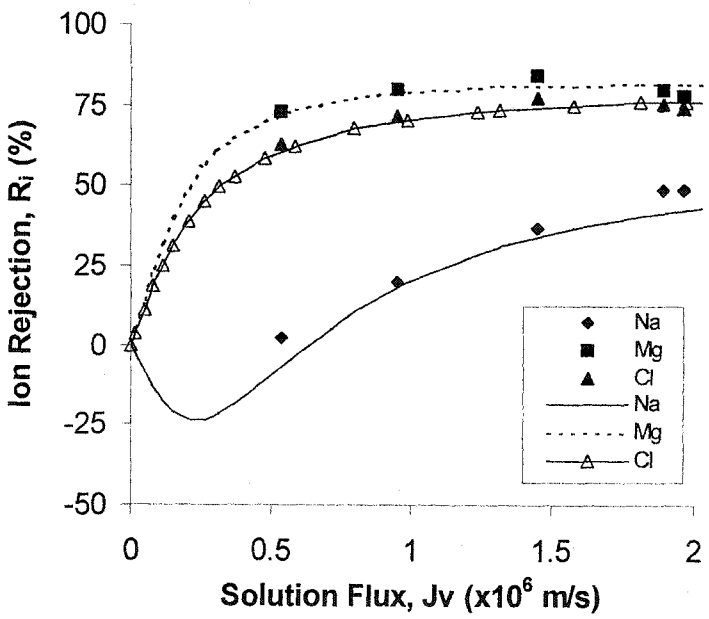

(b) $[Mg^{++}]/[Na^{+}] = 3$

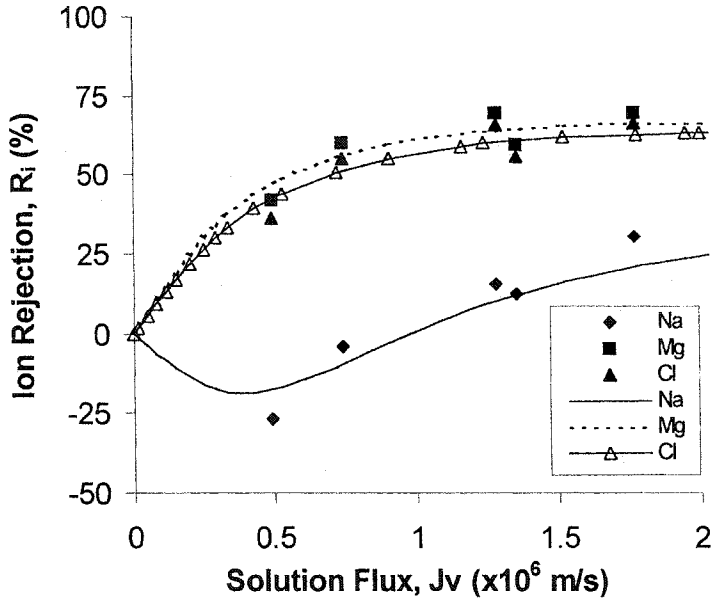

(c) $[Mg^{++}]/[Na^{+}] = 6$

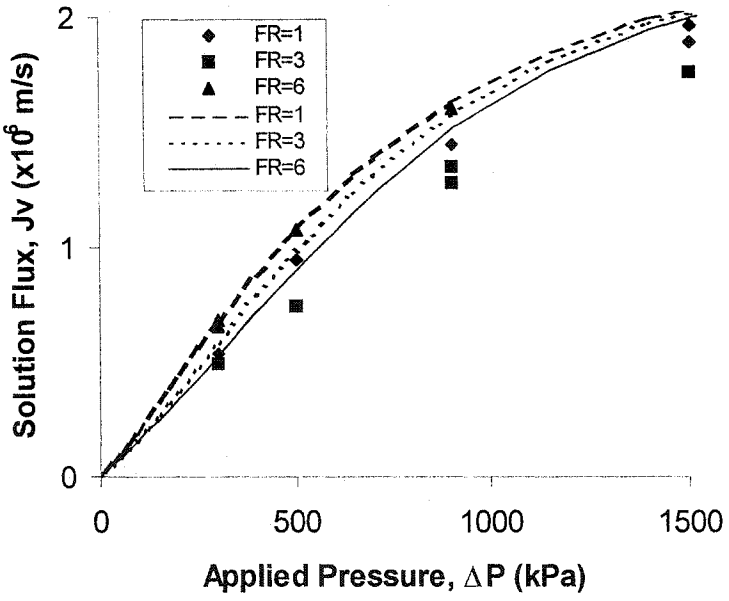

(d)

Figure 6.20 Membrane performance (MacPF 352) for mixed-electrolyte solutions ($NaCl:MgCl_2$) as a function of applied pressure (ΔP = 0.3-1.5 MPa) and feed molar ratio ($[Na^{+}]$ = 5 mol/m^3, FR = $[Mg^{++}]/[Na^{+}]$ = 1-6) Points are experimental data. Lines are model predictions. Ion rejection vs. solution flux at a) FR = 1, b) FR = 3, c) FR = 6 and d) solution flux vs. applied pressure.

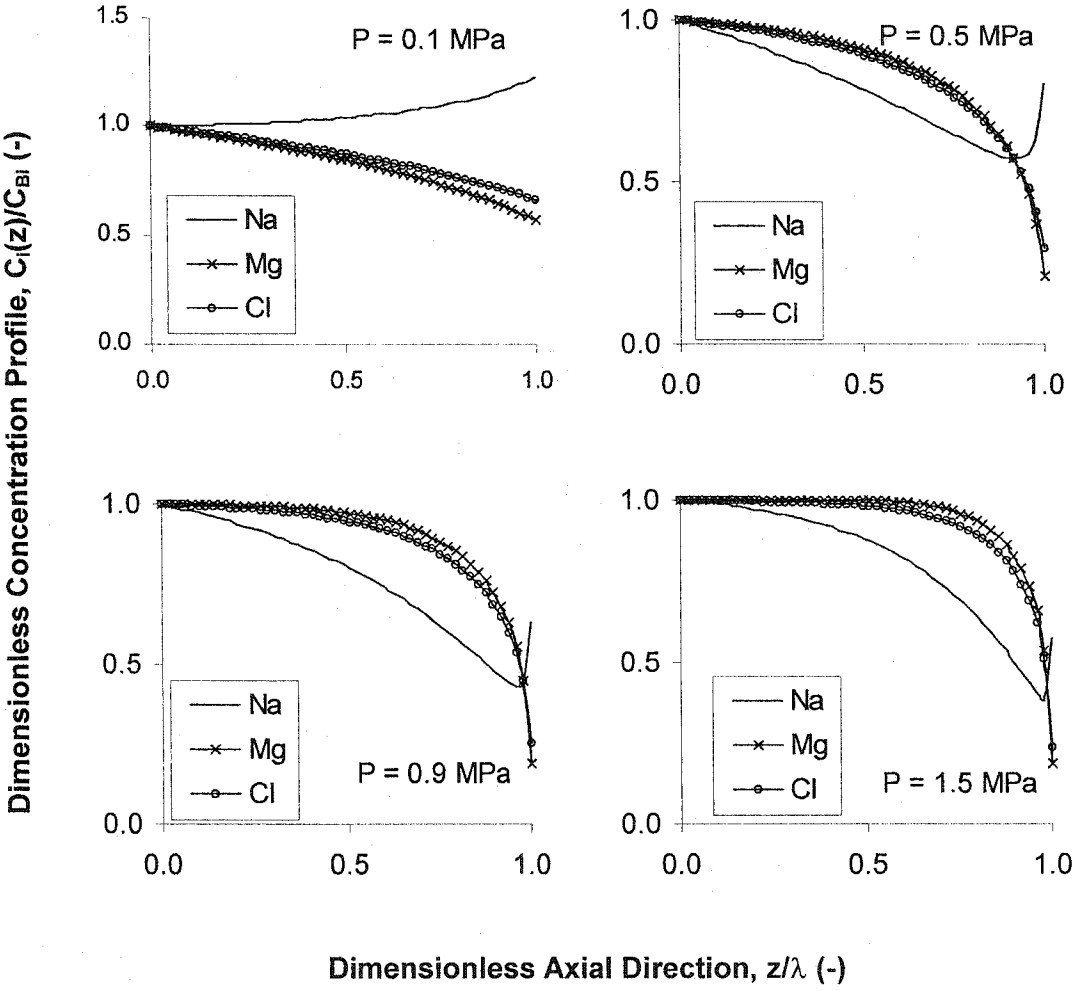

Figure 6.21 For membrane MacPF 352, dimensionless concentration profile vs. dimensionless axial direction for a mixed electrolyte solution containing a common counter-ion NaCl:$MgCl_2$ ($[Na^+]$ = 5 mol/m^3, $[Mg^{++}]/[Na^+]$ = 3).

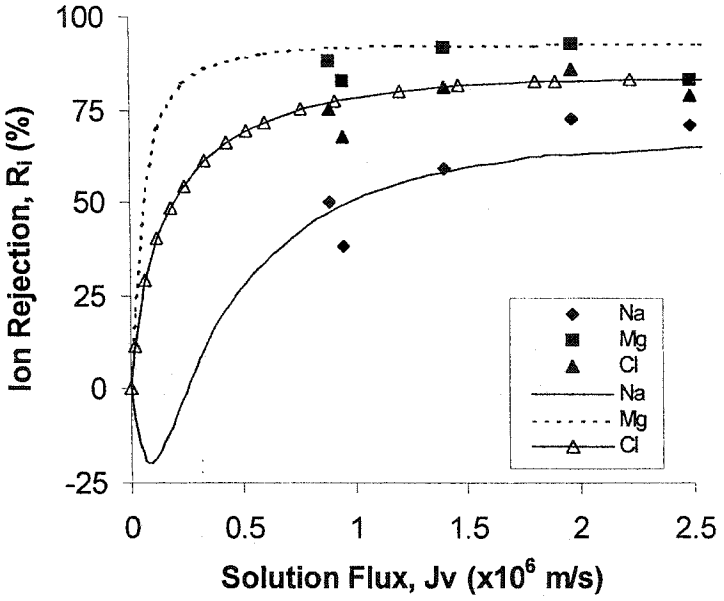

(a) $[Mg^{++}]/[Na^{+}] = 1$

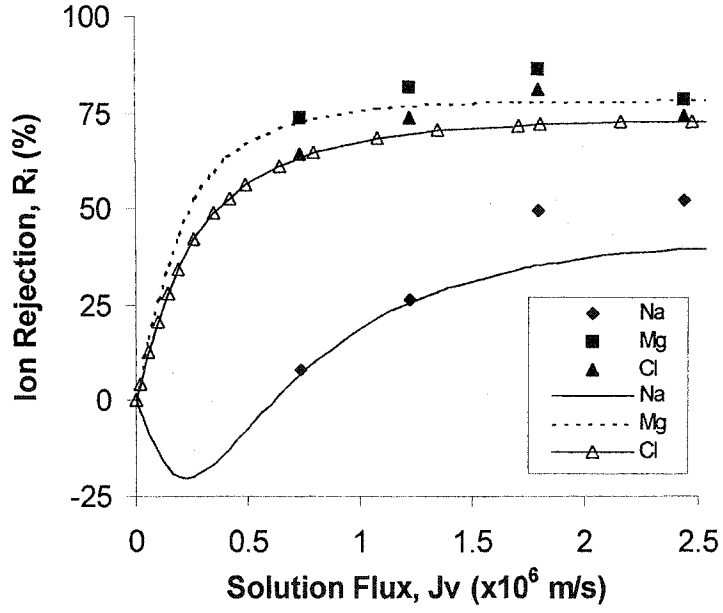

(b) $[Mg^{++}]/[Na^{+}] = 3$

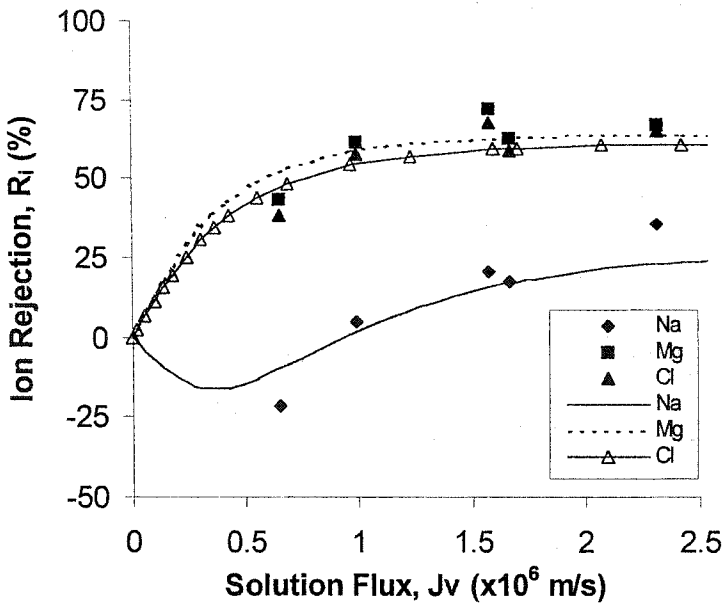

(c) $[Mg^{++}]/[Na^{+}] = 6$

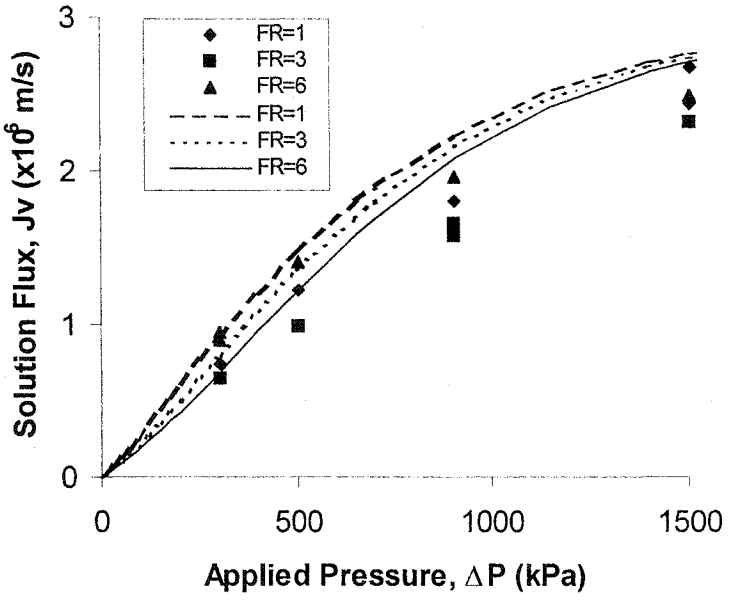

(d)

Figure 6.22 Membrane performance (MacPF 324) for mixed-electrolyte solutions ($NaCl:MgCl_2$) as a function of applied pressure (ΔP = 0.3-1.5 MPa) and feed molar ratio ($[Na^+]$ = 5 mol/m^3, FR = $[Mg^{++}]/[Na^+]$ = 1-6) Points are experimental data. Lines are model predictions. Ion rejection vs. solution flux at a) FR = 1, b) FR = 3, c) FR = 6 and d) solution flux vs. applied pressure.

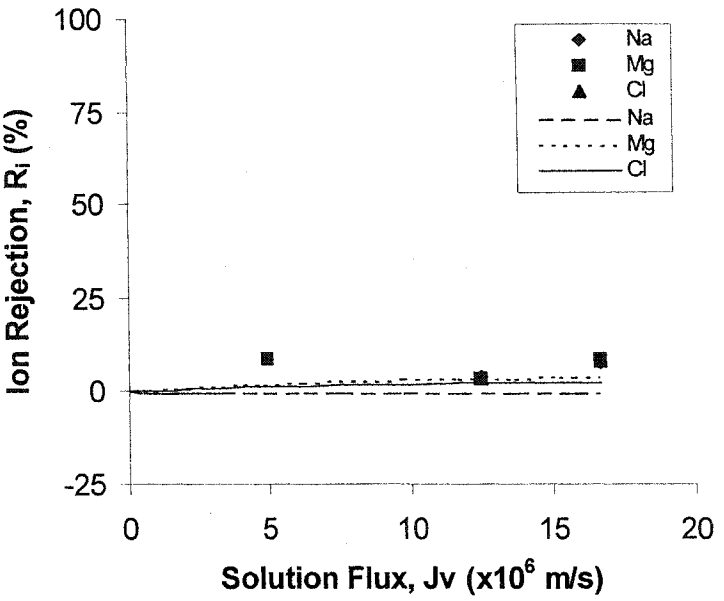

(a) $[Mg^{++}]/[Na^{+}] = 1$

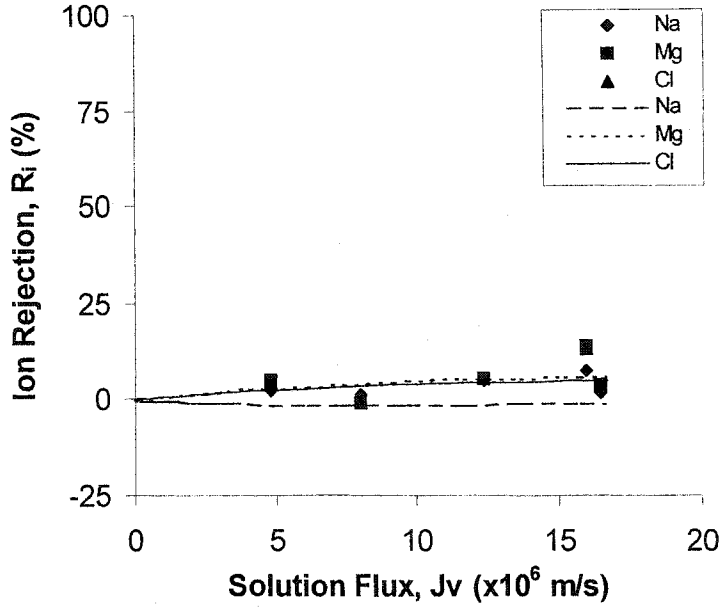

(b) $[Mg^{++}]/[Na^{+}] = 3$

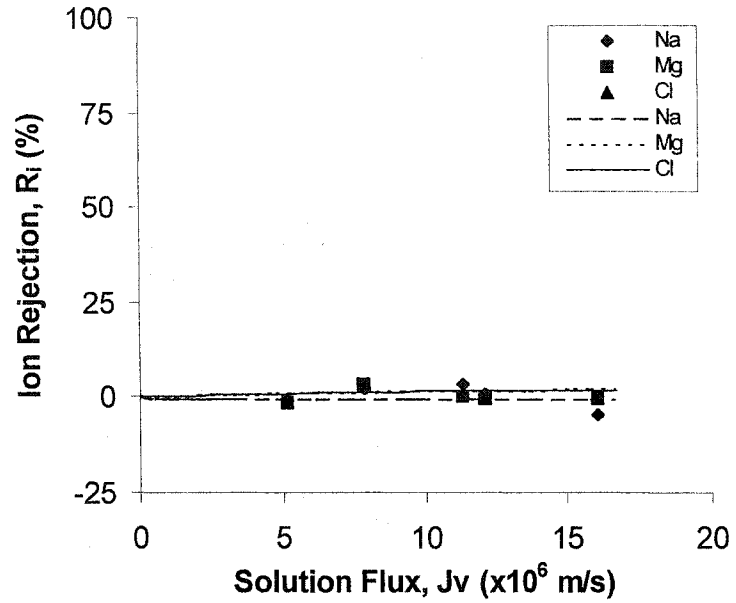

(c) $[Mg^{++}]/[Na^{+}] = 6$

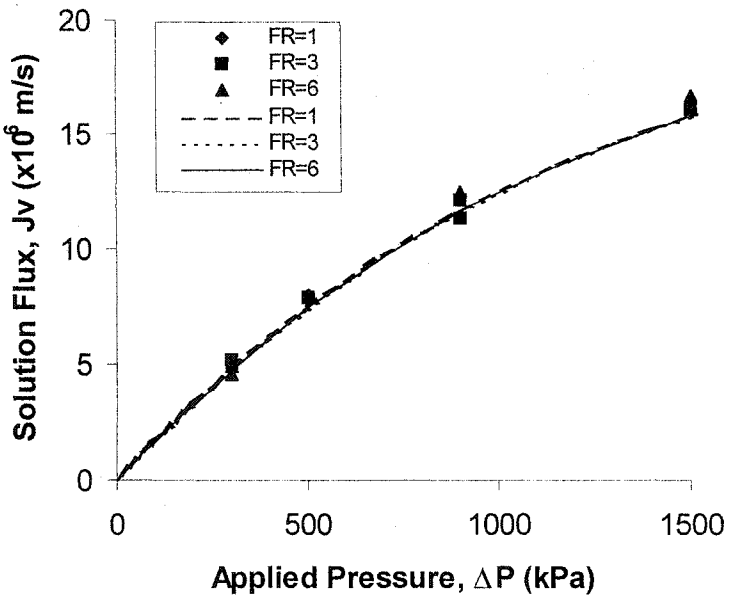

(d)

Figure 6.23 Membrane performance (MacPF 382) for mixed-electrolyte solutions ($NaCl:MgCl_2$) as a function of applied pressure (ΔP = 0.3-1.5 MPa) and feed molar ratio ($[Na^+]$ = 5 mol/m^3, FR = $[Mg^{++}]/[Na^+]$ = 1-6) Points are experimental data. Lines are model predictions. Ion rejection vs. solution flux at a) FR = 1, b) FR = 3, c) FR = 6 and d) solution flux vs. applied pressure.

6.2.6.2 Effect of Common Co-ion on Membrane Performance

Membrane performance with mixed-electrolyte solutions containing a common co-ion is presented in this section. The experimental data and model predictions for these solutions are presented in Figs. 6.24 to 6.30. Initial model predictions are presented in Fig. 6.24. Model predictions with the inclusion of charge inversion are presented in Figs. 6.25-6.30.

In theory, a similar qualitative behavior (Donnan exclusion) should be observed in both types of membranes when using mixed electrolytes with a common co-ion (see model predictions in Fig. 6.24). Based on Donnan exclusion, the counter-ions are attracted by the charged membrane and the common co-ion is repulsed. Normally, the membrane has a greater attraction for a divalent counter-ion. Thus, the divalent counter-ion permeates preferentially through the membrane along with the co-ion. The monovalent counter-ion is rejected preferentially by the membrane.

As presented in Figure 6.24, the model predicts the membrane performance according to the Donnan exclusion mechanism. The commercial membrane should retain sodium ions preferentially and magnesium ions should be allowed to permeate through the membrane. The same qualitative performance is predicted for the MacPF membranes. However, the experimental performance is the opposite as the predicted one. The experimental data (Fig. 6.24) for the TFC commercial membrane show that the permeability of sodium ions is enhanced by the presence of magnesium ions. Similar findings have been reported by others,

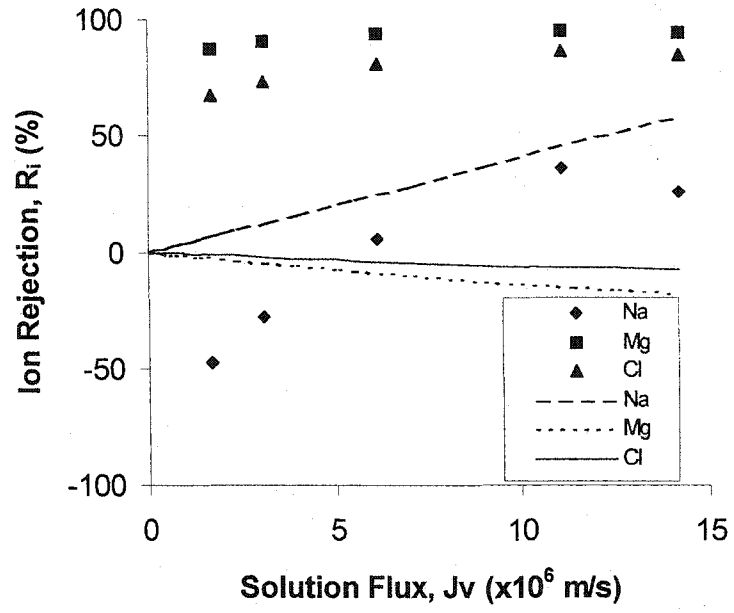

(a)

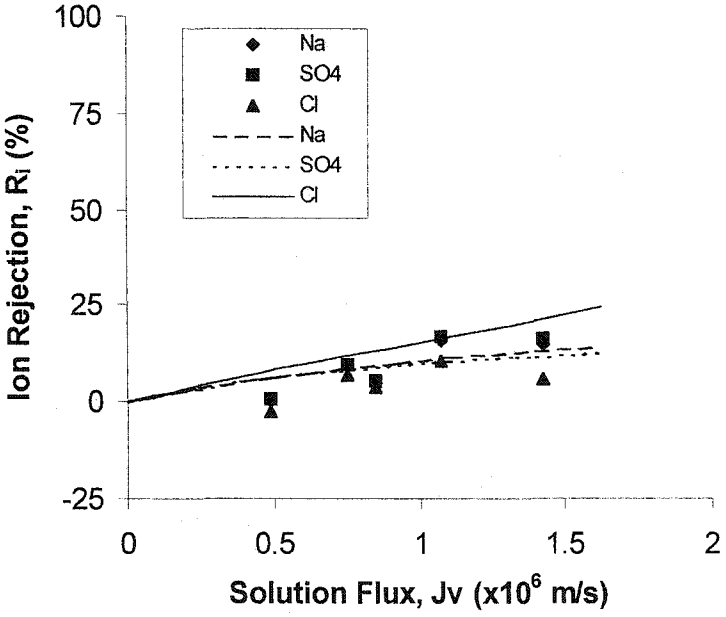

(b)

Figure 6.24 Membrane performance (ion rejection vs. solution flux) for mixed-electrolyte solutions as a function of applied pressure (ΔP = 0.3-1.5 MPa). Points are experimental data. Lines are model predictions. Membrane: a) HN-7450 ($NaCl:MgCl_2$, $[Na^+]$ = 5 mol/m^3, FR = $[Mg^{++}]/[Na^+]$ = 3) and b) MacPF 352 ($NaCl: Na_2SO_4$, $[Cl^-]$ = 5 mol/m^3, FR = $[SO_4^=]/[Cl^-]$ = 3).

including Kimura and co-workers (Tsuru et al., 1991a; 1991b) and Shaep et al. (1999). There are can be two explanations to the discrepancy between experimental observation and model predictions. The first explanation is based on Donnan exclusion; however, this theory does not explain all the observed behavior, as discussed below. The second explanation is based on counter-ion induced charge inversion and is discussed in the next section (6.2.6.3).

The first explanation for this phenomenon is that normally the membrane has a greater attraction for a divalent counter-ion. However, due to the condition of electroneutrality, two co-ions are forced to permeate for every divalent counter-ion that passes through the membrane. Thus, in the presence of a monovalent counter-ion, the counter-ion that "carries" less co-ions is forced to permeate preferentially. The rejection of the monovalent counter-ion decreases as more divalent counter-ion is added to the solution (Figs. 6.25a-c).

One important quantitative difference between the commercial and MacPF membranes is the degree of fractionation (see eq. 2.6). In the MacPF membrane the degree of fractionation is controlled mainly by Donnan exclusion and differences in the mobility of the competing ions. These contributions are normally large between co-ions of different valences, thus a large degree of fractionation is observed in these solutions (Fig. 6.20a). However, these contributions are small between counter-ions, thus a small degree of fractionation ($\approx$10%) and low rejection are observed (Fig. 6.27a). Figures 6.27a-6.27c show

that total salt rejection and ion fractionation decrease with increasing feed concentration.

On the other hand, both steric effects and electrostatic effects determine the degree of fractionation in the commercial membrane (Fig. 6.25). A larger degree of fractionation is observed on the commercial membrane for several reasons (Figs. 6.25a-c). Firstly, there is a significant contribution of steric hindrance by the commercial membrane compared to the MacPF membrane. The commercial membrane discriminates between Mg^{++} and Na^{+} based on size and charge. This effect also increases the total salt rejection of the system compared to the MacPF membrane. Secondly, the commercial membrane has a higher charge density, thus Donnan exclusion (fractionation) is enhanced. For both types of membranes the fractionation between competing counter-ions is always lower than between competing co-ions.

Once again the performance between the membranes 352 and 324 is similar quantitatively and qualitatively (Fig. 6.27 and Fig. 6.29). The degree of fractionation and total salt rejection is small in both membranes. On the other hand, the membrane 382 has a higher overall rejection and degree of fractionation (Fig. 6.30) than the other two MacPF membranes, even though the charge density of this membrane is lower. This behavior cannot be explained directly by Donnan exclusion. However, this behavior is consistent with charge inversion of the membrane induced by counter-ion permeation.

The solution flux of the commercial membrane is not strongly related to the feed concentration in a dilute solution, as observed in Fig. 6.25d. The solution flux of the MacPF membrane 352 and 324 appears to be dependent on counter-ion valence as observed in Figs. 6.27d and 6.29d. However, there is no clear explanation for this behavior, since the membranes HN-7450 and 382 (Fig. 6.30d) do not show the same behavior.

6.2.6.3 Charge Inversion with Solutions Containing Multivalent Counter-ions

The second explanation to the anomalous permeation of mixed electrolyte solutions containing a common co-ion is based on ion absorption in the membrane. Several authors have found that permeating ions, typically co-ions, are adsorbed by highly charged membranes, thus increasing the effective charge of the membrane as a function of salt concentration (Wang et al., 1997; Xu et al., 1997; Bowen and Mohammad, 1998; Garcia-Aleman, 1998). However, such adsorption is not limited to co-ions, thus counter-ions of higher valences that are adsorbed by the membrane can completely shield the charged groups in the membranes, hence neutralizing or changing the sign of the effective charge of the membrane.

Such adsorption can explain the behavior found in (Figs. 6.25-6.30) both commercial and MacPF membranes when using a common co-ion. For example, if in the commercial membrane Mg^{++} ions are adsorbed the membrane could become positively charged, thus Na^{+} ions will permeate preferentially compared

to Mg^{++} ion, as it is observed experimentally. Shaep et al. (1999) reported similar findings in commercial cellulose acetate and polyethersulfone membranes. Charge inversion was observed for these negatively charged membranes and $MgCl_2$ solutions. The cause of the charge inversion was linked to the presence, and apparent adsorption, of the divalent counter-ion. However, no satisfactory mechanism was discussed as to charge inversion being salt or counter-ion specific.

Counter-ion adsorption can explain the larger degree of fractionation encountered in the MacPF membrane (382) with the lowest charge density (Fig. 6.30). A lower charge density is more easily screen and inverted by a solution containing multivalent counter-ion compared to membranes with higher charge densities. The large degree of fractionation observed in the commercial membrane (Fig. 6.25) is due in part by the counter-ion induced charge inversion, but mainly by steric effects hindering Mg^{++} ions permeation through the membrane.

However, other issues still arise from this theory: is such adsorption dependent only on electrostatic interactions between the membrane and permeating ions or are other non-electrostatic forces contributing?

The dependency of charge density on divalent counter-ion concentration is for solutions containing common co-ion was modeled using the semi-empirical correlations described earlier in this chapter (eq. 4.41), as proposed by Shaep et al. (1999). After this dependency is included in the transport model, the model

predicts membrane performance accurately, as discussed below and shown in Figs. 6.25-6.30.

Model predictions for salt rejection are in qualitative and quantitative agreement with experimental data within ±9.36% (Cl^-) and ±1.62% ($SO_4^=$) for the commercial membrane; and, ±5.38-17.18% (Cl^-) and ±3.12-4.46% ($SO_4^=$) for the MacPF membranes. Model predictions for solution flux are in agreement with experimental data within ±0.66 m/s (HN-7450) and ±0.1-0.45 m/s (MacPF).

As discussed earlier, the rejection mechanisms for mixed-electrolyte solutions (common co-ion) are qualitatively the same for the commercial (Fig. 6.26) and the MacPF membranes (Fig. 6.28). Ions are transported by the same mechanisms and the quantitative differences in concentration originate from the steric and electrostatic contributions of each membrane.

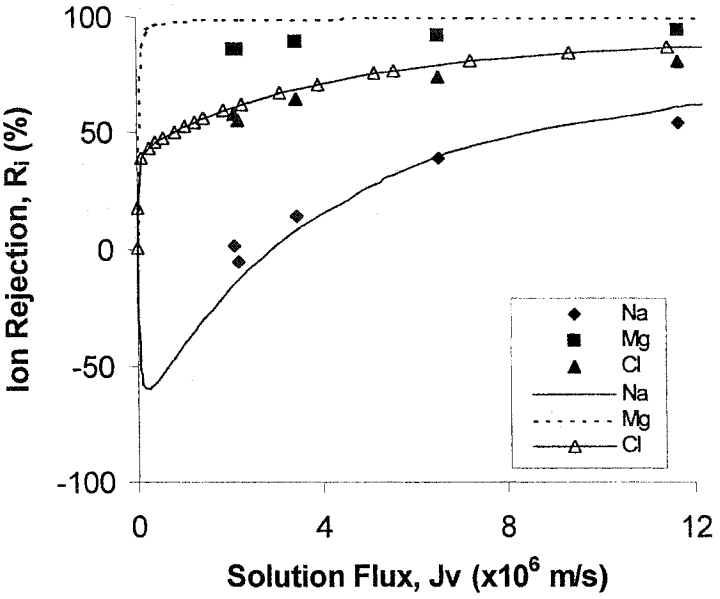

(a) $[Mg^{++}]/[Na^{+}] = 1$

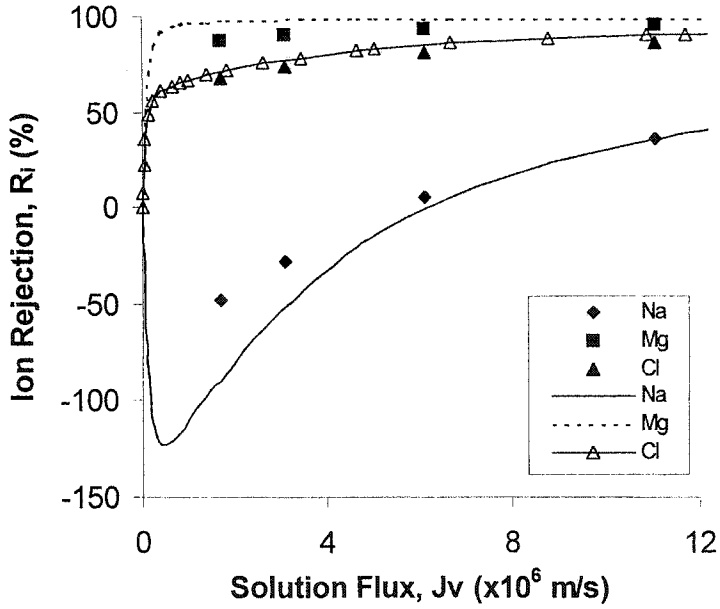

(b) $[Mg^{++}]/[Na^{+}] = 3$

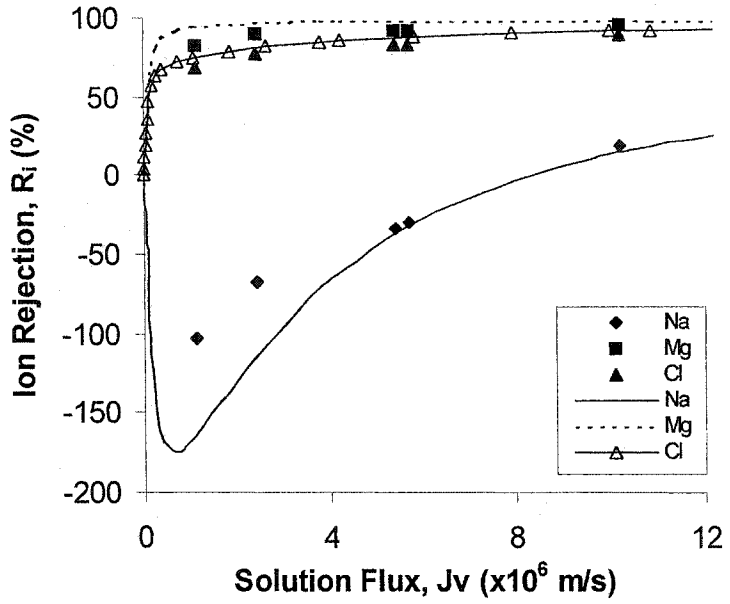

(c) $[Mg^{++}]/[Na^{+}] = 6$

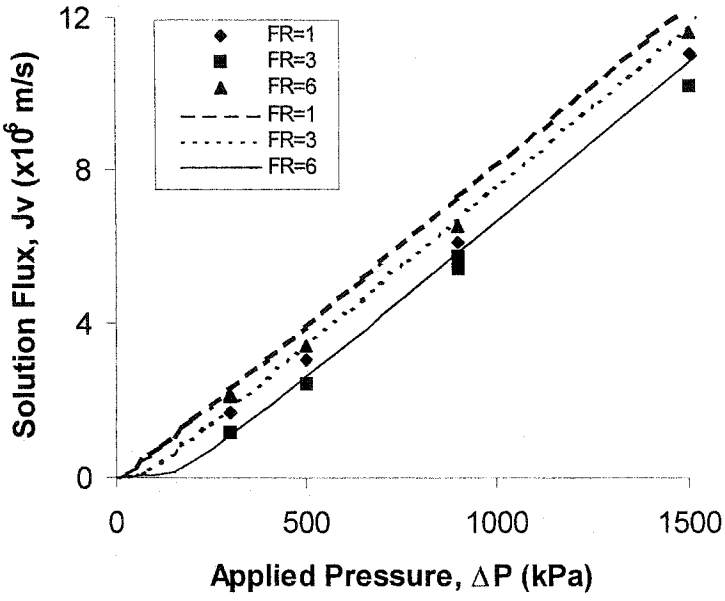

(d)

Figure 6.25 Membrane performance (HN-7450) for mixed-electrolyte solutions ($NaCl:MgCl_2$) as a function of applied pressure (ΔP = 0.3-1.5 MPa) and feed molar ratio ($[Na^+]$ = 5 mol/m^3, FR = $[Mg^{++}]/[Na^+]$ = 1-6) Points are experimental data. Lines are model predictions. Ion rejection vs. solution flux at a) FR = 1, b) FR = 3, c) FR = 6 and d) solution flux vs. applied pressure. The effect of counter-ion adsorption is included, as described in section 6.2.6.3.

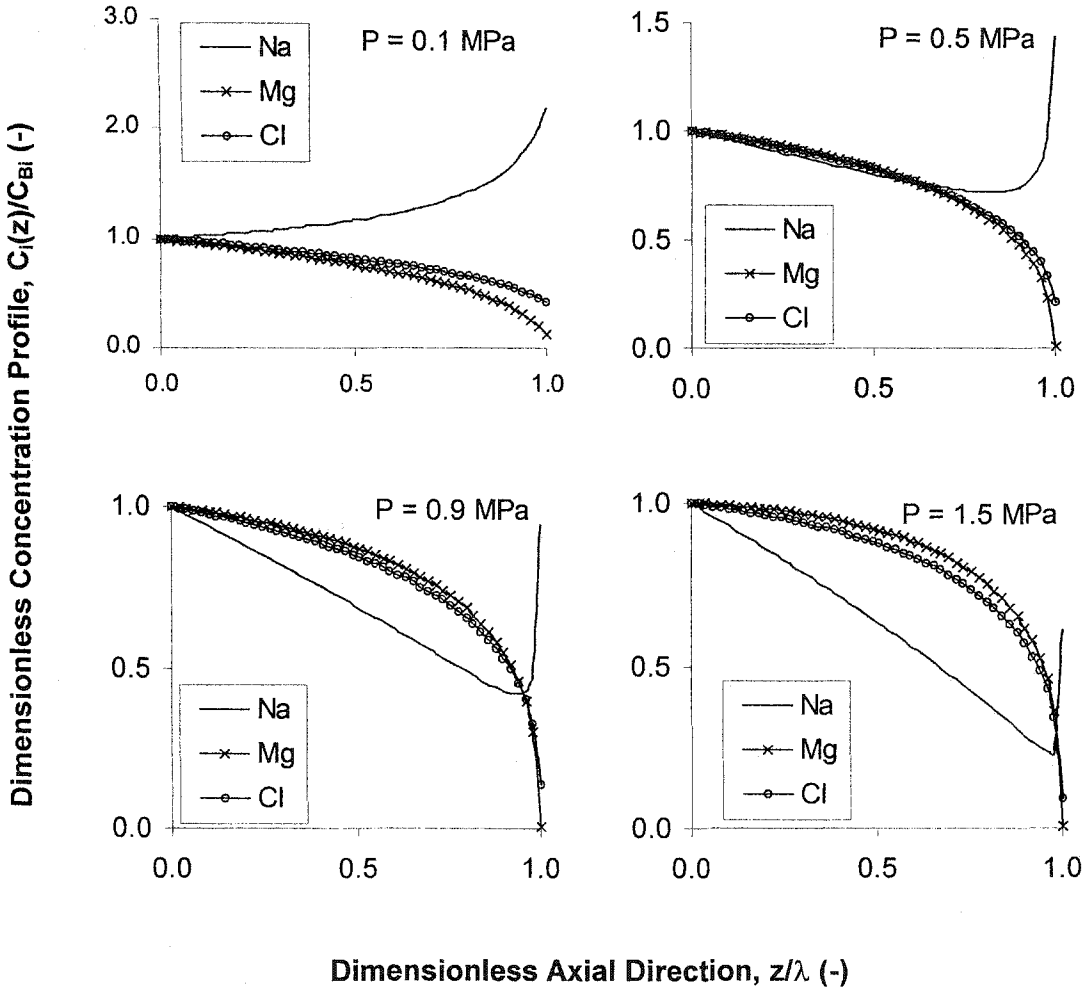

Figure 6.26 For membrane HN-7450, dimensionless concentration profile vs. dimensionless axial direction for a mixed electrolyte solution containing a common co-ion NaCl:$MgCl_2$ ($[Na^+]$ = 5 mol/m^3, $[Mg^{++}]/[Na^+]$ = 3). The effect of counter-ion adsorption is included, as described in section 6.2.6.3.

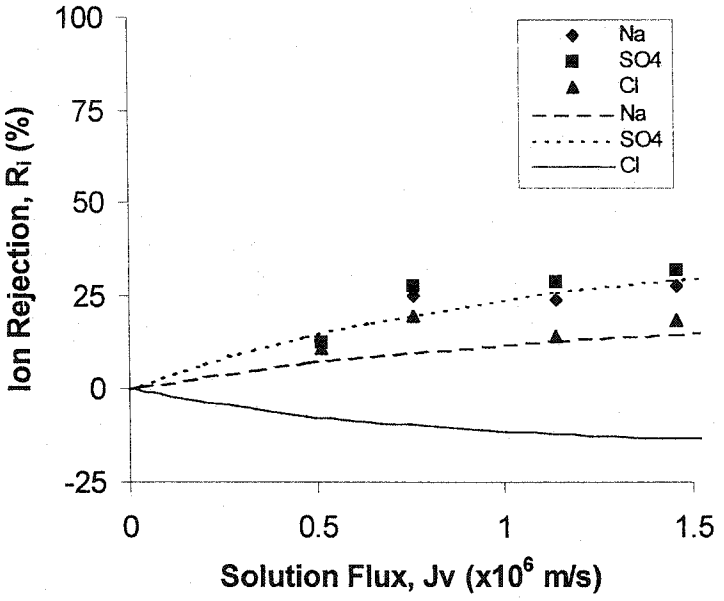

(a) $[SO_4^{=}]/[Cl^-] = 1$

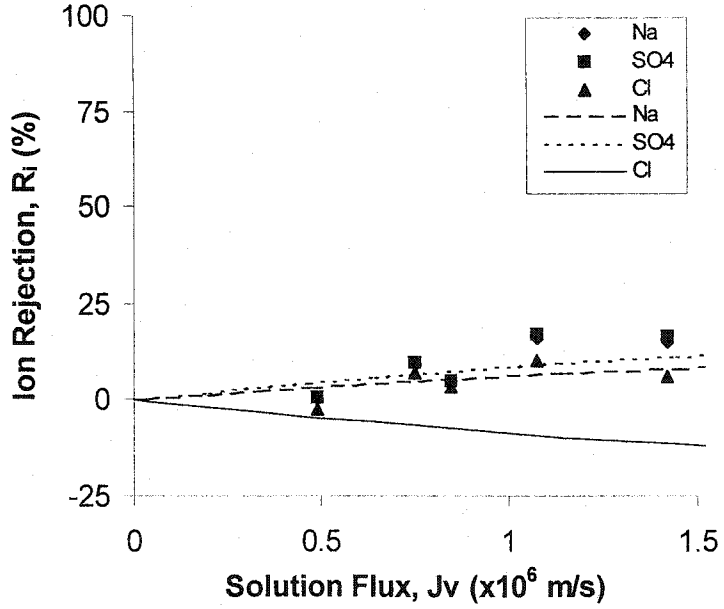

(b) $[SO_4^{=}]/[Cl^-] = 3$

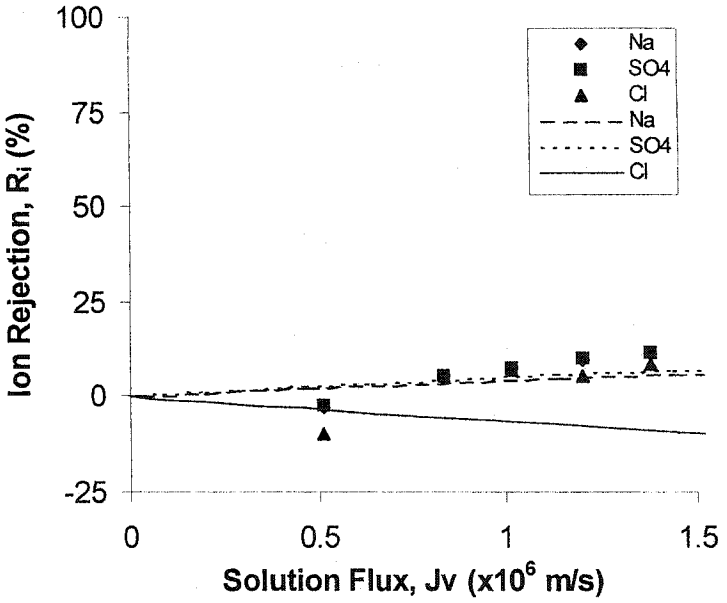

(c) $[SO_4^{=}]/[Cl^-] = 6$

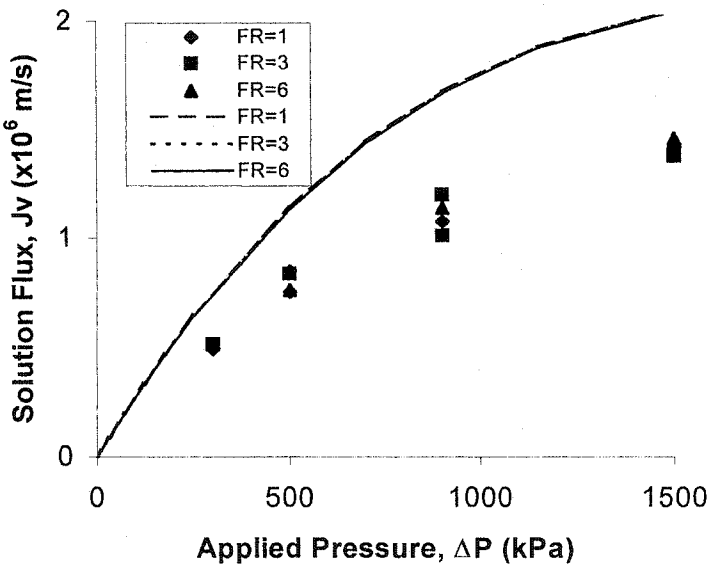

(d)

Figure 6.27 Membrane performance (MacPF 352) for mixed-electrolyte solutions ($NaCl:Na_2SO_4$) as a function of applied pressure (ΔP = 0.3-1.5 MPa) and feed molar ratio ($[Cl^-]$ = 5 mol/m^3, FR = $[SO_4^{=}]/[Cl^-]$ = 1-6) Points are experimental data. Lines are model predictions. Ion rejection vs. solution flux at a) FR = 1, b) FR = 3, c) FR = 6 and d) solution flux vs. applied pressure. The effect of counter-ion adsorption is included, as described in section 6.2.6.3.

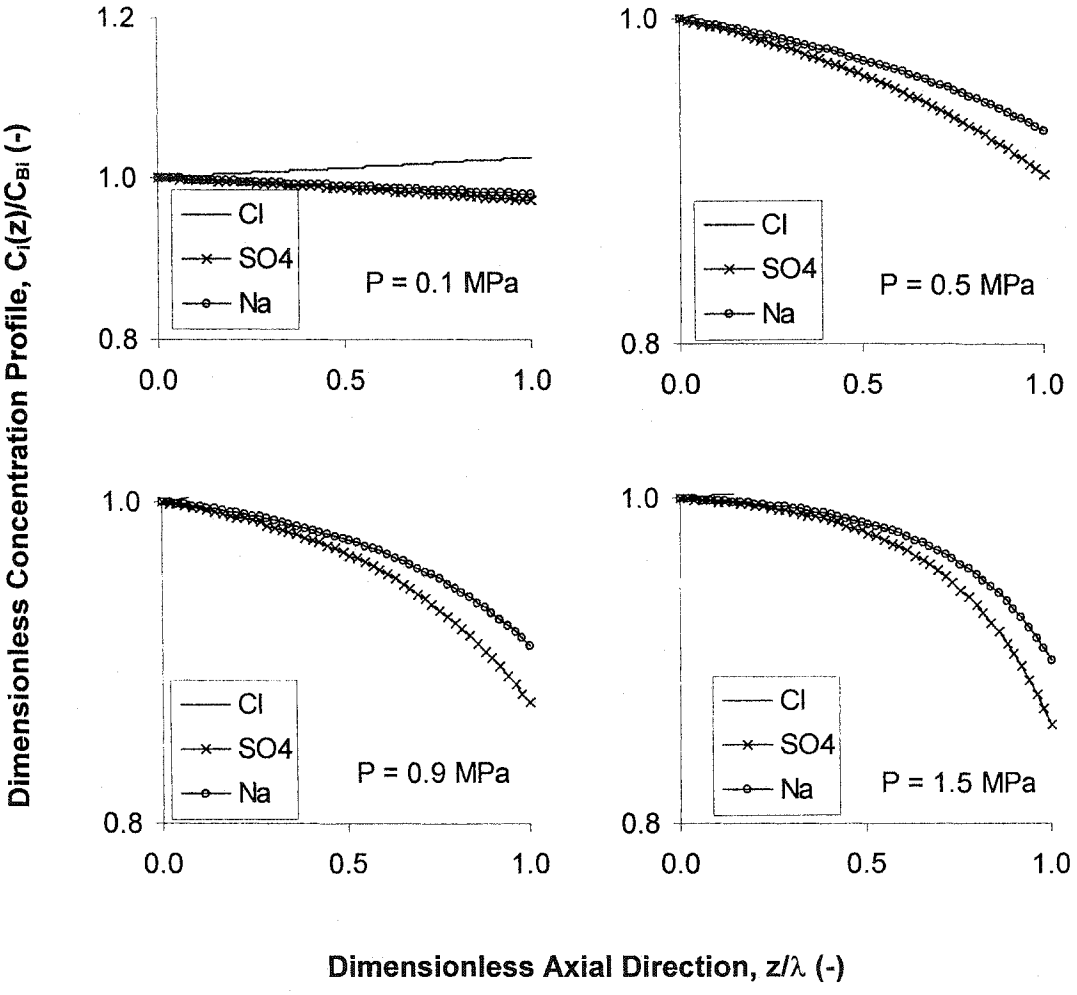

Figure 6.28 For membrane MacPF 352, dimensionless concentration profile vs. dimensionless axial direction for a mixed electrolyte solution containing a common co-ion NaCl:Na_2SO_4 ($[Cl^-]$ = 5 mol/m^3, $[SO_4^{=}]/[Cl^-]$ = 3). The effect of counter-ion adsorption is included, as described in section 6.2.6.3.

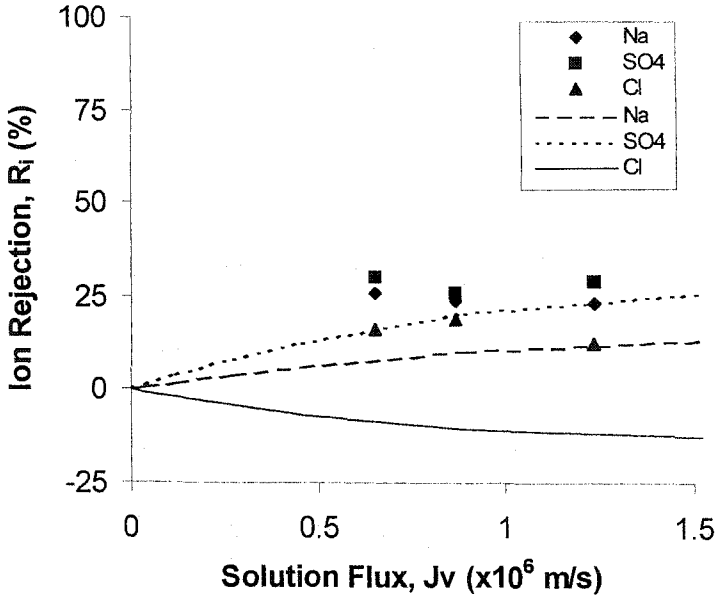

(a) $[SO_4^{=}]/[Cl^-] = 1$

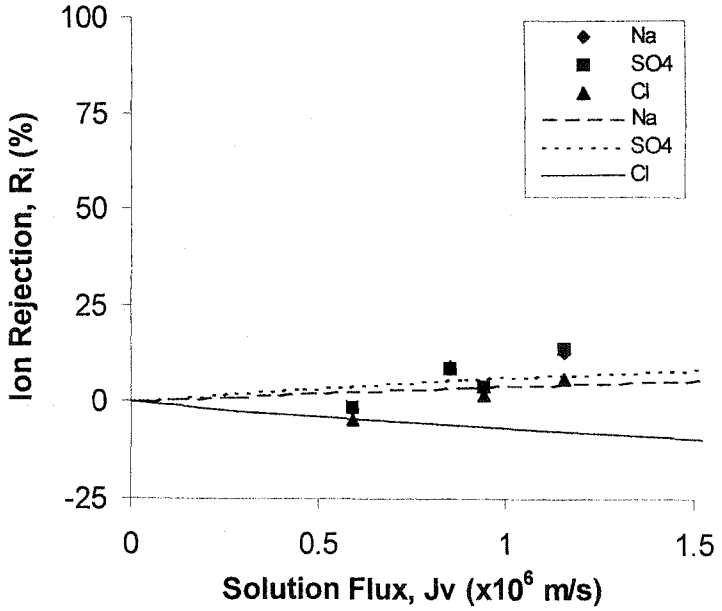

(b) $[SO_4^{=}]/[Cl^-] = 3$

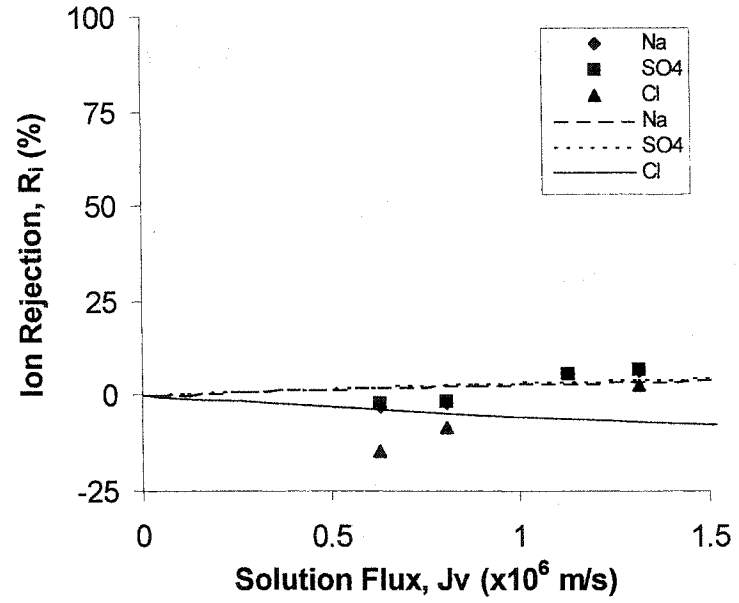

(c) $[SO_4^{=}]/[Cl^-] = 6$

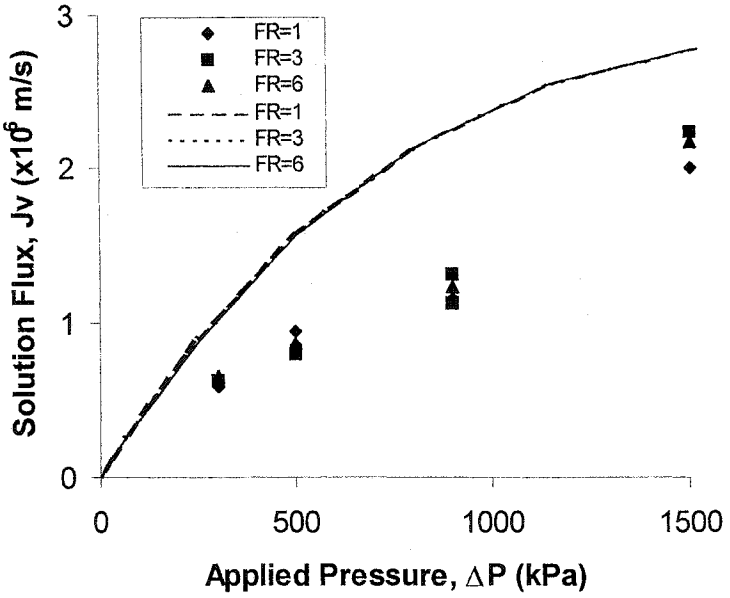

(d)

Figure 6.29 Membrane performance (MacPF 324) for mixed-electrolyte solutions ($NaCl:Na_2SO_4$) as a function of applied pressure (ΔP = 0.3-1.5 MPa) and feed molar ratio ($[Cl^-]$ = 5 mol/m^3, FR = $[SO_4^{=}]/[Cl^-]$ = 1-6) Points are experimental data. Lines are model predictions. Ion rejection vs. solution flux at a) FR = 1, b) FR = 3, c) FR = 6 and d) solution flux vs. applied pressure. The effect of counter-ion adsorption is included, as described in section 6.2.6.3.

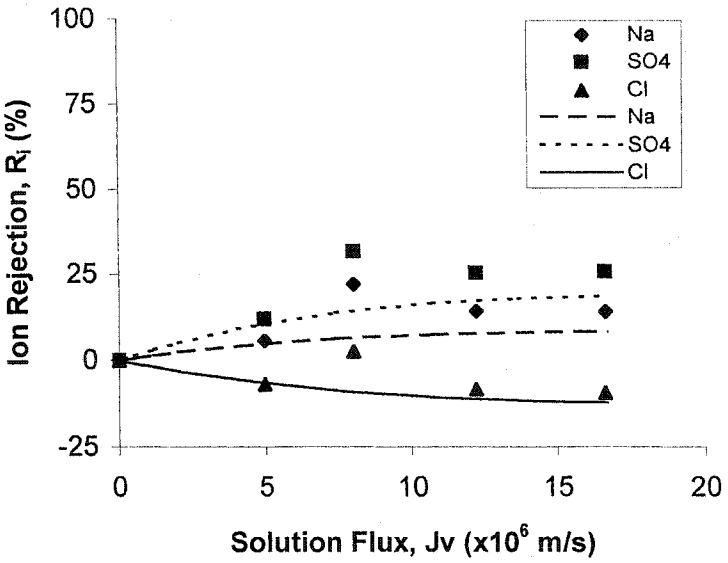

(a) $[SO_4^{=}]/[Cl^-] = 1$

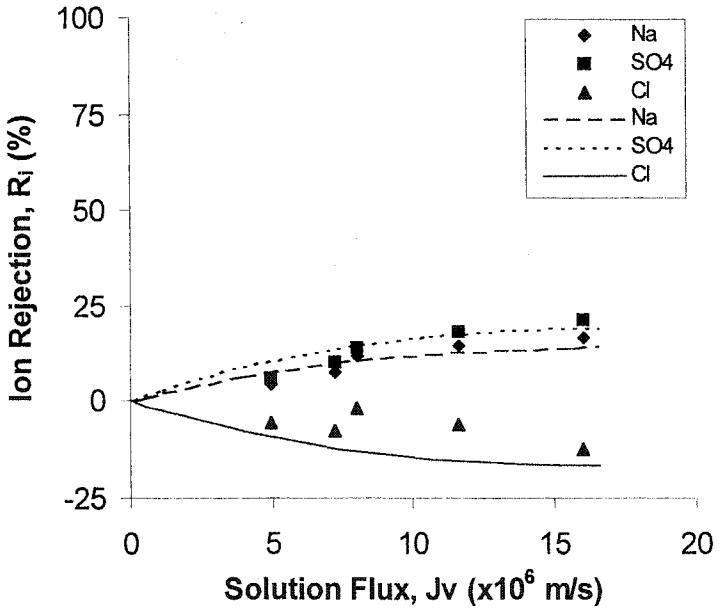

(b) $[SO_4^{=}]/[Cl^-] = 3$

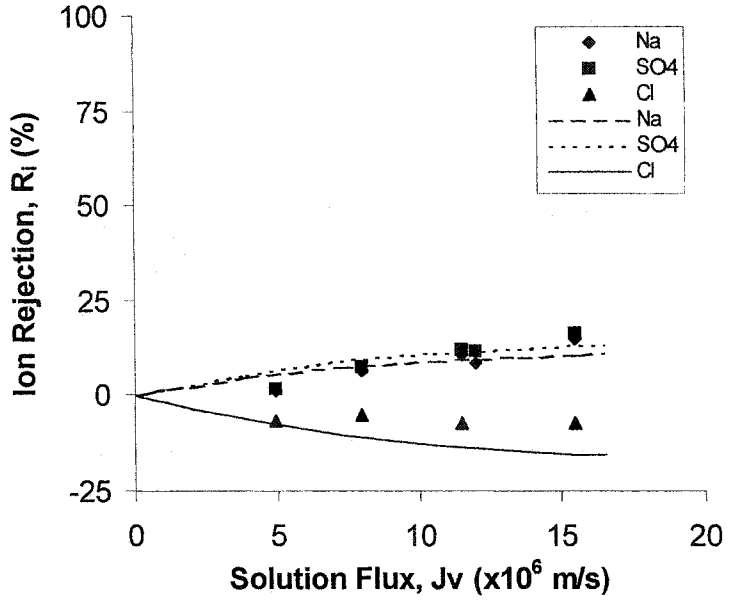

(c) $[SO_4^{=}]/[Cl^-] = 6$

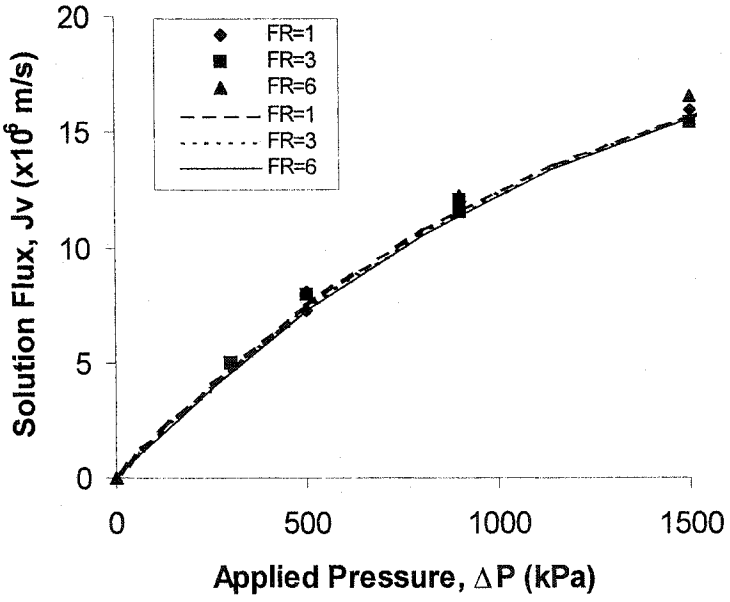

(d)

Figure 6.30 Membrane performance (MacPF 382) for mixed-electrolyte solutions ($NaCl:Na_2SO_4$) as a function of applied pressure (ΔP = 0.3-1.5 MPa) and feed molar ratio ($[Cl^-]$ = 5 mol/m^3, FR = $[SO_4^{=}]/[Cl^-]$ = 1-6) Points are experimental data. Lines are model predictions. Ion rejection vs. solution flux at a) FR = 1, b) FR = 3, c) FR = 6 and d) solution flux vs. applied pressure. The effect of counter-ion adsorption is included, as described in section 6.2.6.3.

6.3 Summary

The experimental performance of the McMaster Pore-filled membranes has been analyzed using a combination of single and mixed solute solutions under different concentrations and pressures. The experimental performance of these membranes was also compared to a standard commercial membrane.

Two mechanistic models were used to determine the physicochemical parameters for the MacPF membranes. The first model (gel model) predicts the conformation of the pore-filling gel and hence the structure of the membrane. The second model (transport model) can be used in combination with the gel model, experimental data or independent measurements to obtain the membrane parameters.

The transport model was used to predict the performance of the commercial and MacPF membranes for single and mixed solute solutions. Transport model predictions and the experimental performance of the MacPF membranes were also compared.

Chapter VII.

Conclusions and Recommendations

This chapter outlines the conclusions and recommendations resulting from the experimental and modeling work done with the McMaster Pore-filled membranes. The contributions of this work are outlined and several recommendations for future work in this area are made based on the results and conclusions drawn from the experimental data and model performance.

7.1 Conclusions on Experimental Findings

The performance (solution flux and rejection) of the MacPF membranes was studied with different mixed solute and salt solutions. This performance was compared to a commercial membrane (HN-7450).

The main contribution of this dissertation (experimentally) is the determination of the contributions of the main transport and rejection mechanisms in the MacPF membranes.

Ionic transport in the MacPF membranes is similar to that in commercial membranes. Convection, diffusion, and electromigration are the main contributors to ionic flux, however these contributors have different relative importance in the MacPF membranes compared to commercial nanofiltration membranes.

Solute rejection in the MacPF and commercial membranes depends primarily on both steric effects and charge repulsion. Whereas, experimental findings make clear that both separation and selectivity of the MacPF membranes are primarily determined by Donnan exclusion and not by steric effects. Both types of membranes have an intermediate (60-70%) rejection of sodium chloride. However, lactose rejection is low (10-20%) in the MacPF membrane; whereas, rejection is high (99%) in the commercial membrane.

7.2 Conclusions on Transport Model

The performance of the commercial membranes was described successfully using a transport model based on the extended Nernst-Planck equation, the Poisson-Boltzmann equation, and hydrodynamic calculations. The model has three fitting parameters that describe four membrane structural parameters: the pure water permeability (L_P), pore radius (r_P), the surface charge density (q_w), and ratio of membrane thickness to water content (λ/E).

The pure water permeability was obtained form experimental pure water flux vs. pressure data. The surface charge density and pore radius were obtained by fitting the model using data from mixed-solute solutions (NaCl and lactose). The ratio of membrane thickness to pore radius was calculated from the Hagen-Poiseuille equation.

The transport model predicted qualitatively and quantitatively membrane performance for other single salts, mixed electrolytes, and mixed solutes. The

parameters obtained for these membranes are statistically significant (small 95% confidence intervals) and are in agreement with previous findings (Garcia-Aleman, 1998). An insightful interpretation of the performance of the membrane was given based on model performance and parameters. Discrepancies between model calculations and experimental data were interpreted from assumptions in the model.

The following is a summary of the key elements that were modified or improved from previous work (Garcia-Aleman, 1998):

- This model combines and modifies, for the first time, existing theory to describe the pressure-driven performance of the MacPF membrane. A modified PBE is used to describe the radial distribution of the electrostatic potential and concentrations.
- The model uses a pseudo-2-dimensional approach as opposed to a 1-dimensional approach. The 2-dimensional approach allows the description of the axial and radial contributions of the transport mechanisms inside the membrane. The approach proposed here used radially-averaged quantities, which provided an accurate description of membrane performance, without the computational expense associated with full 2-D approaches.
- This model uses only 3 fitting parameters to describe 4 structural parameters of the membrane. The parameters are independent of operating conditions, except for the charge density of the membrane. The

model proposed by Garcia-Aleman (1998) uses the same number of parameters, however the charge density of the membrane is assessed differently, as discussed later.

- The model requires a smaller data set to fit the parameters, compared to other models in the literature (see for example, Bowen et al., 1997 or Chevalier, 1999).
- Two of the model parameters are obtained simultaneously (pore radius and surface charge density) by fitting the model to data from mixed-solute solutions (NaCl plus lactose). Normally, a combination of measurement, single salts, and/or single solute experiments are used to determine the model parameters. This is the first time, to our knowledge, that mixed-solute experiments are used to determine these parameters simultaneously.
- The charge density-concentration dependency is described by semi-empirical correlations as opposed to a mechanistic approach (Garcia-Aleman, 1998). Novel concepts were not created in this area, however, the approach is mentioned since it is different from the original formulation.
- Minor modifications include the inclusion of the effect of osmotic pressure on the compressibility of the membrane and the inclusion of a linearized version of the streaming potential term in the solution flux equation for a NF model.

7.3 Conclusions on Tailor-making of MacPF Membrane

A model for gel conformation and a model for membrane transport were presented in this investigation. Both models can be used to predict membrane performance with only knowledge of the physicochemical parameters of the polyelectrolyte gel-filled membrane.

The physicochemical parameters and the transport model parameters were estimated using experimental data. These parameters were compared to the parameters estimated from theory (gel model) and some agreement was found. Agreement was found between both models, especially on predictions of rejection. However, additional work is required to implement these models as a single predictive tool, as discussed later.

7.4 Recommendations and Future Work

No work is ever complete. No model is perfect. From this investigation the following recommendations for future work are made:

- The transport model presented here takes into account only two main rejection mechanisms, steric and electrostatic effects. Hydration effects, attractive forces, and dielectric effects can affect membrane performance. However, at the moment, there is no accurate quantitative description of these phenomena that can be used in a mechanistic transport model. These effects should be accounted for in the model.

- The underlying mechanisms that cause charge inversion inside a membrane are not clearly understood (Shaep et al., 1999). Additional data need to be collected to understand the role of the valence and concentration of the counter-ion in this phenomenon. Based on the data presented by Shaep et al. (1999) and the data presented here, this phenomenon may occur for single- or mixed-electrolyte solutions.
- The effect of a common counter-ion (mixtures) on membrane performance is clearly understood. Membrane selectivity (Donnan exclusion) is normally determined by the valence of the co-ion, and to a lesser extent by the valence of the counter-ion. However, this 'common' idea does not take into account the role of the counter-ion in charge inversion. Data need to be collected with mixtures containing common counter-ions and common co-ion, in order to determine the effect of each ion on membrane rejection.
- The concept of 'tailor-making' involves the development of a procedure and two mechanistic models that describe the structure and the performance of the membrane. In this dissertation these models were developed independently. The parameters for each model (gel and transport) were estimated independently and compared, as depicted in Fig. 7.1. The results obtained so far are promising. However, additional work has to be done to evaluate the full tailor-making concept.

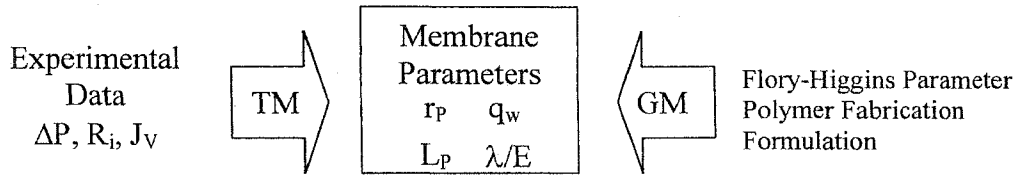

Figure 7.1 Schematic representation of the procedure used to compared independent estimates of the membrane parameters using the gel (GM) and transport (TM) models.

- The ultimate check to the concept of 'tailor making' is to test the procedure and models together, as depicted in Fig. 1.10. A pore-filled membrane will be prepared using the two mechanistic models based on a desired membrane performance (flux and separation). Then, the performance of this membrane will be tested to confirm that the actual membrane performance is indeed the same as the desired performance.
- The experiments performed in here are made at relatively low concentrations, where the effect of osmotic pressure is small. Experimental conditions should be extended to higher total concentrations to test the predictive capabilities of the model and the performance of the MacPF membranes.
- The model can be used to simulate and optimize the performance of the MacPF membrane for different module configurations under different operating conditions (for example, number and type of solutes, pressure, concentration, cross-flow velocity).

Nomenclature

A	:	Contour distance between charged groups, (m)
	:	empirical coefficient in eq. 4.41, dimensionless
a	:	number of bonds on a polymer chain, dimensionless
B	:	empirical coefficient in eq. 4.41, dimensionless
B_i	:	frictional coefficient in Jonsson (1980), dimensionless
b_i	:	hindered diffusion parameter, dimensionless
C_i	:	ion concentration in solution, (mol/m^3)
$C_{i,p}(z)$	:	ion concentration in the pore at point z, (mol/m^3)
C_X	:	volumetric charge density of the membrane, (mol/m^3)
c	:	concentration (mol/m^3)
$D_{i,p}$	:	ionic diffusivity inside the pore, (m^2/s)
$D_{i,\infty}$	:	ionic diffusivity at infinite dilution, (m^2/s)
DF_i	:	degree of fractionation as defined in eq. 2.6, dimensionless
E	:	water content of the membrane, dimensionless
F	:	Faraday's constant, (9,6487.0 C/mol)
g_i	:	least squares dependent function, variable units
h_i	:	least squares independent variable, variable units
I	:	electrical current, (C/s)
	:	ionic strength as defined in eq. 4.42, (mol/m^3)
J_i	:	ion flux based on membrane area, (mol/m^2 s)
J_V	:	solution flux, (m^3/m^2 s)
J_W	:	pure water flux, (m^3/m^2 s)
K_{ei}	:	constant for eq. 3.17, dimensionless
K_i	:	partition coefficient, dimensionless
$K_{i,o}$	:	zero partition coefficient as defined in Jonsson (1980), dimensionless

k : mass transfer coefficient, (m/s)

k_B : Boltzmann constant, (1.38×10^{-23} J/K)

k_m : membrane permeability, (m^{-2})

k_H : gel permeability, (m^{-2})

$L_{i,j}$: phenomenological coefficient as defined in eq. 3.1, variable units

L_P : pure water permeability, (m^3/m^2 s kPa)

L_{PE} : bare persistence length, (m)

L_{Po} : pure water permeability when no pressure is applied, (m^3/m^2 s kPa)

L_e : Electrostatic persistence length, (m)

l_B : Bjerrum length, dimensionless

m_i : molality, (mol/kg)

n : total number of ions or solutes, dimensionless

number of bonds on persistence length, dimensionless

n_{qe} : number of charged groups, (mol/m^3)

P : hydrostatic pressure, (kPa)

P_i : solute permeability, (m/s)

Q_i : volumetric flow, (m^3/s)

: assemblage radius, (m)

Re : Reynold's number, dimensionless

R_e : fluid envelope radius, (m)

R_i : ion or solute rejection, (%)

R'_i : theoretical ion or solute rejection, (%)

r_i : hydrodynamic radius, (m)

r^* : dimensionless radial position, dimensionless

r_P : pore radius, (m)

Sc : Schmidt's number, dimensionless

Sh : Sherwood's number, dimensionless

T : absolute temperature, (K)

t : tortuosity of the membrane, dimensionless

t_i : transport number, dimensionless

u : local solution flux ($m^3/m^2/s$)

q_o : dimensionless surface charge density, dimensionless

q_w : surface charge density, (C/m^2)

w : excluded volume parameter dimensionless

X_j : driving force as defined in eq. 3.1, variable units

x : linear axial coordinate, (m)

y(r) : dimensionless electrostatic potential, dimensionless

z_i : ion valence, dimensionless

z : effective axial coordinate, (m)

z* : dimensionless axial position, dimensionless

Greek

α_i : hindered convection parameter, dimensionless

α_o : compaction coefficient, (kPa^{-1})

γ_i : activity coefficient, dimensionless

δ : polymer volume fraction, dimensionless

ϵ : porosity of the membrane, dimensionless

ϵ_o : dielectric constant of vacuum, (8.8542×10^{12} C^2/J m)

ϵ_r : relative dielectric constant of water, (78.303)

ϵ_S : porosity of substrate, dimensionless

ζ : zeta potential, (V)

η_i : ratio of ion to pore radius, dimensionless

θs : ratio of effective to maximum charge density as defined in eq. 3.17, dimensionless

φ : Surface electrical potential (V)

κ : Debye screening length, (m^{-1})

λ : effective membrane thickness, (m)

μ : viscosity of the solution, (cP = 0.896×10^6 kPa s)

ν_i : stoichiometric coefficient, dimensionless

ν_2 : partial specific volume, dimensionless

ξ : electrostatic component of partition coefficient, dimensionless

ξ_p : correlation length, (m)

$\Delta\pi$: osmotic pressure difference, (kPa)

ρ_C : local charge density, (mol/m^3)

σ : reflection coefficient, dimensionless

χ : Flory-Huggins interaction parameter, dimensionless

$\chi_{i,p}$: solute-membrane friction coefficient, (kJ s/m^2 kmol)

$\chi_{i,w}$: solute-solvent friction coefficient, (kJ s/m^2 kmol)

Ψ : membrane electrical potential, (J/C = V)

$\Delta\Psi_D$: Donnan potential, (V)

Φ_i : steric component of partition coefficient, dimensionless

ϕ : axial component of electrical potential, (V)

Superscripts

P : permeate solution

B : bulk solution

R : retentate solution

Subscripts

i : i^{th}

j : j^{th}

m : just outside the membrane

p : in pore phase

s : salt or solute

x : charge density

+ : cation

- : anion

References

Anderson, J. and D. Malone, "Mechanism of Osmotic Flow in Porous Membranes", Biophys. J., 14, 957, 1974.

Anderson, J. and D. Quinn, "Restricted Transport in Small Pores: A Model for Steric Exclusion and Hindered Particle Motion", Biophys. J., 14, 130, 1974.

Applegate, L., "Membrane Separation Processes", Chem. Eng., June 11, 64, 1984.

Armostrong, M., Personal Communication, 1997.

Atkins, P., "Physical Chemistry", W.H. Freeman and Company, New York, 1994.

Basu, H. and M. Sharma, "An Improved Space-Charge Model for Flow Through Charged Microporous Membranes", J. Membr. Sci., 124, 77, 1997.

Bird, R., W. Stewart and E. Lightfoot, "Transport Phenomena", John Wiley & Sons, New York, 1960.

Bontha J. and P. Pintauro, "Water Orientation and Ion Solvantion Effects during Multicomponent Salt Partitioning in a Nafion Cation Exchange Membrane", Chem. Eng. Sci., 49, 3835, 1994.

Bowen, W., A. Mohammad and N. Hilal, "Characterisation of Nanofiltration Membranes for Predictive Purposes – Use of Salts, Uncharged Solutes and Atomic Force Microscopy", J. Membr. Sci., 126, 91, 1997.

Bowen, W. and A. Mohammad, "Characterization and Prediction of Nanofiltration Membrane Performance-a General Assessment", Trans IChemE, 76(A), 885, 1998.

Bowen, W. and H. Mukhtar, "Characterisation and Prediction of Separation Performance of Nanofiltration Membranes", J. Membr. Sci., 112, 263, 1996.

Bowen, W. and O. Sharif, "Transport Through Microfiltration Membranes – Particle Hydrodynamics and Flux Reduction", J. Colloid and Interface Sci., 168, 414, 1994.

Buck, R., "Kinetics of Bulk and Interfacial Ionic Motion: Microscopic Bases and Limits for the Nernst-Planck Equation Applied to Membrane Systems", J. Membrane Sci., 17, 1, 1984.

Chevalier, S., Modélisation Mathématique des Mécanismes de Séparation en Nanofiltration, Ph.D. Thesis, Université de Bordeaux I, Bordeaux, France, 1999.

Comstock, D., "DESAL-5 Membrane for Water Softening", Desalination, 76, 61, 1989.

Cussler, E., "Diffusion: Mass Transfer in Fluid Systems", Cambridge University Press, Cambridge, 1984.

de Gennes, P., "Scaling Concepts in Polymer Physics", Cornell University Press, Ithaca, 1979.

Deen, W., "Hindered Transport of Large Molecules in Liquid-Filled Pores", AIChE J., 33 (9), 1409, 1987.

Dennis, J. and R. Schnabel, "Numerical Methods for Unconstrained Optimization and Nonlinear Equations", Prentice-Hall, Inc., Englewood Cliffs, 1983.

Dickson, J., "Fundamental Aspects of Reverse Osmosis", in "Reverse Osmosis Technology: Application for High-Purity-Water Production", B. Parekh (ed.), Marcel Dekker, Inc., New York, 1988.

Donnan, F., "The Theory of Membrane Equilibria", Chem. Rev., 1, 73, 1924.

Dresner, L., "Stability of the Extended Nernst-Planck Equations in the Description of Hyperfiltration Through Ion-Exchange Membranes", J. Physical Chem., 76, 2256, 1972.

Dresner, L. and J. Johnson, "Hyperfiltration (Reverse Osmosis)", in "Principles of Desalination Vol. II", K. Spiegler and A. Laird (eds.), Academic Press, New York, 1980.

Eriksson, P., "Nanofiltration Extends the Range of Membrane Filtration", Environmental Progress, 7 (1), 58, 1988.

Ferry, J., "Statistical Evaluation of Sieve Constants in Ultrafiltration", J. Gen. Physiol., 20, 95, 1936.

Fletcher, R., "Practical Methods of Optimization", John Wiley & Sons, Chichester, 1989.

Garcia-Aleman, J., Mathematical Modeling of the Pressure-driven Performance of Nanofiltration Membranes; Mixed Electrolyte Systems, M. Eng. Thesis, McMaster University, Hamilton, Ontario, Canada, 1998.

Gill, P., W. Murray and M. Wright, "Practical Optimization", Academic Press, Inc., San Diego, 1993.

Gross, R. and J. Osterle, "Membrane Transport Characteristics of Ultrafine Capillaries", J. Chem. Phys., 49(1), 228, 1961.

Hagmeyer and R. Gimbel, "Modelling the Salt Rejection of Nanofiltration Membranes for Ternary Ion Mixtures and for Single Salts at Different pH Values", Desalination, 117, 247, 1998.

Hall, M., V. Starov and D. Lloyd, "Reverse Osmosis of Multicomponent Electrolyte Solutions: Part I. Theoretical Development", J. Membr. Sci., 128, 23, 1997.

Haberman, W. and R. Sayre, "David Taylor Model Basin Report No. 1143", Washington, C.C., US Navy Dept. (1958).

Happel, J. and H. Brenner, "Low Reynold Number Hydrodynamics", Noordhof International Publishing, Leyden, 1973.

Happel, J., "Viscous Flow in Multiparticle Systems: Slow Motion Fluids Relative to Beds of Spherical Particles", AIChE J., 4, 197, 1958.

Helfferich, H., "Ion Exchange", McGraw-Hill, New York, 1962.

Hijnen, H. and J. Smit, "The Effect of the pH on Electrolyte Transport Through Microporous Membranes Bearing Either Weakly or Strong Dissociating Acid Groups. A Theoretical Analysis Using the Space-Charge Model for a Cylindrical Capillary", J. Membr. Sci., 99, 285, 1995.

Ho, W. and K. Sirkar, "Membrane Handbook", Van Nostrand Reinhold, New York, 1992.

Jacazio, G., R. Probstein, A. Sonin and D. Yung, "Electrokinetic Salt Rejection in Hyper-filtration Through Porous Materials. Theory and Experiment", J. of Phys. Chem., 76(26), 4015, 1972.

Jonsson, G., "Coupling of Ion Fluxes by Boundary-, Diffusion- and Streaming-Potentials under Reverse Osmosis Conditions", in "Proceedings of the 7th. International Symposium on Fresh Water from the Sea", 2, 153, 1980.

Jonsson, G. and C. Boesen, "Water and Solute Transport Through Cellulose Acetate Reverse Osmosis Membranes", Desalination, 17, 145, 1975.

Kedem, O. and A. Katchalsky, "Thermodynamic Analysis of the Permeability of Biological Membranes to Non-Electrolytes", Biochim. Biophys. Acta, 27, 229, 1958.

Kedem, O. and A. Katchalsky, "A Physical Interpretation of the Phenomenological Coefficients of Membrane Permeability", J. Gen. Physiol, 45, 143, 1961.

Levenberg, K., "A Method for the Solution of Certain Problems in Least Squares", Q. Appl. Math., 2, 164, 1944.

Levenstein, R., D. Hasson and R. Semiat, "Utilization of the Donnan Effect for Improving Electrolyte Separation with Nanofiltration Membranes", J. Membr. Sci., 116, 77, 1996.

Lightfoot, E., "Transport Phenomena and Living Systems, Wiley-Interscience, New York, 186, 1974.

Linde, K. and A. Jönsson, "Nanofiltration of Salt Solutions and Landfill Leachate", Desalination, 103, 223, 1995.

Lonsdale, H., U. Merten and M. Tagami, "Phenol Transport in Cellulosic Acetate Membranes", J. Appl. Poly. Sci., 9, 1341, 1965.

Lloyd, D., K. Kinzer and H. Tseng," Microporous Membrane Formation via Thermally Induced Phase Separation. I. Solid-Liquid Phase Separation", J. Membr. Sci., 52, 239, 1990.

Loeb, S. and S. Sourirajan, "Sea Water Demineralization by Means of an Osmotic Membrane", Advan. Chem. Ser., 38, 117, 1962.

Manning, G., "Limiting Laws and Conterion Condensation in Polyelectrolyte Solutions. I. Colligative Properties", J. Chem. Phys., 51, 924, 1969.

Marquardt, D., "An Algorithm for Least-Squares estimation of Nonlinear Parameters", SIAM J. Appl. Math., 11, 1963.

Mason, E. and H. Lonsdale, "Statistical-Mechanical Theory of Membrane Transport", J. Membrane Sci., 51, 1, 1990.

Matsuura, T. and S. Sourirajan, "Reverse Osmosis Transport Through Capillary Pores Under the Influence of Surface Forces", Ind. Eng. Chem. Process Des., 20, 273, 1981.

Matsuura, T., Y. Taketani and S. Sourirajan, "Estimation of Interfacial Forces Governing the Reverse Osmosis System: Nonionized Polar Organic Solute-Water-Cellulose Acetate Membrane", in "Synthetic Membranes", A. Turbak, Ed., ACS Symposium Series, Washington, D.C., 1981.

Meares, P., J. Thain and D. Dawson, "Transport across Ion-exchange Resin Membranes: the Frictional Model of Transport", in "Membranes: A Series of Advances", G. Eisenman (ed.), 1, 55, 1972.

Mehdizadeh, H., "Modeling of Transport Phenomena in Reverse Osmosis Membranes", Ph.D. Thesis, McMaster University, Hamilton, Ontario, 1990.

Mehdizadeh, H. and J. Dickson, "Theoretical Modification of the Surface Force-Pore Flow Model for Reverse Osmosis Transport", J. Membr. Sci., 42, 119, 1989a.

Mehdizadeh, H. and J. Dickson, "Evaluation of Surface Force-Pore Flow and Modified Surface Force-Pore Flow Models for Reverse Osmosis Transport", Desalination, 42, 119, 1989b.

Merten, U., "Desalination by Reverse Osmosis", MIT Press, Cambridge, 1966.

Meyer, K. and J. Sievers, "La Permeabilite des Membranes 1. Theorie del a Permeabilite Ionique", Helv. Chim. Acta, 19, 649, 1936.

Mika, A., R. Childs, J. Dickson, B. McCarry and D. Gagnon, "Porous, Polyelectrolyte-filled Membranes: Effect of Cross-linking on Flux and Separation", J. Membr. Sci., 135, 81, 1997.

Mika, A., R. Childs, J. Dickson, B. McCarry and D. Gagnon, "A New Class of Polyelectrolyte-filled Microfiltration Membrane with Environmentally Controlled Porosity", J. Membr. Sci., 108, 37, 1995.

Mika, A., R. Childs, J. Garcia-Aleman and J. Dickson, "Theoretical Design and Physical Modeling of Charged 'Gel in Shell' Nanofiltration Membranes", in "The 1999 International Congress on Membranes and Membrane Processes", Toronto, 1999.

Mika, A. and R. Childs, "Calculation of the Hydrodynamic Permeability of Gels and Gel-Filled Microporous Membranes", Ind. Eng. Chem. Research, 40(7), 1694, 2001.

Mika, A., A. Pandey and R. Childs, "Ultra-low-pressure Water Softening with Pore-filled Membranes", Desalination, 140, 265, 2001.

Morrison Jr., F. and J. Osterle, "Electrokinetic Energy Conversion in Ultrafine Capillaries", J. Chem. Phys., 43(6), 2111, 1965.

Mulder, M., "Basic Principles of Membrane Technology", Kluwer, London, 1996.

Murthy, Z. and S. Gupta, "Estimation of Mass Transfer Coefficient Using a Combined Nonlinear Membrane Transport and Film Theory Model", Desalination, 109, 39, 1997.

Nakao, S., "Membrane Transport Phenomena and Ultrafiltration", in Encyclopedia of Fluid Mechanics, P. Cheremisinoff (ed.), 987, 1986.

Nakao, S. and S. Kimura, "Models of Membrane Transport Phenomena and Their Applications for Ultrafiltration Data", J. Chem. Eng. Jpn., 15 (3), 200, 1982.

Nielsen, D. and G. Jonsson, "Bulk-Phase Criteria for Negative Ion Rejection in Nanofiltration of Multicomponent Salt Solutions", Sep. Sci. and Tech., 29 (9), 1165, 1994.

Neogi, P. and E. Ruckenstein, "Viscoelectric Effects in Reverse Osmosis", J. Colloid Interface Sci., 79(1), 159, 1981.

Nernst, W., "Zur Kinetic der in Losung Befindilichen Korper. I. Theorie der Diffusion", Z. Phys. Chem., 2, 613, 1888.

Oasawa, F., "Polyelectrolytes", Marcel Dekker, New York, 1971.

Odijk, T., "Possible Scaling Relations for Semidilute Polyelectrolyte Solutions", Macromolecules, 12, 688, 1979.

Odijk, T., "Polyelectrolytes Near the Rod Limit", J. Polym. Sci., Polym. Phys. Ed., 15, 477, 1977.

Oldham, I., F. Young and J. Osterle, "Streaming Potential in Small Capillaries", J. Colloid Sci., 18, 328, 1963.

Onsager, L., "Reciprocal Relations in Irreversible Processes", Phys. Rev., 37, 405, 1931.

Perry, M. and C. Linder, "Intermediate Reverse Osmosis Ultrafiltration (RO UF) Membranes for Concentration and Desalting of Low Molecular Weight Organic Solutes", Desalination, 71, 233, 1989.

Petersen, R., "Composite Reverse Osmosis and Nanofiltration Membranes", J. Membr. Sci., 83, 81, 1993.

Planck, M., "Ueber die Erregung von Electricitat und Warme in Electrolyten", Ann. Phys., 39, 161, 1890.

Planck, M., "Ueber die Ptentialdifferenz zwischen zwei verdunnten Losungen Binaren Electrolyte", Ann. Phys., 40, 561, 1890.

Probstein, R., A. Sonin and D. Yung, "Brackish Water Salt Rejection by Porous Hyper-filtration Membranes", Desalination, 13, 303, 1973.

Raman, L., M. Cheryan and N. Rajagopalan, "Consider Nanofiltration for Membrane Separations", Chem. Eng. Prog., 90, 68, 1994.

Rautenbach, R., K. Vossenkaul, T. Linn and T. Katz, "Waste Water Treatment by Membrane Processes- New Development in Ultrafiltration, Nanofiltration and Reverse Osmosis", Desalination, 108, 247, 1996.

Schaefer, D., "A Unified Model for the Structure of Polymers in Semi-dilute Solutions", Polymer, 25, 387, 1984.

Schirg, P. and F. Widmer, "Characterisation of Nanofiltration Membranes for the Separation of Aqueous Dye-Salt Solutions", Desalination, 89, 89, 1992.

Schlögl, R., "Membrane Permeation in Systems Far from Equilibrium," Berichte der Bunsegeselschaft, 70, 400, 1966.

Shaep, J., C. Vandecasteele, A. Mohammad and R. Bowen, "Analysis of the Salt Retention of Nanofiltration Membranes using the Donnan-Steric Partitioning Pore Model", Sep. Sci. and Tech., 34, 309, 1999.

Shampine L. and M. Gordon, "Computer Solution of Ordinary Differential Equations: The Initial Value Problem", W.H. Freeman and Company, San Francisco, 1975.

Sherwood, T., P. Brian and R. Fisher, "Desalination by Reverse Osmosis", I&EC Fund., 6(1), 2, 1967.

Skolnick, J. and M. Fixman, "Electrostatic Persistence Length of a Wormlike Polyelectrolyte", Macromolecules, 10, 944, 1977.

Smit, J., "Reverse Osmosis in Charged Membranes: Analytical Predictions from the Space-Charge Model", J. of Colloid Interface Sci., 132(2), 413, 1989.

Soltanieh, M. and W. Gill, "Review of Reverse Osmosis Membranes and Transport Models", Chem. Eng. Commun., 12, 279, 1981.

Sourirajan, S., "The Mechanism of Demineralization of Aqueous Sodium Chloride Solutions by Flow, Under Pressure, Through Porous Membranes", Ind. Eng. Chem. Fundam., 2, 51, 1963.

Sourirajan, S., "Reverse Osmosis", Logos Press, London, 1970.

Spiegler, K., "Transport Processes in Ionic Membranes", Trans. Faraday Soc., 54, 1408, 1958.

Spiegler, K. and O. Kedem, "Thermodynamics of Hyperfiltration (Reverse Osmosis). Criteria for Efficient Membranes", Desalination, 1, 311, 1966.

Staverman, A., "The Theory of Measurement of Osmotic Pressure", Recueil Trav. Chim. Pays-Bas, 70, 344, 1951.

Teorell, T., "Transport Processes and Electrical Phenomena in Ionic Membranes", Progr. Biophysics, 3, 305, 1953.

Thom, A., "Electrostatic Double Layer Interactions in the Transport Modelling of Reverse Osmosis", M.Eng. Thesis, McMaster University, Hamilton, Ontario, 1993.

Tsuru, T., S. Nakao and S. Kimura, "Calculation of Ion Rejection by Extended Nernst-Planck Equation with Charged Reverse Osmosis Membranes for Single and Mixed Electrolyte Solutions", J. Chem. Eng. Jpn., 24(4), 511, 1991.

Tsuru, T., M. Urairi, S. Nakao and S. Kimura, "Reverse Osmosis of Single and Mixed Electrolytes with Charged Membranes: Experiment and Analysis", J. Chem. Eng. Jpn., 24(4), 518, 1991.

Vellenga, E. and C. G. Trägårdh, "Nanofiltration of Combined Salt and Sugar Solutions: Coupling Between Retentions", Desalination, 120, 211, 1998.

Van der Buggen, B. J. Schaep, D. Wilms and C. Vandecasteele, "Influence of Molecular Size, Polarity and Charge on the Retention of Organic Molecules by Nanofiltration", J. Membr. Sci, 156, 29, 1999.

Wang, X., T. Tsuru, S. Nakao and S. Kimura, "Electrolyte Transport Through Nanofiltration Membranes by the Space-Charge Model and the Comparison with Teorell-Meyer-Sievers Model", J. Membr. Sci., 103, 117, 1995a.

Wang, X., T. Tsuru, S. Nakao and S. Kimura, "The Electrostatic and Steric-Hindrance Model for the Transport of Charged Solutes Through Nanofiltration Membranes", J. Membr. Sci., 135, 19, 1997.

Wang, X., T. Tsuru, M. Togoh, S. Nakao and S. Kimura, "Evaluation of Pore Structure and Electrical Properties of Nanofiltration Membranes", J. Chem. Eng. Jpn., 28(2), 186, 1995b.

Wang, X., T. Tsuru, M. Togoh, S. Nakao and S. Kimura, "Transport of Organic Electrolytes with Electrostatic and Steric-Hinderance Effects Through Nanofiltration Membranes", J. Chem. Eng. Jpn., 28(4), 372, 1995c.

Xu, J., X. Xing, S. Yamamoto, Y. Tanji and H. Unno, "Effect of Ion Adsorption on its Permeation Through Nanofiltration Membrane", J. Chem. Eng. Jpn., 30(5), 80, 1997.

Yaroshchuk, A., C. Bardot, E. Gaubert, N. Kulov and A. Nechaev, "Modeling of the Pressure-Driven Transport of Single and Mixed Electrolyte Solutions Across Fine-Porous Inorganic Membranes. Criteria for Efficient Rejection and Separation", in "Proceedings of the Third International Conference on Inorganic Membranes", Worcester 1994.

Yaroshchuk, A. and Y. Vovkogon, "Phenomenological Theory of Pressure-Driven Transport of Ternary Electrolyte Solutions with a Common Coion and its Specification for Capillary Space-Charge Model", J. Membr. Sci., 86, 1, 1994.

Appendix A

Fabrication Procedure of the McMaster Pore-filled Membranes

This section details the materials and methods used to fabricate the MacPF membranes. The methods for membrane characterization are briefly presented at the end of this section.

A.1 Materials

The microfiltration substrates used in this investigation were made of PE and PP. These substrate membranes were supplied by 3M Company and produced by a thermally-induced phase separation (see Lloyd et al., 1990). The PE substrates had a nominal pore radius of 0.2 μm determined by a bubble point method, a porosity of 60-70 vol%, and a thickness of 51±5 μm (Mika et al., 1995). The PP substrates had a nominal pore radius of 0.82 μm, a porosity of 80.5 vol%, and a thickness of 79 μm (Mika et al., 2001).

A.1.1 Materials for the MacPF Membranes with a PE Substrate

The membranes with the polyethelene substrate were pore-filled with 4-vinylpyridine (Aldrich), which was purified by vacuum distillation. The cross-linking agent, DVB (technical grade), was washed with 1 M NaOH and water and

dried over anhydrous Na_2SO_4 prior to vacuum distillation. The fraction of DVB in the distillate was 55% (determined by proton NMR). 2,2-Dimethoxy-2-phenylacetophenone (DMPA) (Aldrich) was used as a photochemical initiator.

A.1.2 Materials for the MacPF Membranes with a PP Substrate

The membranes with the PP substrate were pore-filled with 4-vinylpyridine (Aldrich) and cross-linked with dibromo-*p*-xylene (Aldrich). *N,N*-dimethylformamide (DMF) (Caledon) was used as a solvent for the polymer solution. Quaternization was performed with benzyl bromide (Aldrich). Methanol (Caledon) was used for washing. All other reagents were used without further purification.

A.2 Membrane Preparation

The membranes MacPF 352, 324 and 382 were fabricated by pore-filling polyethylene substrates with 4-vinylpyridine (4VP) cross-linked with divinylbenzene (DVB). The membranes MacPF 515, 508, 509, and AL7 were fabricated by pore-filling polypropylene substrates with 4-vinylpyridine cross-linked with dibromo-*p*-xylene (DBX).

These membranes were quaternized by methylation, as discussed later. The membrane MacPF AL7 was quaternized by cross-linking only. No subsequent quaternization was performed.

A.2.1 Membrane Preparation: Photografting

The MacPF membranes with a PE substrate were prepared by an *in situ* polymerization (photo-grafting) of 4VP/DVB mixtures in the pores of the porous substrates according to the procedure described in detail in the literature (Mika et al., 1995) and summarized below. In the case of the MacPF membrane 382, the 4VP/DVB mixture was diluted with pyridine (20 wt%).

The grafting procedure was carried out in a Rayonet-type photo-reactor (Mika et al., 1995). The PE substrates were cut into rectangular pieces of appropriate sizes, soaked in acetone for 16 h, and vacuum dried at room temperature. A substrate of know mass was placed on the inner wall of the reactor and 1-2 mL of the monomer, or the monomer with DVB, containing 1-1.5 wt/vol% photo-initiator was poured into the bottom. The reactor and contents were degassed in 2-3 freeze-thaw cycles. The membrane was wetted with the monomer by rotating the vessel in a horizontal position. The wetted membrane was then irradiated with 10 UV lamps at 300 nm for a given time (1-2 h).

Unreacted monomers, oligomers, and unbound homopolymers were extracted with boiling methanol until no change in mass of the vacuum-dried membranes could be detected. The pyridine groups of the *in situ* formed cross-linked polymer were quaternized by *N*-methylation using a solution of 5-10 vol% of dimethyl sulfate in methanol. The reaction was carried out at room temperature for about 16 h. The pore-filled membranes were subsequently washed with methanol and, finally, with de-ionized water.

A.2.2 Membrane Preparation: *in situ* Cross-linking

The MacPF membranes with a polypropelene substrate were made by *in situ* cross-linking of 4VP with DBX (Mika et al., 2001) according to the following procedure. A weighed sample of a substrate was placed on a glass plate, and a 4VP/DBX mixture was applied to the sample. After the excess solution was removed using a Teflon roller, a Teflon gasket was placed around the sample and another glass plate put on top of it. The gasket thickness was such that a gap of a few millimeters was left between the sample and the top plate. A few drops of DMF were placed around the membrane to saturate the space with DMF vapor and prevent the membrane from drying. The cross-linking reaction occurred at room temperature for 16-48 h.

Subsequently, the sample was removed from the glass plate and immersed in a quaternization solution to convert the remaining pyridine moieties into pyridinium sites. The quaternization solutions used contained 5 vol% of benzyl bromide in DMF. The reactions were carried out at room temperature for 16-24 h. The pore-filled membranes were washed with methanol followed by thorough washing with de-ionized water. The membranes were conditioned in 0.1 M HCl, washed with de-ionized water and stored in dilute HCl (pH 2-3).

Appendix B

Tabulated Data for Experimental Runs

The experimental data for the membranes HN-7450 and MacPF 352, 324, 382, 515, 508, 509 and AL7 are presented. The tabulated data are divided into single electrolyte (Tables B.1-B.6), mixed solute (Tables B.7-B.10) and mixed electrolyte solutions (Tables B.11-B.18).

Table B.1 Experimental data for single salt solutions (NaCl) as a function of applied pressure (ΔP = 0.3-1.5 MPa) and constant feed concentration (5 mol/m^3). Membranes: 352, 324, 382 and HN-7450.

Applied Pressure, ΔP (kPa)	Target Feed Conc. (mol/m^3)	Actual Feed Conc. (mol/m^3)	Pure Water Flux, J_W x 10^6(m/s)				Solution Flux, J_V x 10^6(m/s)				Rejection, R_i (%)			
			352	324	382	HN-7450	352	324	382	HN-7450	352	324	382	HN-7450
500	5	6.08	1.11	1.38	8.18	3.45	1.10	1.38	8.22	3.39	86.34	87.72	21.22	77.09
500	5	6.24	1.17	1.47	8.54	3.65	1.12	1.40	8.64	3.52	80.40	82.36	7.45	70.85
300	5	6.24	0.85	1.09	5.63	3.88	0.77	0.99	5.62	2.14	73.67	77.62	8.52	61.95
900	5	6.28	1.27	1.45	12.63	6.65	1.46	1.75	12.42	6.40	82.77	83.96	4.33	80.50
900	5	5.59	1.69	2.29	10.33	7.70	1.67	2.26	10.50	6.91	77.45	77.69	8.53	77.45
500	5	5.41	1.16	1.45	7.25	4.10	1.22	1.56	7.33	4.03	75.92	77.41	7.65	76.39
300	5	5.43	0.81	1.14	4.63	2.54	0.81	1.11	4.57	2.34	68.56	72.59	7.56	70.18
1500	5	5.04	2.30	2.95	16.85	13.43	2.32	3.08	16.56	13.28	82.69	77.19	6.19	88.22
1500	5	5.07	1.85	18.67	15.62	13.57	2.06	19.15	15.55	13.39	81.40	11.30	7.34	87.06
1500	5	4.95	1.60	9.23	14.92	13.52	2.02	14.51	14.51	13.14	81.17	15.05	8.34	87.27
500	5	4.47	1.11	1.77	5.19	3.43	1.23	1.88	5.41	3.41	79.62	79.41	11.60	86.67
300	5	4.47	0.82	1.42	3.41	2.17	0.86	1.41	3.41	2.05	80.40	82.49	7.98	76.03
900	5	4.40	1.77	2.61	8.08	5.51	1.75	2.59	7.82	5.02	88.15	88.26	7.77	89.63
700	5	4.37	1.51	2.31	6.24	4.24	1.49	2.28	6.01	3.92	87.12	86.20	11.73	88.98

Table B.2 Experimental data for single salt solutions (Na_2SO_4) as a function of applied pressure (ΔP = 0.3-1.5 MPa) and constant feed concentration (5 mol/m^3). Membranes: 352, 324, 382 and HN-7450.

Applied Pressure, ΔP (kPa)	Target Feed Conc. (mol/m^3)	Actual Feed Conc. (mol/m^3)	Pure Water Flux, J_W x 10^6(m/s)				Solution Flux, J_V x 10^6(m/s)				Rejection, R_i (%)			
			352	324	382	HN-7450	352	324	382	HN-7450	352	324	382	HN-7450
500	5	4.89	0.99	1.16	8.83	3.56	0.76	0.84	8.76	3.27	16.55	17.82	21.13	97.27
300	5	4.93	0.72	0.89	5.78	2.29	0.55	0.65	5.91	2.00	7.02	15.54	14.98	96.48
900	5	4.93	1.11	1.15	13.63	6.73	1.03	1.08	13.45	6.44	19.22	17.82	29.64	98.34
900	5	4.20	1.55	4.05	10.64	7.80	1.18	1.41	10.81	7.28	20.90	17.04	20.24	99.34
500	5	4.22	1.08	1.31	7.43	4.26	0.90	1.01	7.30	3.93	14.17	14.26	21.20	97.57
300	5	4.15	0.76	1.01	4.68	1.91	0.63	0.77	4.60	2.13	20.27	15.62	15.46	96.77
1500	5	4.78	1.95	16.72	15.78	13.38	1.61	12.69	15.98	13.11	30.53	7.65	35.87	99.22
1500	5	4.82	1.93	17.86	14.83	13.32	1.53	9.43	14.67	12.70	31.90	6.47	37.62	99.17

Table B.3 Experimental data for single salt solutions ($MgCl_2$) as a function of applied pressure (ΔP = 0.3-1.5 MPa) and constant feed concentration (5 mol/m^3). Membranes: 352, 324, 382 and HN-7450.

Applied Pressure, ΔP (kPa)	Target Feed Conc. (mol/m^3)	Actual Feed Conc. (mol/m^3)	Pure Water Flux, J_W x 10^6(m/s)				Solution Flux, J_V x 10^6(m/s)				Rejection, R_i (%)			
			352	324	382	HN-7450	352	324	382	HN-7450	352	324	382	HN-7450
500	5	7.30	0.98	1.16	8.66	3.58	1.05	1.32	8.36	3.33	94.03	95.46	4.72	88.53
300	5	7.27	0.82	1.07	5.54	3.86	0.71	20.06	5.41	1.96	93.48	94.55	4.24	82.12
900	5	7.48	1.53	1.89	12.26	6.72	1.50	1.88	12.10	6.45	95.65	96.64	2.47	93.92
900	5	6.51	1.78	4.48	10.46	7.78	1.66	2.25	10.36	7.28	86.28	85.57	7.07	94.69
500	5	6.06	1.12	1.34	7.52	4.36	1.18	1.53	7.19	3.96	93.15	91.64	2.29	89.41
300	5	6.46	0.86	1.18	4.62	2.51	0.77	1.05	4.58	2.22	92.61	90.53	8.36	85.37
1500	5	4.91	2.32	12.69	16.07	13.60	2.35	55.78	16.30	13.41	92.81	7.28	4.24	95.81
1500	5	4.95	2.24	23.28	15.01	13.18	2.26	21.96	15.28	13.30	92.99	12.17	5.28	95.67

Table B.4 Experimental data for single salt solutions (NaCl) as a function of applied pressure (ΔP = 0.3-0.9 MPa) and constant feed concentration (5 mol/m^3). Membranes: 515, 508, 509 and AL7.

Applied Pressure, ΔP (kPa)	Actual Feed Conc. (mol/m^3)	Solution Flux, $J_V \times 10^6$(m/s)				Rejection, R_i (%)			
		515	508	509	AL7	515	508	509	AL7
300	5.18	17.96	4.57	6.84	5.98	6.10	81.87	61.05	68.12
510	6.15	26.31	7.15	11.15	9.53	3.71	80.31	58.47	64.71
720	5.93	27.30	8.71	13.14	11.04	9.31	83.97	59.51	69.64
900	4.52	36.87	10.87	16.45	14.35	9.66	82.59	59.34	67.09

Table B.5 Experimental data for for a NaCl solution as a function of feed concentration (0-4000 ppm) at constant applied pressure (ΔP = 0.5 MPa). Membranes: 352, 324, 382 and HN-7450.

Applied Pressure, ΔP (kPa)	Actual Feed Conc. (mol/m^3)	Solution Flux, $J_V \times 10^6$(m/s)				Rejection, R_i (%)			
		352	324	382	HN-7450	352	324	382	HN-7450
500	4.19	1.44	3.10	5.18	3.17	81.31	76.27	8.01	59.71
500	8.34	1.38	2.97	4.81	3.12	67.83	61.75	4.62	50.81
500	16.18	1.29	2.79	4.97	2.99	47.11	42.70	2.64	40.58
500	34.69	1.20	2.62	4.82	2.84	32.57	28.89	8.50	39.77
500	66.93	1.12	2.52	4.73	2.65	16.36	14.69	4.37	28.52
500	4.27	1.42	3.06	4.82	3.25	82.30	77.13	7.42	61.42
500	33.36	1.21	2.74	4.22	2.77	34.72	29.34	2.44	36.20

Table B.6 Experimental data for for a NaCl solution as a function of feed concentration (0-4000 ppm) at constant applied pressure (ΔP = 0.5 MPa). Membranes: 515, 508, 509 and AL7.

Applied Pressure, ΔP (kPa)	Actual Feed Conc. (mol/m^3)	Solution Flux, J_V x 10^6(m/s)				Rejection, R_i (%)			
		515	508	509	AL7	515	508	509	AL7
500	4.16	23.81	70.77	13.95	9.50	9.82	10.04	50.88	60.21
500	8.30	19.86	35.10	14.74	8.56	6.21	14.74	36.70	48.25
500	16.64	20.89	54.25	14.65	8.34	4.34	4.50	20.75	33.76
500	34.01	19.44	19.44	17.00	8.69	2.78	2.78	8.00	19.03
500	65.93	18.94	38.06	20.88	8.33	1.82	7.90	3.23	8.47
500	4.24	19.74	32.46	14.19	8.36	10.56	26.27	50.26	63.81
500	33.75	16.65	18.38	16.23	7.45	1.94	5.58	11.12	20.52

Table B.7 Experimental data for a NaCl:lactose solution as a function of NaCl feed concentration (0-4000ppm) at constant lactose concentration (500 ppm) and constant applied pressure (ΔP = 0.5 MPa). Membranes: 352, 324, 382 and HN-7450.

Applied Pressure, ΔP (kPa)	Feed Conc. (mol/m^3)		Solution Flux, J_V x 10^6(m/s)				NaCl Rejection, R_i (%)				Lactose Rejection, R_i (%)			
	NaCl	Lactose	352	324	382	HN-7450	352	324	382	HN-7450	352	324	382	HN-7450
500	0.00	1.58	1.41	3.07	4.24	3.11	0.00	0.00	0.00	0.00	7.99	4.47	14.48	97.90
500	4.25	1.58	1.44	3.08	4.76	3.15	82.51	77.55	9.71	60.62	7.39	5.00	15.06	96.73
500	8.34	1.58	1.35	2.90	4.67	3.04	67.86	62.38	4.14	49.07	5.47	5.81	15.49	97.62
500	16.13	1.58	1.26	2.89	4.26	2.89	58.01	48.83	3.63	44.77	6.14	4.76	14.78	98.14
500	35.02	1.58	1.17	2.71	3.75	2.40	32.44	25.67	2.07	35.34	7.55	5.11	14.63	98.26
500	68.17	1.58	1.08	2.64	4.11	2.47	15.09	12.28	2.03	27.39	7.60	4.51	14.94	97.70

Table B.8 Experimental data for a NaCl:lactose solution as a function of NaCl feed concentration (0-4000ppm) at constant lactose concentration (500 ppm) and constant applied pressure (ΔP = 0.5 MPa). Membranes: 515, 508, 509 and AL7.

Applied Pressure,	Feed Conc. (mol/m^3)		Solution Flux, $J_V \times 10^6$(m/s)				NaCl Rejection, R_i (%)				Lactose Rejection, R_i (%)			
ΔP (kPa)	NaCl	Lactose	515	508	509	AL7	515	508	509	AL7	515	508	509	AL7
500	0.00	1.58	18.13	21.45	13.80	8.33	0.00	0.00	0.00	0.00	5.81	3.20	1.25	3.42
500	4.19	1.58	19.46	32.75	14.27	8.56	12.91	25.91	51.34	64.86	6.09	2.67	3.57	2.49
500	8.24	1.58	19.35	33.02	14.30	8.15	5.30	15.73	38.65	49.53	5.49	2.41	2.86	4.51
500	16.19	1.58	17.42	21.73	14.33	6.88	3.12	11.63	25.20	40.29	6.19	5.97	0.35	2.06
500	33.75	1.58	12.97	9.36	15.57	8.64	3.60	7.63	11.47	18.32	6.52	11.06	0.35	2.39
500	67.75	1.58	16.61	19.15	19.45	8.04	2.16	3.32	6.01	9.05	7.55	8.23	1.26	3.13

Table B.9 Experimental data for a NaCl:lactose solution as a function of lactose feed concentration (0-4000ppm) at constant NaCl concentration (2000 ppm) and constant applied pressure (ΔP = 0.5 MPa). Membranes: 352, 324, 382 and HN-7450.

Applied Pressure,	Feed Conc. (mol/m^3)		Solution Flux, $J_V \times 10^6$(m/s)				NaCl Rejection, R_i (%)				Lactose Rejection, R_i (%)			
ΔP (kPa)	NaCl	Lactose	352	324	382	HN-7450	352	324	382	HN-7450	352	324	382	HN-7450
500	34.80	0.00	1.20	2.62	4.82	2.84	32.57	28.89	8.50	39.77	0.00	0.00	0.00	0.00
500	34.80	1.60	1.17	2.71	3.75	2.40	32.44	25.67	2.07	35.34	7.55	5.11	14.63	98.26
500	34.80	2.81	1.16	2.58	3.82	2.48	32.37	28.29	2.62	34.99	7.76	4.74	15.31	98.02
500	34.80	5.83	1.17	2.61	3.74	2.30	31.33	26.27	2.33	33.02	6.99	5.17	15.78	98.06
500	34.80	11.92	1.13	2.56	3.90	2.38	33.70	29.26	3.15	33.85	9.14	4.25	16.48	98.02

Table B.10 Experimental data for a NaCl:lactose solution as a function of lactose feed concentration (0-4000ppm) at constant NaCl concentration (2000 ppm) and constant applied pressure (ΔP = 0.5 MPa). Membranes: 515, 508, 509 and AL7.

Applied Pressure,	Feed Conc. (mol/m^3)		Solution Flux, $J_V \times 10^6$(m/s)				NaCl Rejection, R_i (%)				Lactose Rejection, R_i (%)			
ΔP (kPa)	NaCl	Lactose	515	508	509	AL7	515	508	509	AL7	515	508	509	AL7
500	34.80	0.00	19.44	19.44	17.00	8.69	2.78	2.78	8.00	19.03	0.00	0.00	0.00	0.00
500	34.80	1.53	12.97	9.36	15.57	8.64	3.60	7.63	11.47	18.32	6.52	11.06	0.35	2.39
500	34.80	2.82	14.91	12.72	15.06	7.96	2.42	6.68	12.12	18.37	8.05	9.43	2.27	4.97
500	34.80	5.56	13.54	10.61	15.77	7.06	2.12	5.78	10.46	20.83	7.70	10.71	0.92	3.44
500	34.80	11.74	15.57	14.62	15.34	15.28	2.35	5.56	12.41	18.67	6.56	9.10	3.13	3.55

Table B.11 Experimental data for the membrane MacPF 352 for mixed-electrolyte solutions ($NaCl:MgCl_2$) as a function of applied pressure (ΔP = 0.3-1.5 MPa) and feed molar ratio ($[Na^+]$ = 5 mol/m^3, FR = $[Mg^{++}]/[Na^+]$ = 1-6).

$[Mg^{++}]/[Na^+]$ = 1				$[Mg^{++}]/[Na^+]$ = 3				$[Mg^{++}]/[Na^+]$ = 6			
Applied Pressure, ΔP (kPa)	Solution Flux, $J_V \times 10^6$(m/s)	Rejection, R_i (%) Na^+	Mg^{++}	Applied Pressure, ΔP (kPa)	Solution Flux, $J_V \times 10^6$(m/s)	Rejection, R_i (%) Na^+	Mg^{++}	Applied Pressure, ΔP (kPa)	Solution Flux, $J_V \times 10^6$(m/s)	Rejection, R_i (%) Na^+	Mg^{++}
300	0.66	38.70	87.32	300	0.54	2.06	72.64	300	0.49	-26.54	41.79
500	1.08	90.75	90.75	500	0.95	19.78	79.92	500	0.74	-3.88	60.28
900	1.60	92.01	92.01	900	1.45	36.69	84.42	900	1.28	15.62	69.95
1500	2.04	84.51	84.51	1500	1.89	48.82	79.52	1500	1.76	30.98	69.59
300	0.68	80.76	80.76	1500	1.97	49.25	78.19	900	1.35	12.43	59.67

Table B.12 Experimental data for the membrane MacPF 324 for mixed-electrolyte solutions ($NaCl:MgCl_2$) as a function of applied pressure (ΔP = 0.3-1.5 MPa) and feed molar ratio ($[Na^+]$ = 5 mol/m^3, FR = $[Mg^{++}]/[Na^+]$ = 1-6).

$[Mg^{++}]/[Na^+]$ = 1				$[Mg^{++}]/[Na^+]$ = 3				$[Mg^{++}]/[Na^+]$ = 6			
Applied Pressure, ΔP (kPa)	Solution Flux, J_V x 10^6(m/s)	Rejection, R_i (%) Na^+	Mg^{++}	Applied Pressure, ΔP (kPa)	Solution Flux, J_V x 10^6(m/s)	Rejection, R_i (%) Na^+	Mg^{++}	Applied Pressure, ΔP (kPa)	Solution Flux, J_V x 10^6(m/s)	Rejection, R_i (%) Na^+	Mg^{++}
300	0.89	49.84	88.17	300	0.73	8.07	73.69	300	0.65	-21.60	43.26
500	1.40	91.90	91.90	500	1.22	26.29	81.83	500	0.98	5.00	61.86
900	1.96	92.80	92.80	900	1.80	49.53	86.32	900	1.58	20.72	72.01
1500	2.49	83.56	83.56	1500	2.44	52.03	78.24	1500	2.31	35.47	67.51
300	0.95	82.78	82.78	1500	2.67	47.38	72.90	900	1.66	17.29	62.78

Table B.13 Experimental data for the membrane MacPF 382 for mixed-electrolyte solutions ($NaCl:MgCl_2$) as a function of applied pressure (ΔP = 0.3-1.5 MPa) and feed molar ratio ($[Na^+]$ = 5 mol/m^3, FR = $[Mg^{++}]/[Na^+]$ = 1-6).

$[Mg^{++}]/[Na^+]$ = 1				$[Mg^{++}]/[Na^+]$ = 3				$[Mg^{++}]/[Na^+]$ = 6			
Applied Pressure, ΔP (kPa)	Solution Flux, J_V x 10^6(m/s)	Rejection, R_i (%) Na^+	Mg^{++}	Applied Pressure, ΔP (kPa)	Solution Flux, J_V x 10^6(m/s)	Rejection, R_i (%) Na^+	Mg^{++}	Applied Pressure, ΔP (kPa)	Solution Flux, J_V x 10^6(m/s)	Rejection, R_i (%) Na^+	Mg^{++}
300	4.94	8.84	8.93	300	4.85	2.25	4.71	300	5.17	-0.86	-1.23
500	7.87	0.00	0.00	500	8.00	1.39	-1.05	500	7.85	2.35	3.21
900	12.45	3.47	3.47	900	12.31	4.87	5.33	900	12.12	0.73	-0.27
1500	16.63	8.74	8.74	1500	15.96	7.75	14.10	1500	16.04	-4.65	-0.09
300	4.52	0.00	0.00	1500	16.43	1.64	3.94	900	11.31	3.21	0.40

Table B.14 Experimental data for the membrane HN-7450 for mixed-electrolyte solutions ($NaCl:Na_2SO_4$) as a function of applied pressure (ΔP = 0.3-1.5 MPa) and feed molar ratio ($[Cl^-]$ = 5 mol/m^3, FR = $[SO_4^{=}]/[Cl^-]$ = 1-6).

$[SO_4^{=}]/[Cl^-]$ = 1				$[SO_4^{=}]/[Cl^-]$ = 3				$[SO_4^{=}]/[Cl^-]$ = 6			
Applied Pressure, ΔP (kPa)	Solution Flux, J_V x 10^6(m/s)	Rejection, R_i (%) Cl^-	$SO_4^{=}$	Applied Pressure, ΔP (kPa)	Solution Flux, J_V x 10^6(m/s)	Rejection, R_i (%) Cl^-	$SO_4^{=}$	Applied Pressure, ΔP (kPa)	Solution Flux, J_V x 10^6(m/s)	Rejection, R_i (%) Cl^-	$SO_4^{=}$
300	2.04	19.85	99.88	300	1.63	-21.81	92.99	300	1.09	-75.01	99.90
500	3.39	59.88	96.90	500	3.00	33.94	96.20	500	2.37	45.79	99.90
900	6.62	71.25	98.52	900	6.05	56.11	98.14	900	5.29	32.14	99.93
1500	11.80	76.01	99.89	1500	11.12	60.62	99.94	1500	10.09	47.30	98.62
300	2.03	47.83	99.84	500	3.17	35.93	99.94	900	5.77	36.46	97.44

Table B.15 Experimental data for the membrane MacPF 352 for mixed-electrolyte solutions ($NaCl:Na_2SO_4$) as a function of applied pressure (ΔP = 0.3-1.5 MPa) and feed molar ratio ($[Cl^-]$ = 5 mol/m^3, FR = $[SO_4^{=}]/[Cl^-]$ = 1-6).

$[SO_4^{=}]/[Cl^-]$ = 1				$[SO_4^{=}]/[Cl^-]$ = 3				$[SO_4^{=}]/[Cl^-]$ = 6			
Applied Pressure, ΔP (kPa)	Solution Flux, J_V x 10^6(m/s)	Rejection, R_i (%) Cl^-	$SO_4^{=}$	Applied Pressure, ΔP (kPa)	Solution Flux, J_V x 10^6(m/s)	Rejection, R_i (%) Cl^-	$SO_4^{=}$	Applied Pressure, ΔP (kPa)	Solution Flux, J_V x 10^6(m/s)	Rejection, R_i (%) Cl^-	$SO_4^{=}$
300	0.51	10.90	12.50	300	0.49	-2.40	0.48	300	0.51	-10.01	-2.33
500	0.76	19.52	27.39	500	0.75	7.13	9.64	500	0.83	5.44	5.34
900	1.14	14.28	28.70	900	1.08	10.34	16.84	900	1.01	6.89	7.81
1500	1.46	18.59	32.07	1500	1.42	5.78	16.48	1500	1.38	8.78	11.63
300	0.61	4.55	-4.48	500	0.85	3.58	5.09	900	1.20	5.25	9.99

Table B.16 Experimental data for the membrane MacPF 324 for mixed-electrolyte solutions ($NaCl:Na_2SO_4$) as a function of applied pressure (ΔP = 0.3-1.5 MPa) and feed molar ratio ($[Cl^-]$ = 5 mol/m^3, FR = $[SO_4^{=}]/[Cl^-]$ = 1-6).

$[SO_4^{=}]/[Cl^-]$ = 1				$[SO_4^{=}]/[Cl^-]$ = 3				$[SO_4^{=}]/[Cl^-]$ = 6			
Applied Pressure, ΔP (kPa)	Solution Flux, J_V x 10^6(m/s)	Rejection, R_i (%) Cl^-	$SO_4^{=}$	Applied Pressure, ΔP (kPa)	Solution Flux, J_V x 10^6(m/s)	Rejection, R_i (%) Cl^-	$SO_4^{=}$	Applied Pressure, ΔP (kPa)	Solution Flux, J_V x 10^6(m/s)	Rejection, R_i (%) Cl^-	$SO_4^{=}$
300	0.65	16.44	30.48	300	0.59	-4.67	-1.37	300	0.63	-14.47	-1.82
500	0.86	18.74	26.07	500	0.85	8.99	8.37	500	0.80	-8.05	-1.22
900	1.24	12.46	28.97	900	1.16	6.06	13.99	900	1.12	6.05	6.22
1500	2.18	19.44	28.85	1500	2.00	2.29	12.21	1500	2.24	3.97	7.11
300	0.72	2.06	-5.36	500	0.94	2.04	4.09	900	1.31	2.84	6.81

Table B.17 Experimental data for the membrane MacPF 382 for mixed-electrolyte solutions ($NaCl:Na_2SO_4$) as a function of applied pressure (ΔP = 0.3-1.5 MPa) and feed molar ratio ($[Cl^-]$ = 5 mol/m^3, FR = $[SO_4^{=}]/[Cl^-]$ = 1-6).

$[SO_4^{=}]/[Cl^-]$ = 1				$[SO_4^{=}]/[Cl^-]$ = 3				$[SO_4^{=}]/[Cl^-]$ = 6			
Applied Pressure, ΔP (kPa)	Solution Flux, J_V x 10^6(m/s)	Rejection, R_i (%) Cl^-	$SO_4^{=}$	Applied Pressure, ΔP (kPa)	Solution Flux, J_V x 10^6(m/s)	Rejection, R_i (%) Cl^-	$SO_4^{=}$	Applied Pressure, ΔP (kPa)	Solution Flux, J_V x 10^6(m/s)	Rejection, R_i (%) Cl^-	$SO_4^{=}$
300	4.96	-6.91	11.91	300	4.94	-5.39	6.06	300	4.95	-6.88	1.70
500	8.02	2.69	31.87	500	8.00	-1.74	13.92	500	7.98	-5.00	7.67
900	12.21	-8.44	25.48	900	11.63	-6.19	17.81	900	12.02	-28.22	11.74
1500	16.60	-9.33	25.95	1500	16.01	-12.21	21.32	1500	15.50	-7.33	16.69
300	4.50	-4.74	0.14	500	7.21	-7.60	10.19	900	11.53	-7.29	12.48

Table B.18 Experimental data for the membrane HN-7450 for mixed-electrolyte solutions ($NaCl:MgCl_2$) as a function of applied pressure (ΔP = 0.3-1.5 MPa) and feed molar ratio ($[Na^+]$ = 5 mol/m^3, FR = $[Mg^{++}]/[Na^+]$ = 1-6).

$[Mg^{++}]/[Na^+]$ = 1				$[Mg^{++}]/[Na^+]$ = 3				$[Mg^{++}]/[Na^+]$ = 6			
Applied Pressure, ΔP (kPa)	Solution Flux, J_V x 10^6(m/s)	Rejection, R_i (%) Na^+	Mg^{++}	Applied Pressure, ΔP (kPa)	Solution Flux, J_V x 10^6(m/s)	Rejection, R_i (%) Na^+	Mg^{++}	Applied Pressure, ΔP (kPa)	Solution Flux, J_V x 10^6(m/s)	Rejection, R_i (%) Na^+	Mg^{++}
300	2.17	-5.95	86.31	300	1.67	-47.79	86.97	300	1.14	-102.97	82.40
500	3.42	89.37	89.37	500	3.06	-27.91	90.56	500	2.41	-67.13	89.83
900	6.52	92.60	92.60	900	6.12	5.75	93.75	900	5.41	-33.56	92.77
1500	11.65	94.43	94.43	1500	11.04	36.22	95.30	1500	10.20	19.72	95.78
300	2.10	85.86	85.86	1500	14.20	26.43	95.26	900	5.72	-29.23	92.65

Appendix C

Calculation of the Free-Solution Diffusivity and Hydrodynamic Radius

The calculations of the free-solution diffusivity at infinite dilution and the hydrodynamic radius are presented in this section. The data are presented in Table C.1.

For sufficiently dilute solutions, ion diffusivity is independent of ionic concentration and can be expressed as a function of the ionic limiting conductance (λ^0_i) using the Nernst equation (Atkins, 1994).

$$D_{i,\infty} = \frac{RT}{F^2}\frac{\lambda_i^0}{|z_i|} \tag{C.1}$$

The hydrodynamic radius for a hard sphere can be calculated from the Stokes-Einstein equation as:

$$r_P = \frac{kT}{6\pi\mu D_{i,\infty}} \tag{C.2}$$

Table C.1 Calculated values for the hydrodynamic radius and free-solution diffusivity.

Ion	Ionic conductance * $\lambda^0_i \times 10^3$ (m^2/ohm/mol)	Radius r_P (nm)	Diffusivity $D_{i,\infty} \times 10^9$ (m^2/s)
Na^+	5.011	0.1637	1.3343
Mg^{2+}	5.300	0.3463	0.7056
Cl^-	7.635	0.1074	2.0331
$SO_4^=$	8.000	0.2050	1.0651

* From Atkins (1994).

Appendix D

Effective Surface Charge Density as a Function of Ionic Strength

The experimental and modeled results correlating the effective surface charge density of the membrane to ionic strength are presented in this section. The effective surface charge density of each membrane was estimated using the transport model, the known model parameters (pore radius and pure water permeability) and the experimental data presented in section 6.2.5.1. Once the effective charge density for the membrane at each concentration was known, an empirical model (eq. 4.41a or 4.41b) was fitted to the data. The experimental and modeled results are presented in Fig. D1.

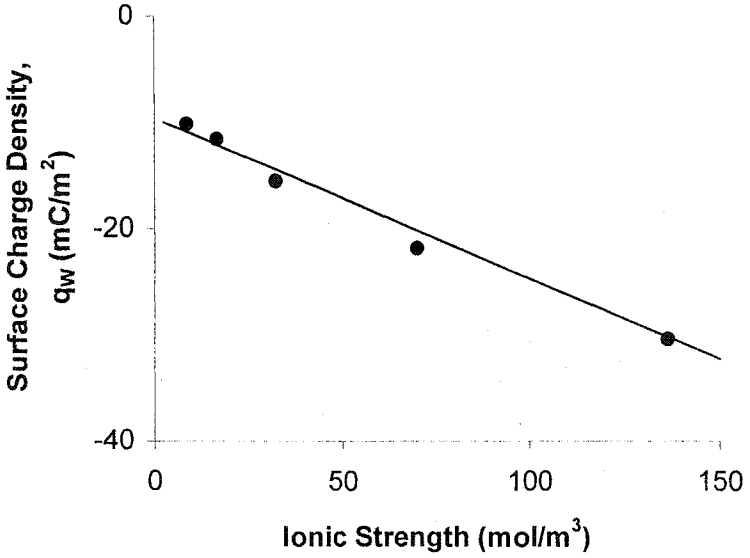

(a)

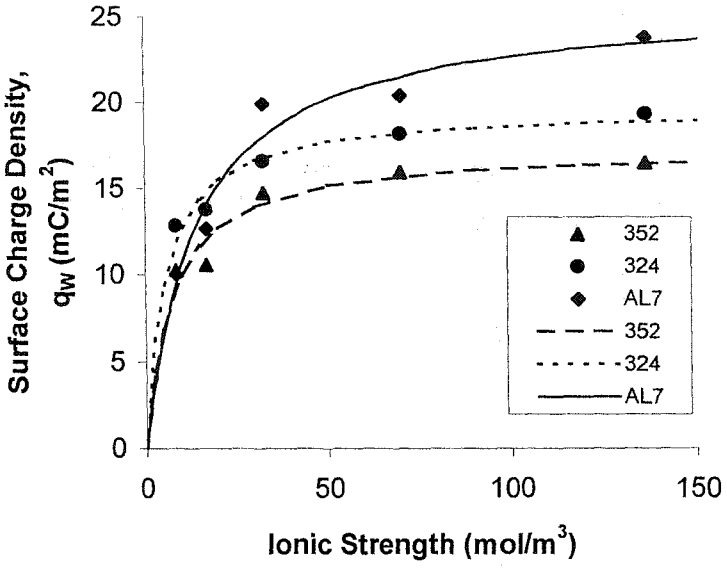

(b)

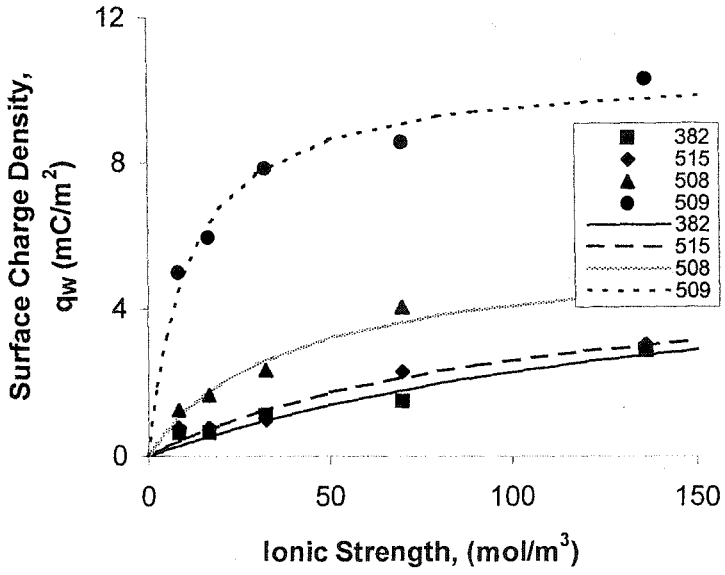

(c)

Figure D.1 Effective surface charge density as a function of the ionic strength of the feed solution (0-150 mol/m^3). Points are experimental data. Lines are model calculations. NaCl (●,–) and Lactose (▲,---). Membranes: a) HN-7450 and MacPF b) 352, 324, AL7, c) 382, 515, 508, 509.